Gadolinium(III) Chelates as MRI Contrast Agents: Structure, Dynamics, and Applications

Peter Caravan,* Jeffrey J. Ellison, Thomas J. McMurry, and Randall B. Lauffer

EPIX Medical, Inc., 71 Rogers Street, Cambridge, Massachusetts 02142

Received February 22, 1999 (Revised Manuscript Received June 24, 1999)

Contents

I. Introduction

Gadolinium, an obscure lanthanide element buried in the middle of the periodic table, has in the course of a decade become commonplace in medical diagnostics. Like platinum in cancer therapeutics and technetium in cardiac scanning, the unique magnetic properties of the gadolinium(III) ion placed it right in the middle of a revolutionary development in medicine: magnetic resonance imaging (MRI). While it is odd enough to place patients in large superconducting magnets and noisily pulse water protons in their tissues with radio waves, it is odder still to inject into their veins a gram of this potentially toxic metal ion which swiftly floats among the water molecules, tickling them magnetically.

The successful penetration of gadolinium(III) chelates into radiologic practice and medicine as a whole can be measured in many ways. Since the approval of $[Gd(DTPA)(H_2O)]^{2-}$ in 1988, it can be estimated that over 30 metric tons of gadolinium have been administered to millions of patients worldwide. Currently, approximately 30% of MRI exams include the use of contrast agents, and this is projected to increase as new agents and applications arise; Table 1 lists agents currently approved or in clinical trials. In the rushed world of modern medicine, radiologists, technicians, and nurses often refrain from calling the agents by their brand names, preferring instead the affectionate "gado." They trust this clear, odorless "magnetic light", one of the safest class of drugs ever developed. Aside from the cost ($50−80/bottle), asking the nurse to "Give him some gado" is as easy as starting a saline drip or obtaining a blood sample.

Gadolinium is also finding a place in medical research. When one of us reviewed the field in its infancy,[1] in 1987, only 39 papers could be found for that year in a Medline search for "gado-" and MRI. Ten years later over 600 references appear each year. And as MRI becomes relied upon by different specialties, "gado" is becoming known by neurologists,

* To whom correspondence should be addressed: Tel.: +1 617 250 6127. Fax: +1 617 250 6127. E-mail: pcaravan@epixmed.com.

10.1021/cr980440x CCC: $35.00
Published on Web 08/20/1999

Peter Caravan grew up in Bay Roberts, Newfoundland. He received a B.Sc. degree in Chemistry from Acadia University in Nova Scotia, Canada, in 1992. He was awarded an NSERC postgraduate scholarship which he took to the University of British Columbia where he studied the coordination chemistry of podand complexes of trivalent metal ions with Chris Orvig. After receiving his Ph.D. in 1996, Peter was awarded an NSERC postdoctoral fellowship to work in the group of André Merbach at the Université de Lausanne. There he probed the dynamics of metal complexes utilizing paramagnetic NMR. In 1998 Peter joined EPIX Medical, Inc., where he is currently investigating various biophysical chemistry problems.

Thomas J. McMurry received his B.S. in Chemistry from Penn State in 1979. He did his graduate work with John T. Groves at the University of Michigan (Ph.D., 1984) where he studied the structure and reactivity of high valent iron porphyrinate models for cytochrome P-450. Tom then moved to Berkeley as an NIH Postdoctoral Fellow in Kenneth N. Raymond's laboratory to work on the synthesis and coordination chemistry of macrobicyclic catechol-based siderophore analogues. In 1987, he joined the NIH as a Staff Fellow in the late Otto Gansow's laboratory and was involved with the development of bifunctional chelating agents for use in radioimmunotherapy. Tom has been employed at EPIX Medical (formerly Metasyn, Inc.) since 1993, where he is currently Senior Director, Chemistry.

Jeff Ellison came to EPIX Medical in 1997. He received a B.S. degree in chemistry from the University of California, Irvine. He earned his Ph.D. at the University of California, Davis, studying the kinetic stabilization of low coordinate metal environments with Phil Power. He did his postdoctoral research with Julie Kovacs at the University of Washington, investigating the role of iron in nitrile hydratase enzymes.

Dr. Lauffer received his Ph.D. in Chemistry from Cornell University in 1983. At the Massachusetts General Hospital, Boston, MA, he served as a National Institutes of Health Postdoctoral Fellow and as director of the NMR Contrast Media Laboratory. He also held positions of Assistant Professor in Radiology at Harvard Medical School and NIH New Investigator. In 1992, Dr. Lauffer founded EPIX Medical, Inc., a developer of MRI contrast agents, and currently serves as Chief Scientific Officer and a member of the board of directors.

cardiologists, urologists, opthamologists, and others in search of new ways to visualize functional changes in the body.

While other types of MRI contrast agents have been approved, namely an iron particle-based agent and a manganese(II) chelate, gadolinium(III) remains the dominant starting material. The reasons for this include the direction of MRI development and the nature of Gd chelates.

A. Signal Intensity in MRI

As described in more detail elsewhere, signal intensity in MRI stems largely from the local value of the longitudinal relaxation rate of water protons, $1/T_1$, and the transverse rate, $1/T_2$. Signal tends to increase with increasing $1/T_1$ and decrease with increasing $1/T_2$. Pulse sequences that emphasize changes in $1/T_1$ are referred to as T_1-weighted, and the opposite is true for T_2-weighted scans.

Contrast agents increase both $1/T_1$ and $1/T_2$ to varying degrees depending on their nature as well as the applied magnetic field. Agents such as gadolinium(III) that increase $1/T_1$ and $1/T_2$ by roughly similar amounts are best visualized using T_1-weighted images since the percentage change in $1/T_1$ in tissue is much greater than that in $1/T_2$. Iron particles, on the other hand, generally lead to a much larger increase in $1/T_2$ than in $1/T_1$ and are best seen with T_2-weighted scans.

The longitudinal and transverse relaxivity values, r_1 and r_2, refer to the amount of increase in $1/T_1$ and $1/T_2$, respectively, per millimolar of agent (often given as per mM of Gd). T_1 agents usually have r_2/r_1 ratios of 1−2, whereas that value for T_2 agents, such as iron oxide particles, is as high as 10 or more.

Table 1. Clinically Relevant Gadolinium(III) Chelates

chemical name	generic name	brand name	company	classification
$[Gd(DTPA)(H_2O)]^{2-}$	gadopentetate dimeglumine	Magnevist[a]	Schering (Germany)	extracellular
$[Gd(DOTA)(H_2O)]^{-}$	gadoterate meglumine	Dotarem[a]	Guerbet (France)	extracellular
$[Gd(DTPA\text{-}BMA)(H_2O)]$	gadodiamide	Omniscan[a]	Nycomed-Amersham (U.K.)	extracellular
$[Gd(HP\text{-}DO3A)(H_2O)]$	gadoteridol	ProHance[a]	Bracco (Italy)	extracellular
$[Gd(DO3A\text{-}butrol)(H_2O)]$	gadobutrol	Gadovist[a]	Schering (Germany)	extracellular
$[Gd(DTPA\text{-}BMEA)(H_2O)]$	gadoversetamide	OptiMARK[b]	Mallinckrodt (U. S.)	extracellular
$[Gd(BOPTA)(H_2O)]^{2-}$	gadobenate dimeglumine	MultiHance[a]	Bracco (Italy)	hepatobiliary/extracellular
$[Gd(EOB\text{-}DTPA)(H_2O)]^{2-}$	gadoxetic acid disodium	Eovist[b]	Schering (Germany)	hepatobiliary
MS-325	gadophostriamine trisodium	AngioMARK[b]	EPIX/Mallinckrodt (U. S.)	blood pool

[a] Approved. [b] In clinical trials.

Advances in MRI have strongly favored T_1 agents and thus gadolinium(III). Faster scans with higher resolution require more rapid radio frequency pulsing and are thus generally T_1-weighted since the MR signal in each voxel becomes saturated. T_1 agents relieve this saturation by restoring a good part of the longitudinal magnetization between pulses. At the same time, a good T_1 agent would not significantly affect the bulk magnetic susceptibility of the tissue compartment in which it is localized, thus minimizing any inhomogeneities which can lead to image artifacts and/or decreased signal intensity. Small iron particles can function as T_1 agents using very T_1-weighted scans, but the resulting changes in magnetic susceptibility are much larger than that for gadolinium(III) chelates.

B. The Nature of Gadolinium(III) Chelates

The choice of Gd(III) would be expected, for no other ion has seven unpaired electrons. But there is a much more subtle reason it performs so well. Two other lanthanide ions, dysprosium(III) and holmium(III), have larger magnetic moments (due to orbital contributions to electron angular momentum) than that of Gd(III), but the asymmetry of these electronic states leads to very rapid electron spin relaxation.[2] The symmetric S-state of Gd(III) is a more hospitable environment for electron spins, leading to a much slower electronic relaxation rate. In the intricate dance that gives rise to relaxivity, water protons hardly feel the effects of ions such as Dy(III), much like a leaf near the incredibly rapid wings of a hummingbird; Gd(III) electrons, on the other hand, are more closely in tune with the proton's frequency.

A bizarre ion does not a drug make. Even with its high relaxivity, how can one inject a whole gram of it into people? This is a toxic heavy metal, with a size approximating calcium(II), but with a higher charge, leading to disruption of critical Ca(II)-required signaling. This is also not cobalt(III) or chromium(III), ions with powerfully bonding orbitals forming chelates that last for years.

The final oddity of gadolinium(III) chelates is that, when proper ligands are chosen, they actually do remain chelated in the body and are excreted intact. Apparently, the off-the-shelf ligands such as DTPA form complexes strong enough so that, for the period that the agent is in the body, there is no detectable dissociation. This is in the face of significant amounts of phosphate, citrate, transferrin, and other chelating substances.

Once the chemist makes the mental leap, however difficult it is, that this exchange-labile metal ion forms essentially inert complexes, then the chelate can be viewed as an intact drug molecule. Traveling over the surface of, say, $[Gd(DTPA)(H_2O)]^{2-}$, it does not look too bad. It is not hydrophobic, so it is unlikely to enter cells. There are no nitrogen mustard or intercalating groups to muck up our DNA. The metal ion is buried in the cage, so it is unlikely to bind to donor groups in proteins and enzymes. There is nothing a good nucleophile or electrophile can attack. It actually does not look like much at all: a little hydrophilic ball, as inocuous as a sugar molecule. And, oddly enough, it appears to be as safe.

C. This Review

A previous review in this journal,[1] now 12 years old, covered a broad range of topics related to MRI agents. A number of other reviews and perspectives have also appeared.[3−15] The present article is to be more focused, especially on the subtle and unique chemical features of Gd(III) chelates which have not been covered in as much detail. Agents for oral or inhalation use in MRI are omitted from this article. Iron particles and manganese complexes are not discussed here, but good summaries can be found in other sources.[8,16,17] Nor are the other fascinating areas of chemical shift reagents[3,15] and, especially, imaging with the hyperpolarized nuclei of noble gases[18] covered in this review.

With regard to Gd(III) chelates, only brief summaries of safety and applications are provided; more can be found elsewhere.[1,4,8] The chelates discussed are those judged by the authors to be of sufficient stability for in vivo use. As opposed to an exhaustive review of every paper on the subject, our major goal is to communicate the critical points needed to understand the development of clinically relevant agents. We regret if we omitted interesting studies for the sake of conciseness.

II. Solution and Solid State Structures

This first section deals with the solid and solution state structures of gadolinium(III) complexes used in MRI or of interest from an MRI perspective. Structural characterization is the first step in understanding the physicochemical and pharmacologic behavior of these compounds. In the second part of section II, the thermodynamic stability and kinetic inertness of

Chart 1

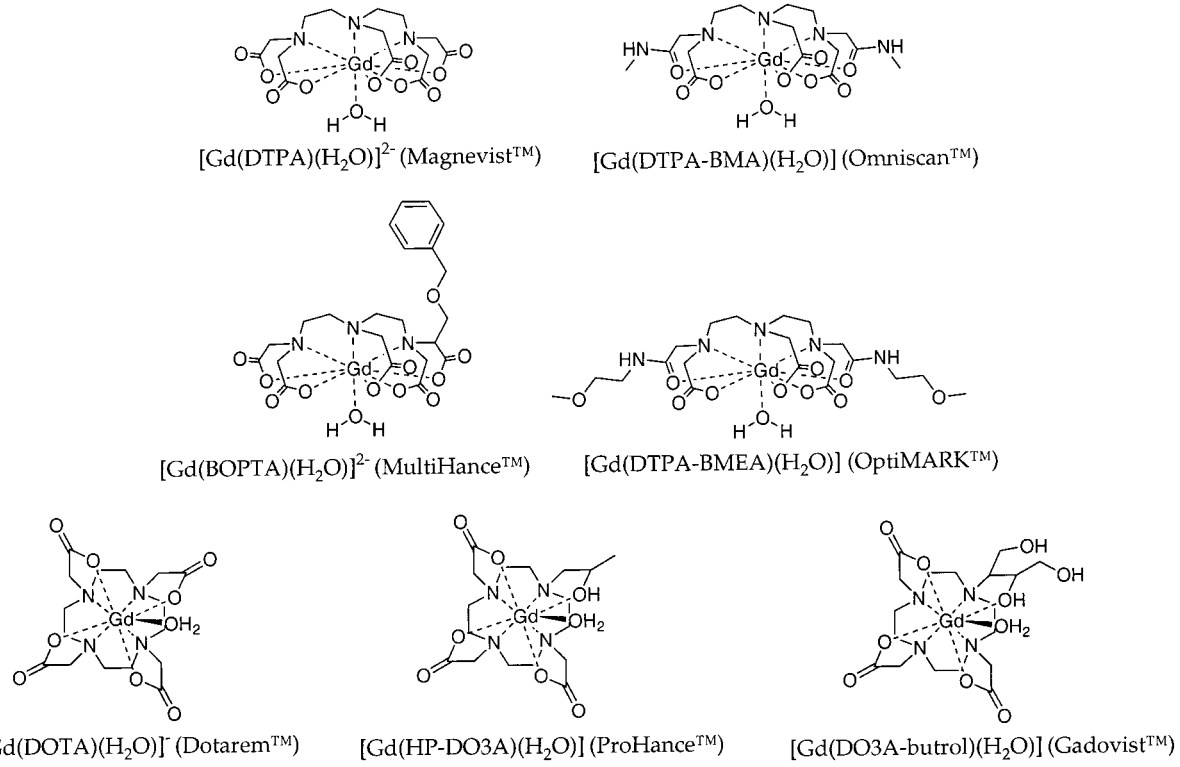

these complexes is discussed, with particular emphasis on in vivo stability.

A. Solid State Structures

Owing to their large size, lanthanides tend to favor high coordination numbers in aqueous media. Currently, all gadolinium(III)-based chelates approved for use in MRI are nine-coordinate complexes in which a ligand occupies eight binding sites at the metal center and the ninth coordination site is occupied by a solvent water molecule (Chart 1). For nine-coordinate complexes the idealized coordination geometries are tricapped trigonal prism (TTP) and capped square antiprism (CSAP) (Figure 1). In the absence of chelate ring steric effects, Guggenberger and Muetterties identified the tricapped trigonal prism as the most favorable polytopal form for an ML_9 coordination complex.[19] When the square basal plane of a CSAP is bent along the (4,7) diagonal, the CSAP is changed to a TTP geometry (Figure 1). Three useful distinguishing features of the two geometries are the dihedral angle between the trigonal faces

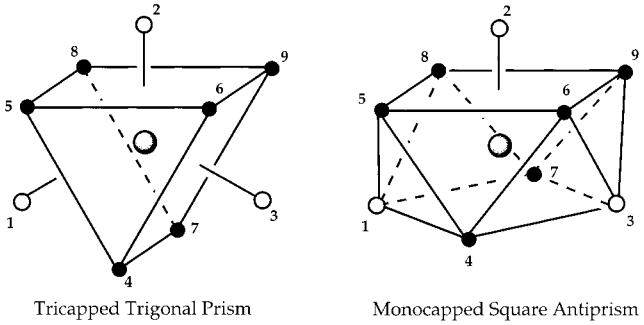

Figure 1. Tricapped trigonal prism (TTP) and monocapped square antiprism (CSAP) geometries.

(4,5,6) and (7,8,9), which in idealized polyhedra is 180° for TTP (coplanar to each other and to the (1,2,3) plane) and 163.5° for CSAP, the dihedral angle between the trigonal faces (1,4,7) and (3,4,7) which should be 26.4° for TTP and 0° for CSAP, and the mean deviation in the basal (1,4,3,7) plane, which should be small in the CSAP case. Nine-coordinate Ln(III) complexes are often described as distorted TTP or distorted CSAP. Because the two geometries are closely related, it is possible that a particular structure is described equally well by both geometries.

X-ray structures for Ln(III) complexes of DTPA (Chart 2) were reported by Gries et al. (Gd(III) complex, Na^+ salt),[20] Stezowski et al. (Nd(III) complex, Ba salt),[21] Jin et al. (Gd(III) complex, Mn salt),[22] Inoue et al. (Gd(III) complex, NH_4^+ salt),[23] Sakagami et al. (Dy(III) complex, Cs salt),[24] and Ruloff et al. (Gd(III) complexes, guanidinium salts).[25] All of these structures contained a nine-coordinate metal ion bonded to three nitrogens and five monodentate carboxylate oxygen atoms of the DTPA ligand. In some cases the observed geometries were distorted from ideal prisms to such a degree that either the TTP or CSAP description is justified. For example, the dihedral angles in the Nd(III) complex (Table 3) were intermediate to those of idealized TTP and CSAP arrangements (Figure 2). In most cases, the geometry is best described as a distorted TTP. The complexes $Na_2[Gd(DTPA)(H_2O)]$, $Mn[Gd(DTPA)(H_2O)]$, $Ba[Nd(DTPA)(H_2O)]$, and $CN_3H_6[Gd(HDTPA)(H_2O)]$ all have similar structures in which the remaining coordination site (position 2 in Figure 1) was occupied by a water molecule. Three examples of dimeric structures, $(NH_4)_4[Gd_2(DTPA)_2]$, $(CN_3H_6)_4[Gd_2(DTPA)_2]$, and $Cs_4[Dy_2(DTPA)_2]$, were also reported.

Chart 2

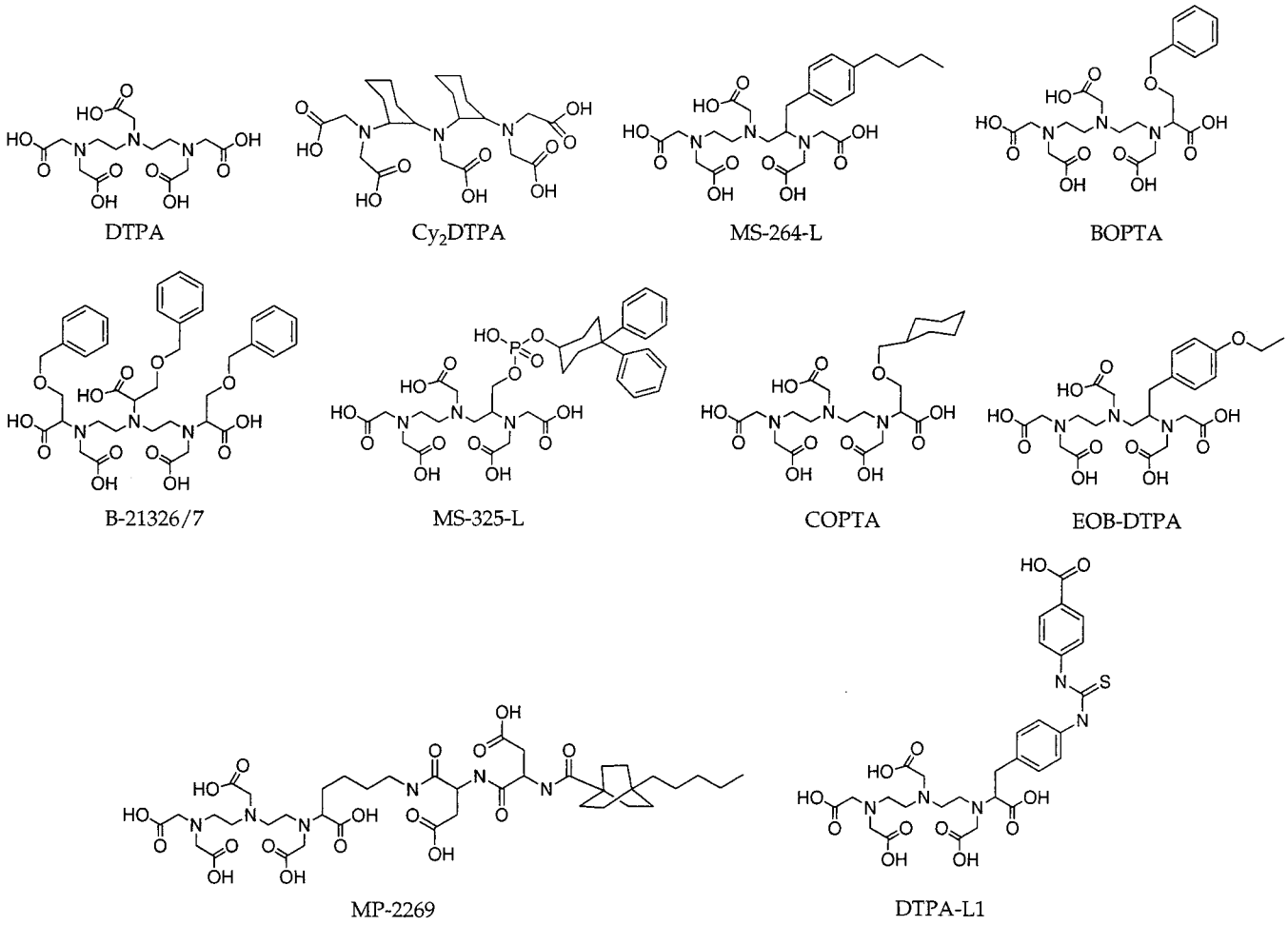

Table 2. Selected Bond Distances (Å) for Ln(III) Complexes of DTPA and Related Ligands

complex	Ln−O_{water}	Ln−$O_{carboxylate}$[a]	Ln−$N_{terminal}$	Ln−$N_{central}$	Ln−O_{amide}	ref
$Na_2[Gd(DTPA)(H_2O)]$	2.490	2.363−2.437	2.629, 2.710	2.582		20
$(NH_4)_4[Gd_2(DTPA)_2]$		2.364−2.413	2.651, 2.728	2.620		23
$(CN_3H_6)_4[Gd_2(DTPA)_2]$		2.371−2.428	2.669, 2.713	2.612		25
$(CN_3H_6)[Gd(HDTPA)(H_2O)]$	2.421[b]	2.340−2.492	(2.659, 2.785)[b]	2.666[b]		25
$Mn[Gd(DTPA)(H_2O)]$	2.441	2.350−2.442	2.588, 2.830	2.621		22
$Ba[Nd(DTPA)(H_2O)]$	2.616	2.361−2.526	2.681, 2.822	2.760		21
$Cs_4[Dy_2(DTPA)_2]$		2.324−2.392	2.648, 2.724	2.609		24
$(NH_4)_2[Gd(Cy_2DTPA)(H_2O)]$	2.434	2.347−2.424	2.622, 2.705	2.800		26
$Na_2[Gd(BOPTA)(H_2O)]$	2.463	2.340−2.416	2.615, 2.800	2.571		28
$Na_2[Gd(MS-264)(H_2O)]$	2.466[b]	2.339−2.419	(2.633, 2.734)[b]	2.605[b]		27
$Na_2[Eu(BOPTA)(H_2O)]$	2.46	2.320−2.437	2.65, 2.81	2.65		29
$[Gd(DTPA\text{-}BBA)(H_2O)]$	2.442	2.368−2.384	2.665, 2.751	2.600	2.427, 2.455	33
$[Gd(DTPA\text{-}BEA)(H_2O)]$	2.423	2.351−2.384	2.702, 2.759	2.645	2.362, 2.425	32
$[Lu(DTPA\text{-}BBA)(H_2O)]$	2.359	2.296−2.308	2.601, 2.739	2.526	2.296, 2.318	35
$[Y(DTPA\text{-}BBA)(H_2O)]$	2.40	2.32−2.34	2.62, 2.74	2.56	2.33, 2.36	36
$[Dy(DTPA\text{-}BMA)(H_2O)]$	2.463	2.318−2.350	2.616, 2.751	2.609	2.348, 2.376	31
$H_2[Eu_2(DTPA-cs124)_2]$		2.35−2.41	2.64, 2.76	2.59	2.50, 2.30	31
$[Gd_2(15\text{-}DTPA-EAM)_2(H_2O)_2]$	2.412	2.380−2.381	2.611, 2.915	2.761	2.406, 2.449	38
$[Gd(16\text{-}DTPA\text{-}PAM)(H_2O)]$	2.474	2.332−2.391	2.664, 2.748	2.618	2.439, 2.451	38
$[Gd(17\text{-}DTPA\text{-}BAM)(H_2O)]$	2.431	2.356−2.387	2.700, 2.785	2.615	2.397, 2.454	40
$[Gd(16\text{-}DTPA\text{-}HPAM)(H_2O)]$	2.408	2.350−2.364	2.695, 2.783	2.643	2.439, 2.454	39
$[Y_2(15\text{-}DTPA-EAM)_2(H_2O)_2]$	2.367	2.320−2.348	2.589, 2.926	2.759	2.403, 2.370	37
$[La_2(15\text{-}DTPA-EAM)_2(H_2O)_2]$	2.534	2.468−2.484	2.718, 2.953	2.842	2.507, 2.559	37
$(CF_3SO_3)_2[La(18\text{-}DTPA-dienH^+)(H_2O)]_2$	2.586	2.555−2.862	2.826, 2.889	2.796	2.615, 2.689	41
$(CF_3SO_3)_2[Eu(18\text{-}DTPA-dienH^+)]_4$		2.361−2.407	2.646, 2.816	2.615	2.408, 2.440	41

[a] Range of observed distances. [b] Average of two independent molecules.

In all three cases a ligand carboxylate donor functions as a bridging bidentate group occupying the ninth coordination site of a neighboring metal center.

The crystal structure of the Gd(III) complex of Cy_2-DTPA (Chart 2), in which the ligand had an all trans configuration in the dicyclohexyltriamine backbone,

Table 3. Selected Dihedral Angles (deg) for Ln(III) Complexes of DTPA and DTPA Derivatives[a]

complexes	(4,5,6) (7,8,9)	(1,7,4) (3,4,7)	ref
idealized CSAP	163.5	0.0	19
$(NH_4)_2$[Gd(Cy$_2$DTPA)(H_2O)]	153.5	0.8	26
Ba[Nd(DTPA)(H_2O)]	166.4	10.2	21
Mn[Gd(DTPA)(H_2O)]	171.7	14.5	22
[Gd(16-DTPA-PAM)(H_2O)]	172.7	14.5	38
[Gd(16-DTPA-HPAM)(H_2O)]	173.9	16.2	39
Na_2[Gd(BOPTA)(H_2O)]	177.0	17.4	28
Na_2[Eu(BOPTA)(H_2O)]	176.9	17.5	29
[Gd(DTPA-BEA)(H_2O)]	175.9	19.8	32
[Dy(DTPA-BMA)(H_2O)]	176.5	22.1	31
[Lu(DTPA-BBA)(H_2O)]	171.2	23.3	35
Na_2[Gd(MS−264)(H_2O)]	178[b]	23[b]	27
idealized TTP	180	26.4	19

[a] Positions are assigned based upon water filling site 2 as described in Figure 11. [b] Average of two independent molecules.

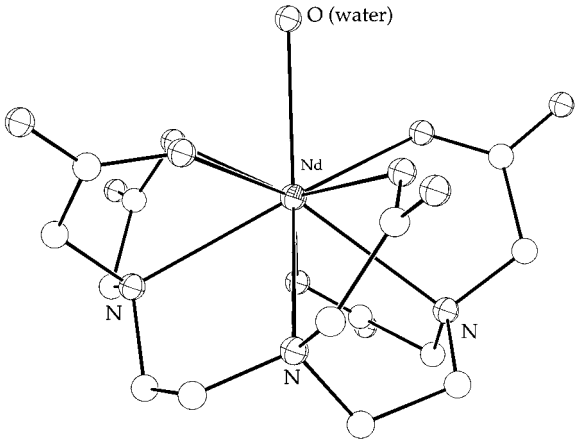

Figure 2. Molecular structure of [Nd(DTPA)(H_2O)]$^{2-}$ (ref 21).

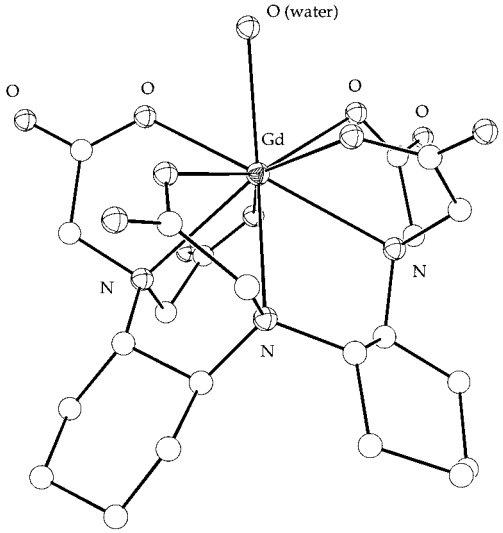

Figure 3. ORTEP drawing of [Gd(Cy$_2$DTPA)(H_2O)]$^{2-}$ (ref 26).

has been reported by Caulfield et al.[26] and is shown in Figure 3. The metal ion was nine-coordinate with the eight donor atoms in a CSAP arrangement. The three amine nitrogens and one carboxylate oxygen were coplanar, forming the basal plane of a prism. The capped plane, comprised of four carboxylate oxygens, was slightly distorted with three of the

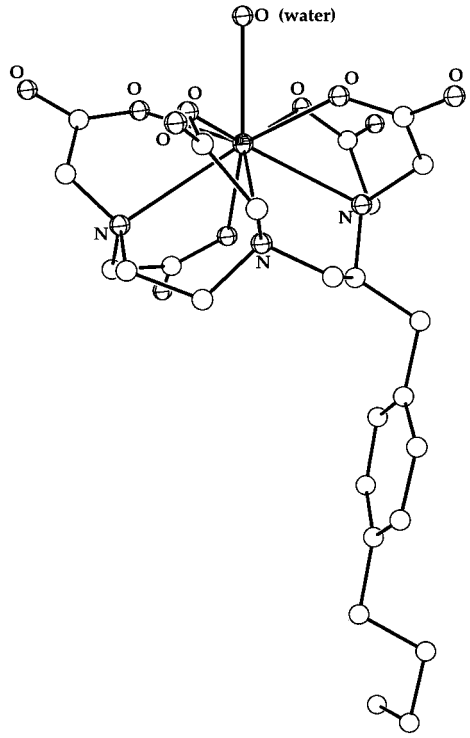

Figure 4. ORTEP drawing of MS-264: one of two independent molecules in the unit cell (ref 27).

oxygens forming a plane that is parallel to the N_3O basal plane. The out of plane carboxylate oxygen was slightly displaced toward the basal plane. The capping position was occupied by a water molecule. The twist angle between the basal and capped planes was ca. 43°. The Gd−N distance to the central nitrogen (2.80 Å) is long relative to those found in Gd(III) complexes of DTPA (2.62 Å average) and likely results from steric constraints of the ligand.

Structures of DTPA derivatives, in which substituents were attached to the acetate arms or diethylenetriamine backbone of the ligand, are known for MS-264 (Gd(III) complex, Na^+ salt)[27] and BOPTA (Gd(III)[28] and Eu(III)[29] complexes, Na^+ salt) (Chart 2). In all four cases the ligand coordinated in the same manner as DTPA, with TTP geometries about the metal centers. As expected for bulky substituents on five-membered rings, these substituents were equatorially positioned from their chelate ring and always directed away from the metal ion. The X-ray crystal structures of the Gd(III) complexes of MS-264 and BOPTA are shown in Figures 4 and 5.

A crystal structure of the Eu(III) complex (Figure 6) of DTPA-cs124 (Chart 3) was reported by Selvin et al.[30] The Eu(III) ion was nine-coordinate with binding sites occupied by three amine nitrogens, four monodentate carboxylate oxygens, and two monodentate amide oxygens. The complex crystallized as an amide bridged dimer in which the ring amide filled a capping position in a distorted TTP arrangement. Interestingly, the Eu−O (bridging amide) distance (2.30 Å) was shorter than the Eu−O (carboxylate) distances. The nonbridging amide distance (Table 2) was 0.2 Å longer.

Several structures of DTPA-bisamide complexes [Dy(DTPA-BMA)(H_2O)],[31] [Gd(DTPA-BEA)(H_2O)],[32]

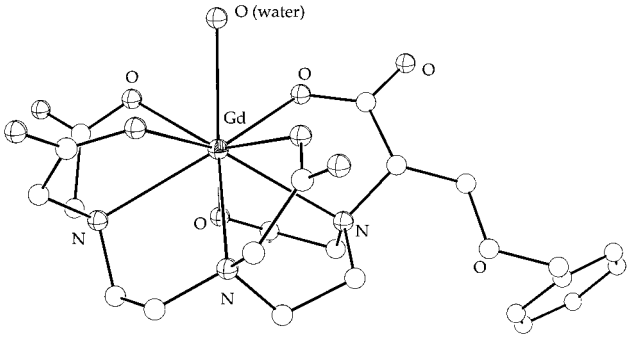

Figure 5. ORTEP drawing of $[Gd(BOPTA)(H_2O)]^{2-}$ (ref 28).

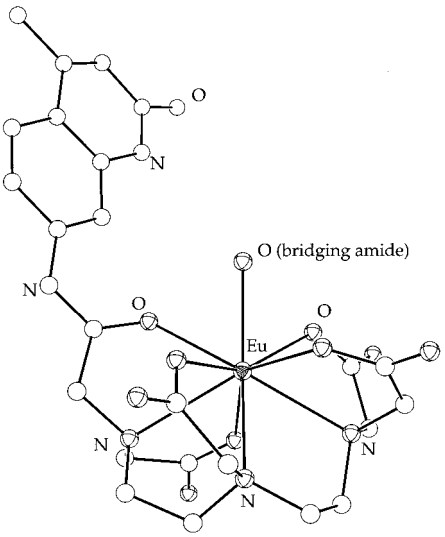

Figure 6. ORTEP drawing of [Eu(DTPA-cs124)]. The capping position is filled by a bridging amide (ref 30).

$[Gd(DTPA\text{-}BBA)(H_2O)]$,[33,34] $[Lu(DTPA\text{-}BBA)(H_2O)]$,[35] and $[Y(DTPA\text{-}BBA)(H_2O)]$[36] were reported (Chart 4). In all of these complexes, nonacoordinate metal ions were observed. The coordination sphere consisted of three nitrogen, three monodentate carboxylate oxygen, two monodentate amide oxygen, and one water oxygen atom donor. There are four possible configurations for placement of the amide groups (syn, cis, anti, and trans), which are illustrated in Figure 7. The Dy(III) complex of DTPA-BMA (Figure 8) and the Gd(III) complex of DTPA-BEA had trans configurations in the solid state. The DTPA-BBA complexes, see Figure 9 for the Gd(III) structure, all exhibited cis configurations. In each case, the geometry was distorted TTP. For $[Dy(DTPA\text{-}BMA)(H_2O)]$, $[Lu(DTPA\text{-}BBA)(H_2O)]$, and $[Y(DTPA\text{-}BBA)(H_2O)]$, the M−O (amide) distances are comparable to those found for M−O (carboxylate), while in the gadolinium complexes $[Gd(DTPA\text{-}BEA)(H_2O)]$ and $[Gd(DTPA\text{-}BBA)(H_2O)]$ the M−O (amide) distances were longer, approaching the M−O (water) distance (Table 2).

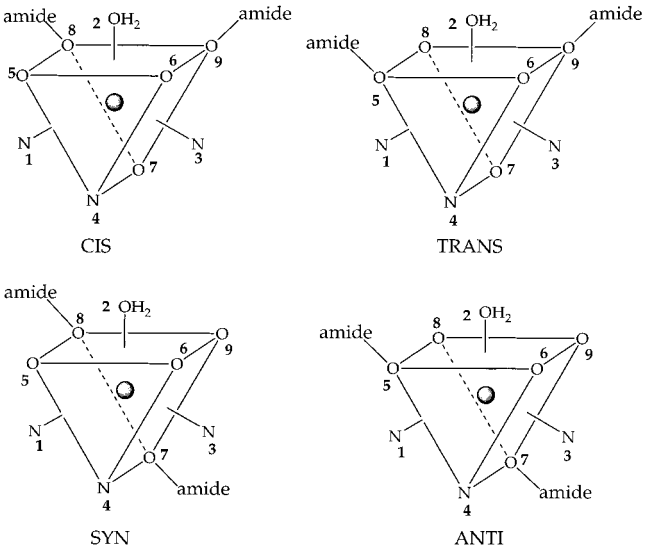

Figure 7. Four possible conformations (cis, trans, syn, and anti) of DTPA-bisamides in a TTP arrangement.

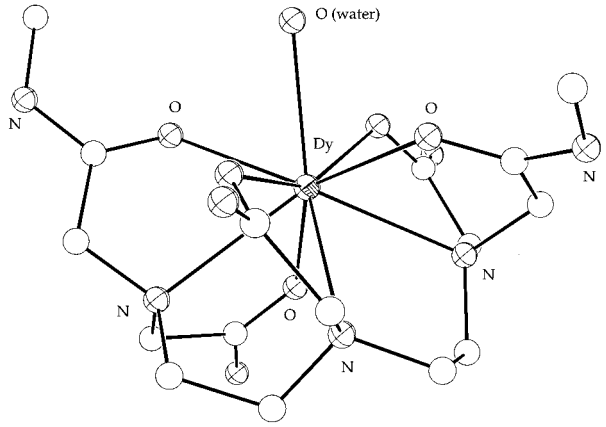

Figure 8. ORTEP drawing of $[Dy(DTPA\text{-}BMA)(H_2O)]$ with the amides in a trans configuration (ref 31).

The isostructural La(III),[37] Y(III),[37] and Gd(III)[38] complexes of 15-DTPA-EAM (Chart 5) crystallized as binuclear centrosymmetric structures with two Ln(III) ions located between two ligand molecules. The Ln(III) ions (CN9) were coordinated to an amide oxygen, two carboxylate oxygens, and two amine nitrogen atom donors from one ligand and an amide oxygen, a carboxylate oxygen, and an amine nitrogen atom donor from the second ligand. The coordination sphere was completed by a water molecule. When the ring is expanded, as with 16-DTPA-PAM,[38] 16-DTPA-HPAM,[39] or 17-DTPA-BAM,[40] the ligand is then able to wrap around the metal center, which resulted in mononuclear structures for the Gd(III) complexes (Chart 5). In the 16-DTPA-PAM (Figure 10), 16-DTPA-HPAM, and 17-DTPA-BAM complexes, the Gd(III) ions were each nine-coordinate, bonded to two amide oxygens, three carboxylate oxygens, three

Chart 3

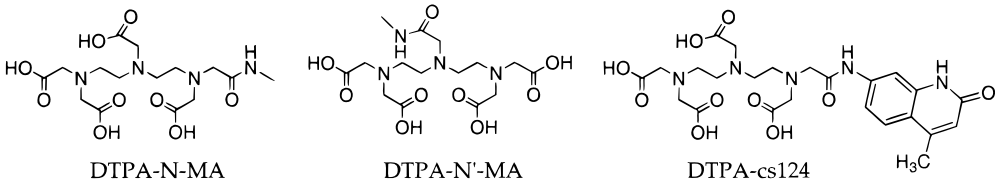

Chart 4

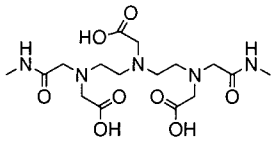

DTPA-BMA

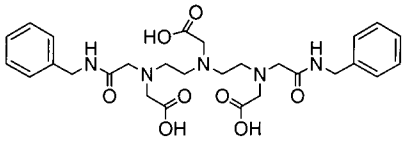

DTPA-BBA

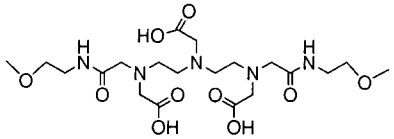

DTPA-BMEA

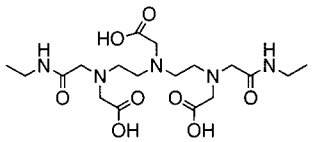

DTPA-BEA

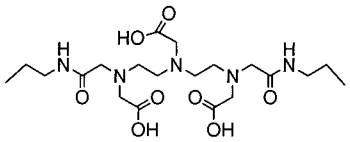

DTPA-B^{n}PA

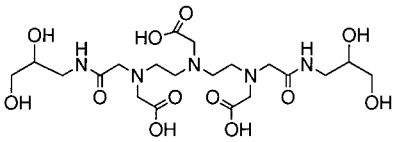

DTPA-BPDA

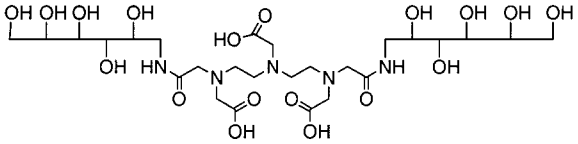

DTPA-BGLUCA

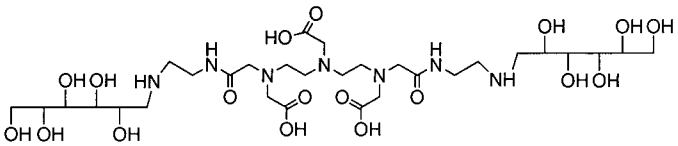

DTPA-BENGALAA

Chart 5

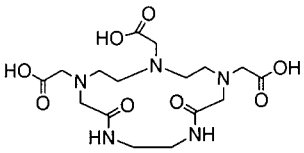

15-DTPA-EAM

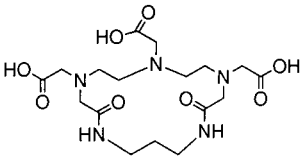

16-DTPA-PAM

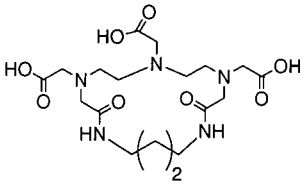

17-DTPA-BAM

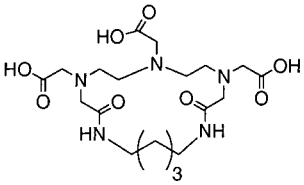

18-DTPA-PenAM

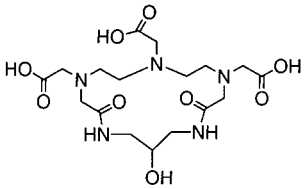

16-DTPA-HPAM

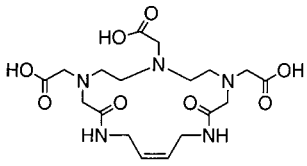

17-DTPA-cisC=CBAM

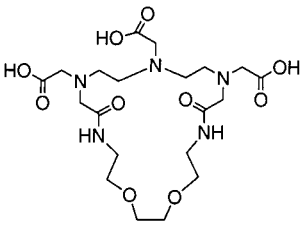

21-DTPA-OAM

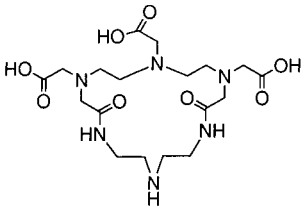

18-DTPA-dien

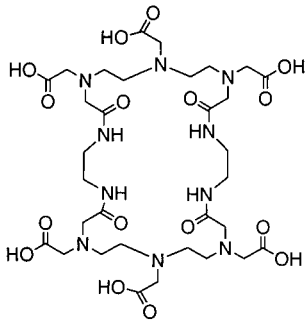

30-DTPA-en-DTPA-en

amine nitrogens, and a single water molecule. In each structure, the geometry around the metal center was distorted TTP with the amides sitting in a syn configuration. The La(III) complex of 18-DTPA-dien (Chart 5) crystallized as an M_2L_2 dimer in which the metal centers are symmetry related.[41] Each La(III) was eleven-coordinate. Three amine nitrogens, two amide oxygens, three carboxylate oxygens, a bridging bidentate carboxylate, and a water molecule filled the coordination sphere. The Eu(III) complex of 18-DTPA-dien crystallized as a M_4L_4 tetramer[41] in which each metal ion was nine-coordinate. Each 18-DTPA-dien provided eight donor atoms to one metal ion and a bridging carboxylate donor to an adjacent Eu(III). The geometry about each metal ion was distorted TTP with the amide oxygen atoms sitting in a syn configuration. The difference in the solid state structures among the cyclic DTPA-bisamides can be ascribed to steric factors. These steric constraints prevent the formation of anti or trans configurations for the amide oxygen donors.

Several structural features are consistent among the lanthanide complexes in which the backbone of the ligand is diethylenetriamine, as with DTPA,

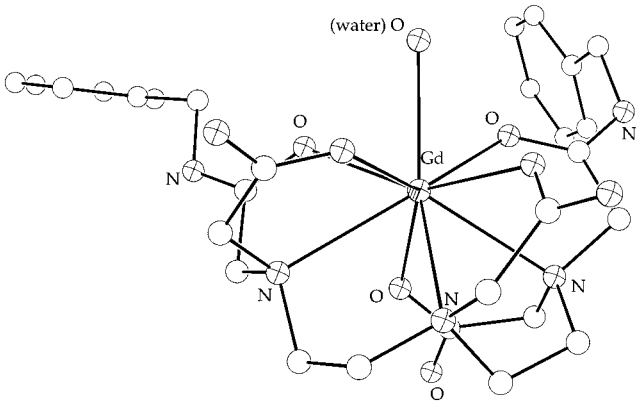

Figure 9. ORTEP drawing of [Gd(DTPA-BBA)(H_2O)] with the amides in a cis configuration (ref 33).

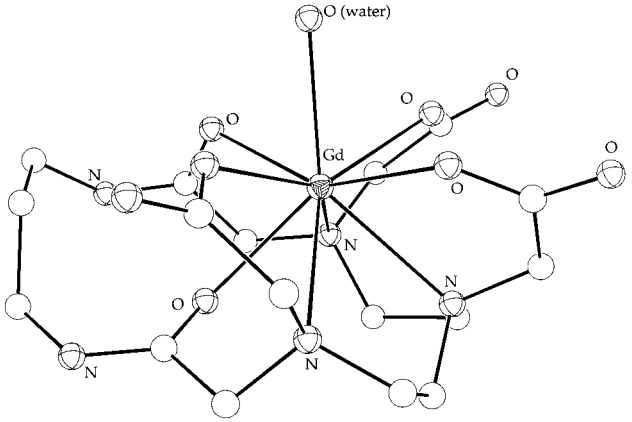

Figure 10. ORTEP drawing of [Gd(16-DTPA-PAM)(H_2O)] with the amides in a syn configuration (ref 38).

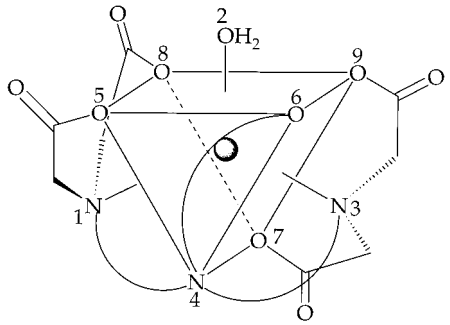

Figure 11. General coordination scheme for complexes of DTPA and DTPA derivatives (one of two wrapping isomers). The terminal backbone nitrogens differ in the position of their pendant acetate/amide groups.

BOPTA, MS-264, DTPA-bisamides (cyclic and linear), and DTPA-cs124. In general, the Ln(III) complexes of these ligands assume distorted TTP geometries. In the TTP arrangement, the neutral donor atoms with longer bond lengths will prefer to occupy a face capping position (positions 1, 2, and 3 in Figure 1) rather than a prismatic corner. However, since it is not possible for all three nitrogens to occupy face capping positions, the central nitrogen of the diethylenetriamine backbone always occupies a prismatic corner, while the terminal backbone nitrogens occupy capping positions (Figure 11). Generally, the shortest Ln(III)−N bond distance belongs to the central backbone nitrogen. The two terminal Ln(III)−N bond distances differ from each other by as much as 9%

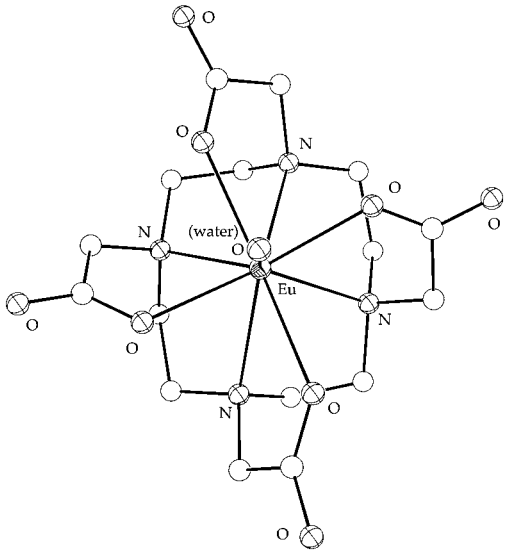

Figure 12. ORTEP drawing of [Eu(DOTA)(H_2O)]$^-$ (CSAP isomer) as viewed looking down the metal−water bond (ref 42).

and exhibit a consistent pattern.[29] The terminal nitrogens are distinguished by the positions of their pendant acetate/amide groups. As shown in Figure 11, at one terminal nitrogen both acetate/amide groups reside at prismatic corners in the (5,6,8,9) plane, while for the other terminal nitrogen one group occupies a prismatic corner in the (5,6,8,9) plane and the other completes the coordination of the basal plane (position 7). The terminal nitrogen associated with the longer Ln(III)−N distance has pendant acetate/amide groups which span the (7,9) edge. The reasons for this bond lengthening are unclear; however, it is worth noting that the trigonal prisms in these structures are very irregular. The (5,8), (6,9), and (4,7) edges tend to be longer than those edges at the triangular faces. The difference in the length of the two edges of interest, (5,8) and (7,9), can be as great as 0.5 Å (for Mn[Gd(DTPA)-(H_2O)] (5,8) = 3.5 Å, (7,9) = 3.0 Å). Dihedral angles for selected complexes are provided in Table 3. Metal−donor atom bond distances are provided in Table 2.

X-ray structures of the Eu(III),[42] Gd(III),[43,44] Y(III),[44] Lu(III),[45] and La(III)[46] complexes of DOTA (Chart 6) showed that the ligand coordinated in an octadentate fashion. Crystals of the Eu(III), Gd(III), Lu(III), and Y(III) complexes were isomorphous; the Eu(III) X-ray structure is shown in Figure 12. These complexes were arranged in a CSAP geometry where the basal plane was occupied by four amine nitrogens, the capped plane was occupied by four carboxylate oxygens, and the capping position was occupied by a water molecule. The twist angle between the basal and capped planes was approximately 39° for these complexes. The La(III) complex crystallized as a helical chain of carboxylate bridged complexes. The asymmetric unit contained two lanthanide chelates in a nine-coordinate monocapped arrangement with capping positions occupied by the bridging carboxylates. In the La(III) complex the twist angle between the basal and capped planes was approximately 22°, halfway between a prismatic (0°) and an antipris-

Table 4. Selected Bond Distances (Å) and Twist Angles (deg) for Ln(III) Complexes of DOTA and Related Macrocycles

complex	Ln−O_{water}	Ln−$O_{carboxylate}$[a]	Ln−N_{amine}[a]	Ln−O	twist angle	ref
Na[Eu(DOTA)(H_2O)]	2.480	2.247−2.511	2.519−2.900		38.9	42
Na[Gd(DOTA)(H_2O)]	2.458	2.362−2.370	2.648−2.679		38.7	43
Na[Y(DOTA)(H_2O)]	2.435	2.316−2.327	2.633−2.666		39.2	44
Na[Lu(DOTA)(H_2O)]	2.416	2.269−2.282	2.597−2.640		39.7	45
{Na[La(DOTA)]}$_n$		2.750−2.806	2.478−2.510		22[c]	46
[Gd(HP-DO3A)(H_2O)]	2.50[c]	2.31−2.38	2.64−2.65	2.33[c,d]	26.0, 37.9	47
[Y(HP-DO3A)(H_2O)]	2.49[c]	2.27−2.35	2.58−2.63	2.36[c,d]	28.1, 37.9	47
[Gd_2(DO3A−butrol)$_2$]		2.342−2.427	2.648−2.741	2.405[d]	27.9	48
H_5[Eu(TCE−DOTA)(H_2O)]	2.445	2.38[i]	2.68[i]		38.4	50
[Gd(DO3A−L2)(H_2O)]	2.429	2.337−2.360	2.627−2.719	2.392[h]	39.1	49
[Gd_2(DO3MA)$_2$(H_2O)$_2$]	2.420, 2.526	2.311−2.392[j]	2.66[k], 2.58[l]		29.7, 38	51
Na_2[{Gd(DO3A)}$_3$(CO_3)]		2.34−2.35[b]	2.61[k], 2.57[l]	2.46[b,e]	38.1[b]	44
[Gd(ODOTRA)(H_2O)]$_n$	2.559	2.327−2.357	2.644−2.674	2.574[f]	30.8	55
[Y(DOTBzP)]$^-$			2.64−2.67	2.20−2.31[g,a]	29.0	52
[Eu(DOTBzP)]$^-$			2.65−2.72	2.30−2.35[g,a]	29.5	53
[Yb(DOTBzP)]$^-$			2.62−2.64	2.22−2.29[g,a]	30.5	53
[La(DOTBzP)(H_2O)]$^-$	2.66		2.69−2.84	2.41−2.50[g,a]	28.8	53

[a] Range of distances. [b] Average of three independent molecules. [c] Average of two independent molecules. [d] M−O (hydroxyalkyl). [e] M−O (carbonate). [f] M−O (ether). [g] M−O (phosphinate). [h] M−O (amide). [i] Average bond distance in molecule. [j] Nonbridging carboxylates. [k] Average M−N distance to tertiary nitrogens. [l] Average M−N distance to secondary nitrogens.

Chart 6

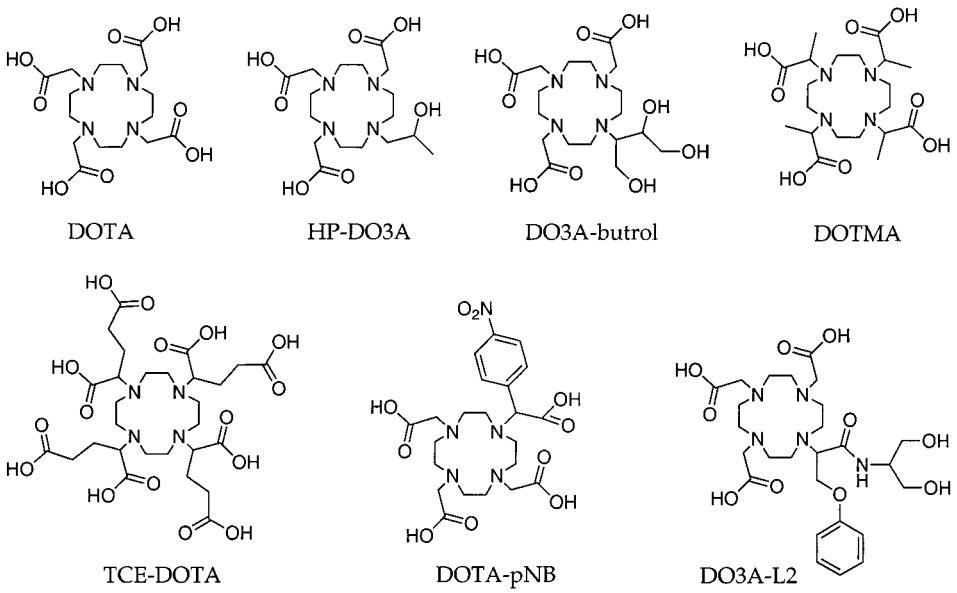

matic (45°) arrangement. This geometry is described as twisted CSAP (also referred to as inverted CSAP). In all five structures the four amine nitrogens were coplanar as were the four carboxylate oxygens in the capped plane.

Neutral Gd(III) complexes of ligands in which one of the acetate arms of DOTA is replaced by a hydroxyalkyl group are approved for use under the brand names ProHance and Gadovist. Crystal structures for both the Gd(III) and Y(III) complexes of HP-DO3A[47] and the Gd(III) complex of DO3A-butrol[48] were reported (Chart 6). In all three structures the metal ion (CN9) was coordinated by four nitrogens, three monodentate carboxylate oxygens, and one hydroxyalkyl oxygen. A water molecule in the capping position completed the coordination sphere in the isostructural HP-DO3A complexes of Gd(III) and Y(III). The unit cell was comprised of two independent molecules with diastereomeric conformations (Figures 13 and 14). The twist angle between the basal and capped planes was ca. 38° in one molecule and ca. 26° in the other. Thus both CSAP (Figure 13) and twisted CSAP (Figure 14) geometries were present in the crystal. The Gd(III) complex of DO3A-butrol crystallized as a carboxylate bridged dimer, with a single unique metal ion in the asymmetric unit. The twist angle between the basal and capped planes was ca. 28° (twisted CSAP geometry). In all three structures, the M−O (hydroxyalkyl) distances were comparable to the M−O (carboxylate) distances (Table 4).

The neutral Gd(III) complex of DO3A-L2 (Chart 6) in which one of the acetate arms of DOTA is replaced by an amide group was reported by Aime et al.[49] The Gd(III) ion was nine-coordinate with bonding to four amine nitrogens, three monodentate carboxylates, one monodentate amide oxygen, and one water molecule. The twist angle between the basal and capped planes was 39.1°, resulting in CSAP geometry (Figure 16). The M−O (amide) distance was compa-

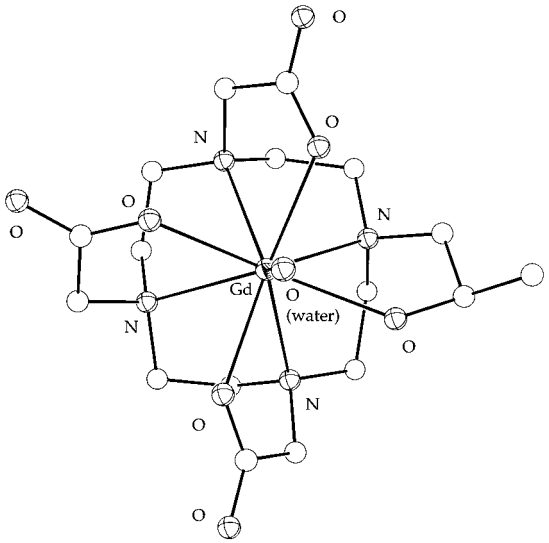

Figure 13. ORTEP drawing of the CSAP diastereomer of [Gd(HP-DO3A)(H_2O)] as viewed looking down the metal−water bond (ref 47).

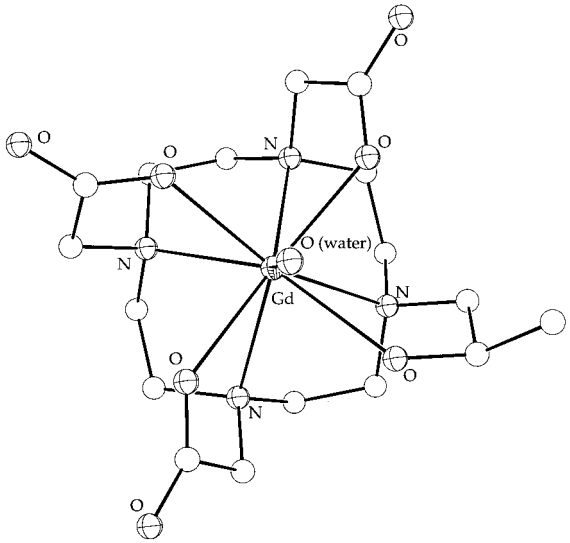

Figure 14. ORTEP drawing of the twisted CSAP diastereomer of [Gd(HP-DO3A)(H_2O)] as viewed looking down the metal−water bond (ref 47).

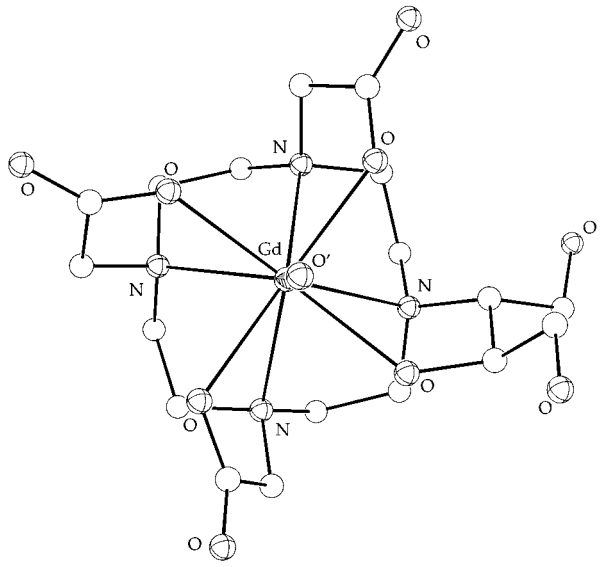

Figure 15. ORTEP drawing of [Gd(DO3A-butrol)] (twisted CSAP isomer). The capping position (O′) is occupied by a bridging carboxylate oxygen (ref 48).

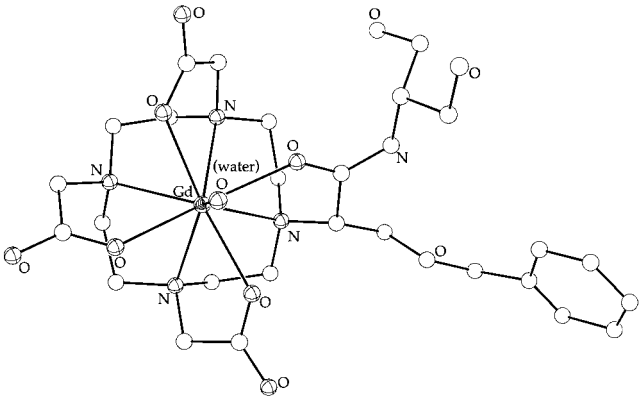

Figure 16. ORTEP drawing of [Gd(DO3A-L2)(H_2O)] (CSAP isomer) as viewed looking down the metal−water bond (ref 49).

rable to the M−O (carboxylate) distances and significantly shorter than the M−O (water) distance (Table 4).

Howard et al. reported the crystal structure for the Eu(III) complex of TCE-DOTA (Chart 6).[50] The ligand was synthesized as a mixture of stereoisomers defined by the absolute configuration at the chiral carbon. Two enantiomers, the (*RRRR*) and (*SSSS*) complexes, with opposite helicities crystallized together. The Eu(III) ion (CN9) was coordinated to four amine nitrogen atoms, four carboxylate oxygen atoms, and a water molecule. The twist angle between the basal and capped planes was 38.4° (CSAP). The X-ray structure for the complex is shown in Figure 17.

Crystal structures of the Gd(III) complexes of DO3A and DO3MA (Chart 7) were reported.[44,51] In both structures, the Gd(III) ions were nine-coordinate with the ligands binding in a heptadentate fashion. The DO3A complex crystallized as a carbonate bridged trimer with three crystallographically independent complexes sharing the same conformation and chirality (Figure 20). The eighth and ninth coordination sites for all three complexes in the trimer were filled by a single carbonate ion. The twist angle between the basal and capped planes was 39° (CSAP). When the ligand is DO3MA, two crystallographically independent complexes formed a dimer, Figures 18 and 19. The remaining two coordination sites in one of the metal centers were occupied by water molecules. The remaining two coordination sites of the second metal center in the dimer were filled by a bidentate carboxylate group which bridged from the first complex. The two complexes have diastereomeric conformations with a twist angle between the basal and capped planes of 38° around one metal center and 29.7° around the other, so that both CSAP and twisted CSAP geometries were present in the structure. In both crystal structures, the four amine nitrogens in each complex were coplanar as were the four oxygens that defined the capped face. The Gd(III)−N distances to the secondary nitrogens were shorter than those to the tertiary nitrogens by ca. 0.1 Å.

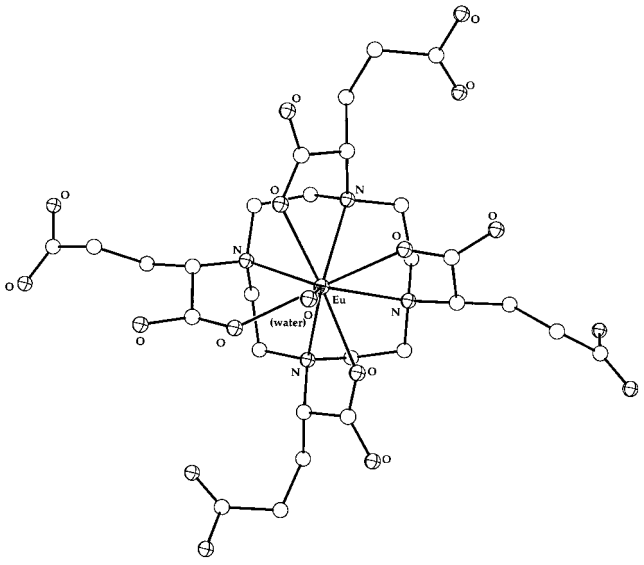

Figure 17. ORTEP drawing of $[Eu(TCE\text{-}DOTA)(H_2O)]^{5-}$ (CSAP isomer) as viewed looking down the metal−water bond (ref 50).

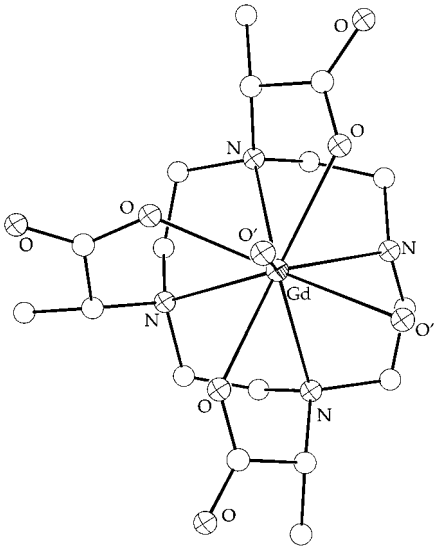

Figure 18. ORTEP drawing of the CSAP diastereomer contained in the dimer $[Gd_2(DO3MA)_2(H_2O)_2]$. Two water molecules (O′) occupy prismatic and capping positions around the metal center (ref 51).

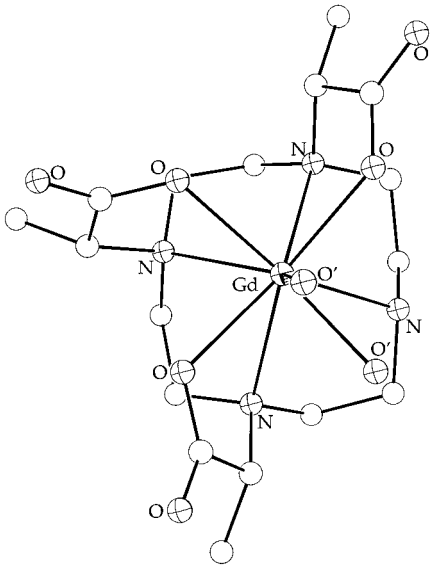

Figure 19. ORTEP drawing of the twisted CSAP diastereomer contained in the dimer $[Gd_2(DO3MA)_2(H_2O)_2]$. Two bridging carboxylates (O′) occupy prismatic and capping positions around the metal center (ref 51).

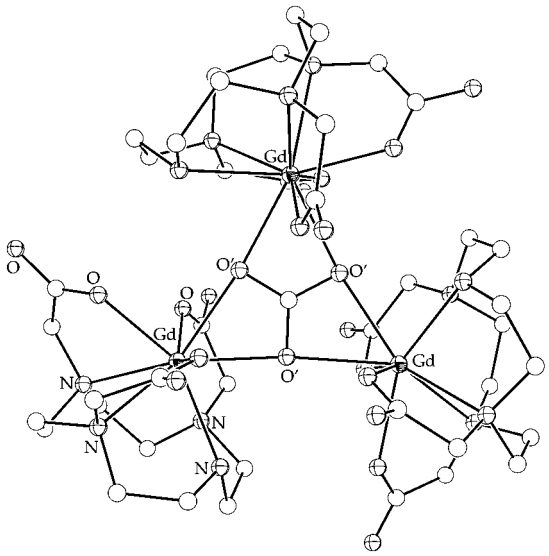

Figure 20. ORTEP drawing of the trimer $\{[Gd(DO3A)]_3[CO_3]\}^{2-}$. Carbonate oxygens (O′) occupy prismatic and capping positions around each metal center (ref 44).

The structures of the Y(III), La(III), Eu(III), and Yb(III) complexes of DOTBzP (Chart 8) were reported.[52,53] The eight-coordinate Y(III), Eu(III), and Yb(III) complexes crystallized without a water molecule in the inner coordination sphere. The X-ray crystal structure for the Y(III) complex is shown in Figure 21. The four amine nitrogens were coplanar, as were the four donor phosphinate oxygens. The twist angle between the nitrogen and oxygen planes was ca. 29°, resulting in twisted square antiprismatic geometries. In contrast, the La(III) complex was nine-coordinate with a water molecule capping the phosphinate oxygen face of the molecule. The four amine nitrogens in this complex were slightly folded at 6.5°. The twist angle between the N_4 and O_4 planes was also ca. 29° (twisted CSAP).

Chart 7

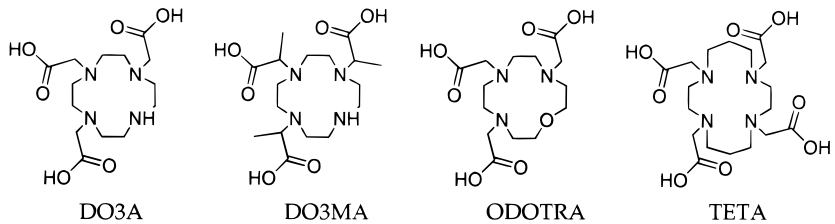

Chart 8

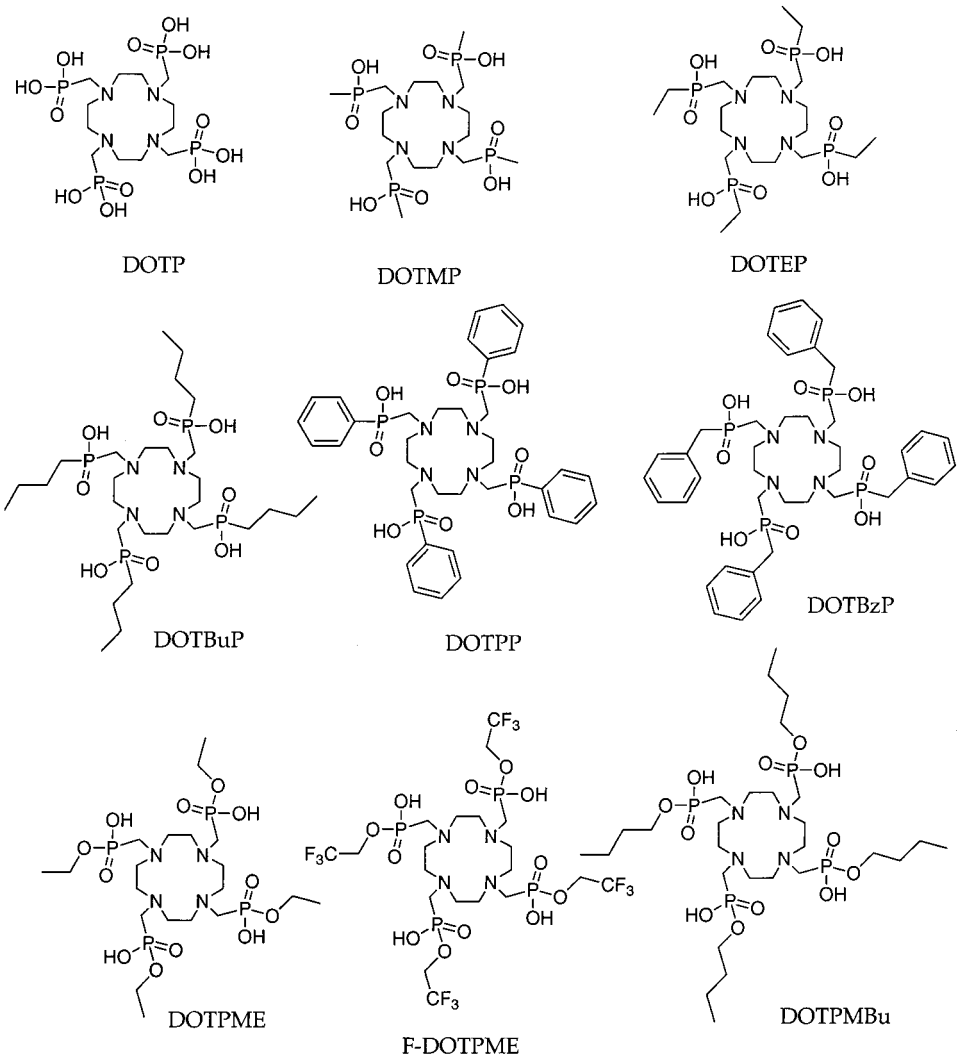

Several structural features are common to the Ln(III) complexes of ligands derived from tetraazacyclododecane. In these structures the macrocycle adopts a square [3333] conformation,[54] forming the basal plane in a square antiprismatic arrangement of donor atoms (see Figure 1). In the examples provided here, the opposite face of the prism is occupied by a planar arrangement of oxygen donors (carboxylate, water, hydroxyalkyl, amide, or phosphinate). As expected for square antiprismatic arrangements, the N_4 plane and the O_4 plane are parallel to each other. The metal ions typically do not occupy the center of the polyhedron, but are shifted toward the O_4 face. This was also observed for the Tb(III) complex of the cyclam-derived ligand TETA and presumably results from differences in donor atom affinity rather than differences in donor atom radii or ligand constraints. One defining feature in these cyclen-derived complexes is the twist angle between the N_4 and O_4 planes. Two angles are possible depending upon the quadrangular conformation of the tetraazacyclododecane ring and the helicity of the complex (see Figures 29 and 31). As a result, two diastereomeric conformations, CSAP and twisted CSAP, are found among the solid state structures. Important bond distances are provided in Table 4.

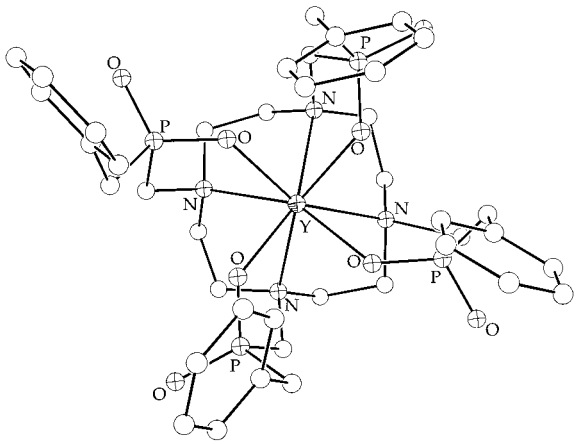

Figure 21. ORTEP drawing of $[Y(DOTBzP)]^-$ (twisted CSAP) as viewed looking down the metal−water bond (ref 52).

Spirlet et al. reported the crystal structure for the Gd(III) complex of ODOTRA (Chart 7).[55] The complex contained a nonacoordinate Gd(III) ion coordinated to three amine nitrogens, one ether oxygen, four carboxylate oxygens, and a water molecule in the capping position (Figure 22). The complex crystallized as an infinite chain with bridging η^1 carboxylate groups shared between adjacent chelates. The three

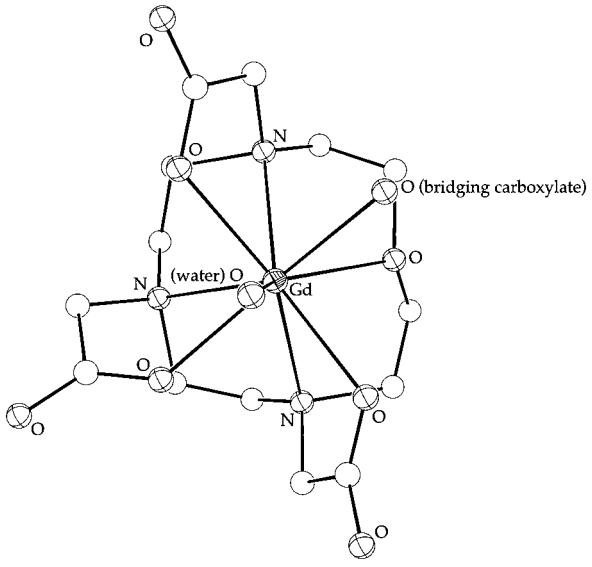

Figure 22. ORTEP drawing of [Gd(ODOTRA)(H_2O)] as viewed looking down the metal−water bond. A prismatic corner is occupied by a bridging carboxylate (ref 55).

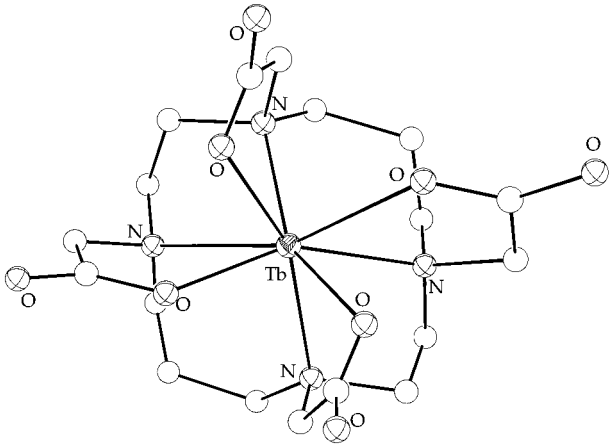

Figure 23. ORTEP drawing of $[Tb(TETA)]^-$ (ref 56).

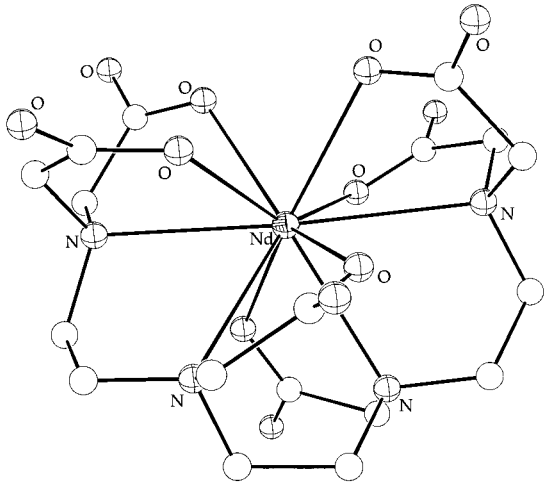

Figure 24. ORTEP drawing of $[Nd(TTHA)]^{3-}$ (ref 62).

amine nitrogens and one ether oxygen were coplanar, forming the basal plane of the prism. The four carboxylates forming the monocapped plane were also coplanar. The twist angle between the faces averaged 30.7° (twisted CSAP).

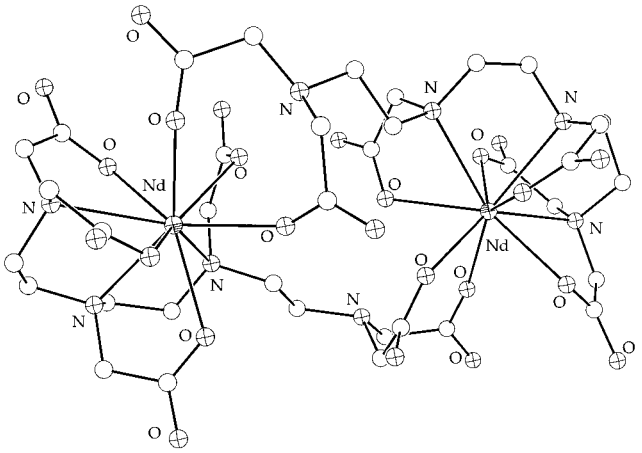

Figure 25. ORTEP drawing of the dimer $[Nd_2(HTTHA)_2]^{4-}$ (ref 60).

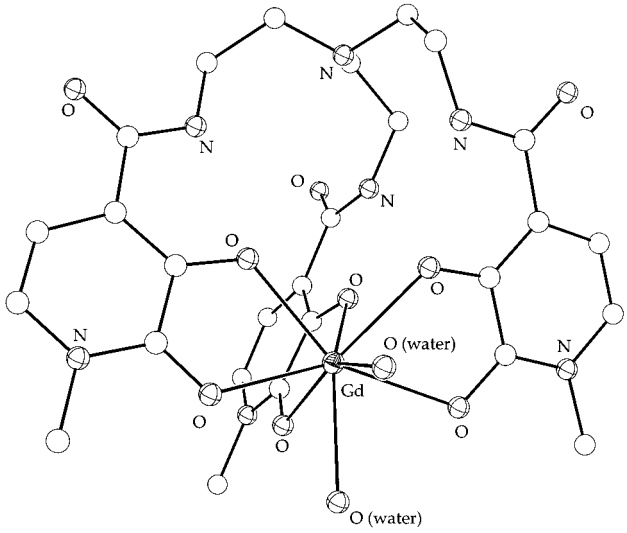

Figure 26. ORTEP drawing of [Gd(HOPO)(H_2O)$_2$] (ref 64).

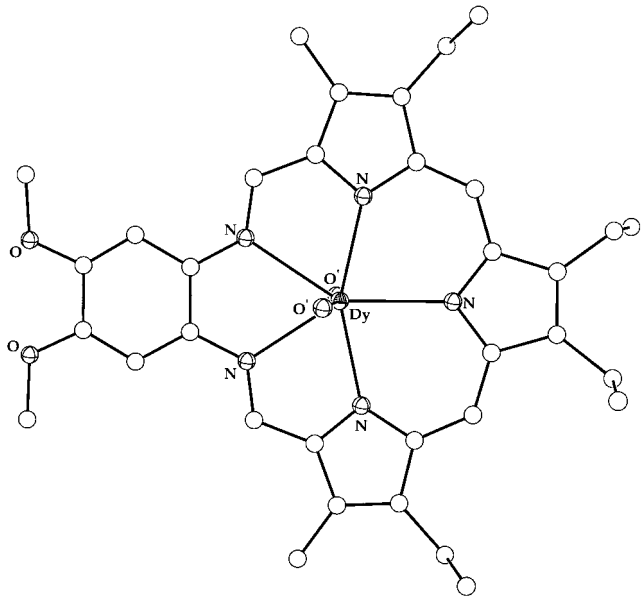

Figure 27. ORTEP drawing of $[Dy((C_6H_5)_2PO_4)_2]$. Two diphenyl phosphate oxygens (O′) occupy axial coordination sites in the complex (ref 66).

The Tb(III) structure of TETA (Chart 7) was reported by Spirlet et al.[56] The Tb(III) ion, which was completely encapsulated by the ligand, was eight-

Chart 9

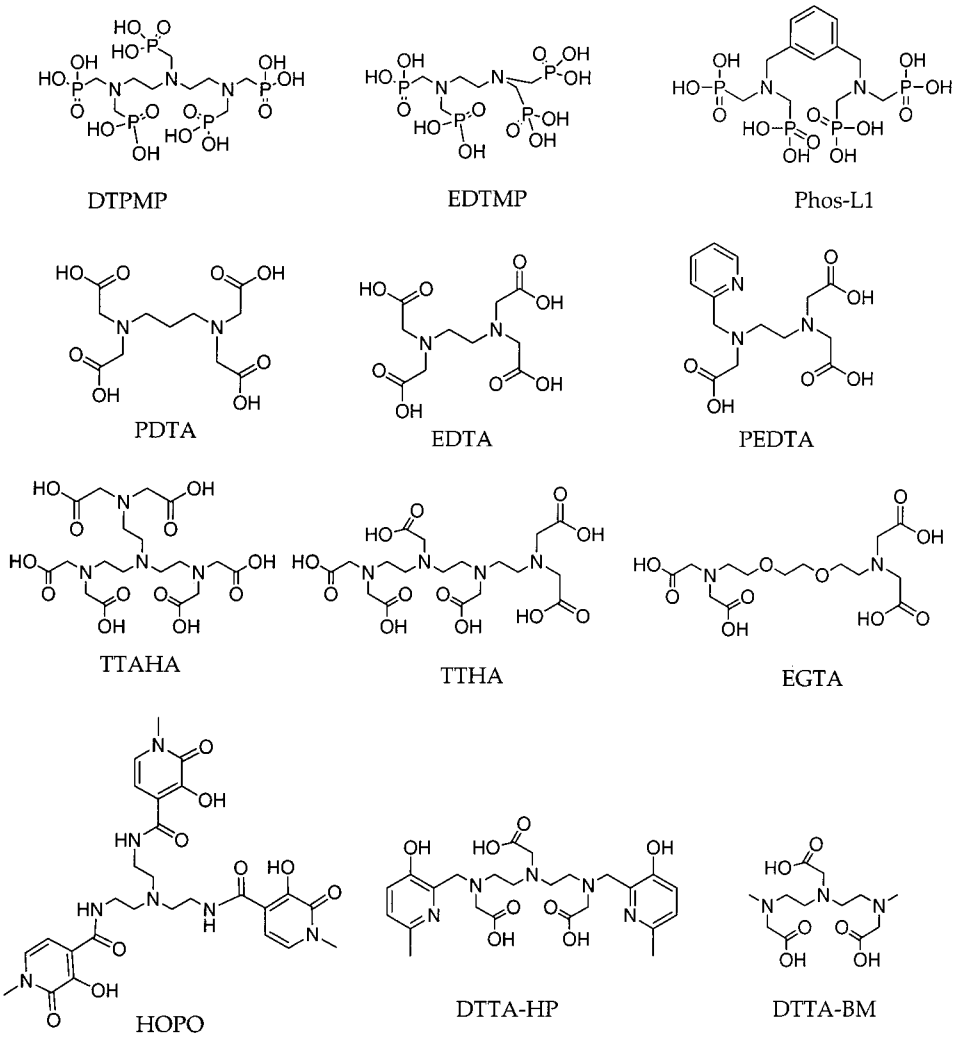

coordinate with bonds to four amine nitrogens and four carboxylate oxygens. Unlike the related DOTA complexes, the Tb(III) complex of TETA did not have a water molecule in the inner coordination sphere. The geometry about the metal center in the TETA complex approximates a dodecahedron, Figure 23. As expected for such a geometry, a large deviation from planarity in the four nitrogens was observed. Two nitrogens were displaced from the mean plane by 0.28 Å toward the carboxylate oxygens, and two nitrogens are displaced 0.28 Å away from the carboxylate oxygens. The same pattern was observed for the oxygen donor atoms. The metal−donor atom bond distances form pairs of longer (Tb−N = 2.620 and 2.606 Å, Tb−O = 2.322 and 2.330 Å) and shorter (Tb−N = 2.575 and 2.595 Å, Tb−O = 2.302 and 2.304 Å) bonds depending upon their position in the dodecahedron.

Crystal structures of the TTHA (Chart 9) complexes of La(III),[57,58] Dy(III),[57] Gd(III),[59] Nd(III),[60] and Yb(III)[61] were recently reported. The smaller lanthanides, Dy(III), Gd(III), and Yb(III), formed nine-coordinate complexes with coordination to four amine nitrogens and five carboxylate oxygens in a distorted CSAP arrangement. The larger lanthanides, La(III) and Nd(III), formed ten-coordinate complexes involving bonding to all four amine nitrogens and all six carboxylate oxygens of TTHA, Figure 24. The ten-coordinate complexes assumed a distorted bicapped square antiprismatic geometry. In addition to their mononuclear structures, dimeric structures were observed for Nd(III),[62] Figure 25, and Gd(III)[63] complexes as well. In both dimers the metal centers were nine-coordinate with bonding to three amine nitrogens and four carboxylate oxygens from one TTHA ligand. Two free carboxylate oxygens from a ligand molecule in a neighboring complex completed the coordination sphere. Important bond distances are provided in Table 5.

The crystal structure of the Gd(III) complex of TREN-Me-3,2-HOPO (Chart 9) was reported by Xu et al.[64] The structure featured an eight-coordinate Gd(III) center coordinated to six hydroxypyridinone oxygens and two water molecules, Figure 26. The coordination geometry about the metal ion was described as a slightly distorted bicapped trigonal prism in which one water molecule occupied a prismatic corner and the other occupied a capping position. One interesting feature of the structure was the close contact between the amide nitrogen atoms and the coordinated hydroxyl oxygen atoms (2.65 and 2.73 Å), resulting from internal hydrogen bonds (N−H···O) within the complex. The Gd(III)−O (hydroxypyridinone) distances fell in the range of 2.34−2.43

Table 5. Selected Bond Distances (Å) for Ln(III) Complexes of TTHA

complex	Ln−$O_{carboxylate}$[a]	Ln−N_{amine}[a]	ref
Na_3[Nd(TTHA)]	2.430−2.537	2.724−2.823	62
$Na_{0.5}H_{5.5}$[Nd_2(TTHA)$_2$]	2.397−2.471	2.629−2.732	60
$(CN_3H_6)_2$[La(HTTHA)]	2.464−2.535 (2.801)[b]	2.757−2.875	57
K_2[La(HTTHA)]	2.469−2.555 (2.711)[b]	2.788−2.843	58
$(CN_3H_6)_2$[Dy(HTTHA)]	2.317−2.419	2.574−2.712	57
$(CN_3H_6)_2$[Gd(HTTHA)]	2.352−2.437	2.590−2.733	59
K_3[Yb(TTHA)]	2.264−2.365	2.568−2.721	61

[a] Range of observed distances. [b] One significantly longer bond distance is listed in parentheses.

Scheme 1

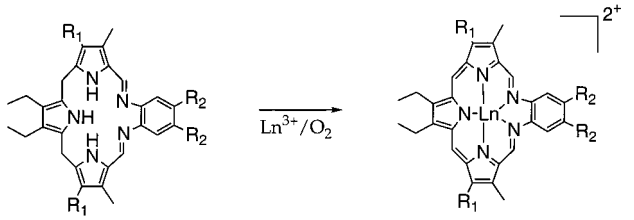

Tx_1 $R_1 = CH_2CH_3$, $R_2 = OCH_3$
Tx_2 $R_1 = CH_2CH_3$, $R_2 = OCH_2CH_2CH_2OH$
Tx_3 $R_1 = CH_2CH_2CH_2OH$, $R_2 = OCH_2CH_2CH_2OH$ (PCI-0101)
Tx_4 $R_1 = CH_2CH_2CH_2OH$, $R_2 = O(CH_2CH_2O)_3OCH_3$ (PCI-0120)

Å. The Gd(III)−O (water) distances were essentially equal at 2.44 Å.

A series of pyrrole-based ligands of the type shown in Scheme 1 were reported by Sessler and co-workers. The ligand formed 1:1 complexes with Ln(III) ions in the solid state. Oxidation and metalation of the texaphyrin in the presence of a Ln(III) cation yields $[Ln(Tx)]^{2+}$ in which the texaphyrin ring has lost a proton and acts as a monoanion. Structures for the La(III), Gd(III), and Dy(III) (Figure 27) complexes ($R_1 = CH_2CH_3$, $R_2 = OCH_3$), the Lu(III) complex ($R_1 = CH_2CH_3$, $R_2 = OCH_2CH_2CH_2OH$), and the Eu(III) and Gd(III) complexes ($R_1 = CH_2CH_2CH_2OH$, $R_2 = OCH_2CH_2CH_2OH$) were reported.[65,66,244] In the latter instance the crystals of the Eu(III) and Gd(III) complexes were isomorphous. In all of the structures the Ln(III) cations coordinated to all five ring nitrogens of the macrocycle and were axially ligated by counterions and solvent molecules. A buckling of the macrocycle framework was observed which increased with increasing size of the Ln(III) cation. Important bond distances are provided in Table 6.

A comprehensive review of lanthanide complexes of macrocyclic ligands was recently published by Alexander.[67] Lanthanide complexes of EGTA[68−70] as well as Eu(III)[71,72] and Gd(III)[73] complexes of DOTA tetraamides have also been reported.

B. Solution Methods

Contrast agents function in an aqueous environment. Solid state structures provide a wealth of information, but it is imperative to confirm the solution structure in order to to understand the biophysical properties of the molecule. Contrast agents are generally ternary complexes—Gd(III), a multidentate ligand, and one or more water ligands. Determination of the hydration number, q, of a gadolinium complex is crucial to understanding its contrast agent properties. One method to determine q is laser induced luminescence. Horrocks and Sudnick[74] showed that Tb(III) or Eu(III) fluorescence is better quenched in H_2O than in D_2O because of better coupling to the O−H oscillators than to the O−D oscillators. If the fluorescent lifetimes are measured in D_2O and H_2O, the ratio of the fluorescence decay constants in both solvents is proportional to q. Parker and co-workers have extended this approach by applying a correction which allows for the contributions of closely diffusing water molecules and of other proton exchangeable oscillators.[343] Since this method involves the use of Tb(III) or Eu(III), ions which flank Gd(III) in the periodic table and have similar radii, the result should be an excellent indication of the hydration number for the Gd(III) complex. A further benefit of this method is the scant amount (micromolar) of material required. Hydration numbers for selected complexes are provided in Table 7.[75−87]

Any difference in chemical or structural behavior among a series of Ln(III) complexes of a particular ligand can usually be ascribed to the decrease in ionic radius on going from La(III) (1.36 Å) to Lu(III) (1.17 Å).[88] With the gradual change in metal ion radii, it is not uncommon for a ligand to form isostructural chelates within the lanthanide series. The ability to confirm an isostructural relationship between Ln(III) chelates is particularly important since solution studies often involve the use of a surrogate lanthanide to probe the structure and dynamics of a complex.

In the presence of a paramagnetic lanthanide ion, NMR chemical shifts are much larger than in the presence of a diamagnetic ion. This is referred to as the lanthanide induced shift (LIS), $\Delta\omega$. The LIS can be parametrized into a contact, ($\Delta\omega_c$) and a pseudocontact ($\Delta\omega_p$) term, eq 1. The contact term can be

$$\Delta\omega = \Delta\omega_c + \Delta\omega_p \quad (1)$$

$$\Delta\omega = \langle S_Z\rangle F + C_D G \quad (2)$$

written as the product of an entity that is characteristic of the lanthanide ion, $\langle S_Z\rangle$, and one which is characteristic of the ligand in question, F, eq 2. Similarly the pseudocontact term has a lanthanide dependent, C_D, and ligand dependent, G, factor. Calculated values for $\langle S_Z\rangle$ and C_D have been reported.[15] Equation 2 can be rewritten as eqs 3 and 4. If the observed shifts are plotted as $\Delta\omega/\langle S_Z\rangle$ versus $C_D/\langle S_Z\rangle$ (or $\Delta\omega/C_D$ versus $\langle S_Z\rangle/C_D$), the data will fall on a straight line if the lanthanide complexes are isostructural. Any major structural differences in the

$$\left(\frac{\Delta\omega}{\langle S_Z\rangle}\right) = \left(\frac{C_D}{\langle S_Z\rangle}\right)G + F \quad (3)$$

$$\left(\frac{\Delta\omega}{C_D}\right) = \left(\frac{\langle S_Z\rangle}{C_D}\right)F + G \quad (4)$$

series are indicated by a break in the pattern.[15,89]

Table 6. Selected Bond Distances (Å) for Texaphyrin Ln(III) Complexes

complex	Ln−$N_{pyrrole}$[a]	Ln−N_{imine}	Ln−O_{anion}[b]	Ln−O_{MeOH}	ref
[La(III)(Tx_1)(NO_3)$_2$(MeOH)]	2.484−2.615	2.631, 2.685	2.68	2.72	65
[Gd(III)(Tx_1)(NO_3)$_2$(MeOH)]	2.401−2.517	2.564, 2.579	2.60	2.51	65
[Dy(III)(Tx)$_1$(Ph_2PO_4)$_2$]	2.317−2.437	2.438, 2.459	2.23		66
(NO_3)[Lu(III)(Tx_2)(NO_3)(MeOH)]	2.312−2.421	2.428, 2.455	2.37	2.27	65
(NO_3)[Gd(III)(Tx_3)(NO_3)(MeOH)$_2$]	2.383−2.494	2.517, 2.536	2.49	2.49	65
(NO_3)[Eu(III)(Tx_3)(NO_3)(MeOH)$_2$]	2.395−2.500	2.517, 2.538	2.50	2.49	65

[a] Range of observed distances. [b] Average.

Table 7. Hydration Numbers for Selected Eu(III), Tb(III), and Dy(III) Complexes

ligand	q	method	ref
DTPA	1.2 ± 0.5	Eu(III) luminescence	75
DTPA	1.3 ± 0.2	^{17}O Dy.I.S.	76
DTPA	1.2 ± 0.2	Eu(III) luminescence	77
DTPA	1.1	Tb(III) luminescence	78
DTPA	1.08 ± 0.11	Eu(III) luminescence	343
DTPA	1.10 ± 0.11	Tb(III) luminescence	343
BOPTA	1.2 ± 0.5	Eu(III) luminescence	79
DTPA-BPA	1.0 ± 0.2	^{17}O Dy.I.S.	80
DTPA-BPA	1.0 ± 0.2	Eu(III) luminescence	77
15-DTPA-en	1.2 ± 0.2	^{17}O Dy.I.S.	81
15-DTPA-en	2.3 ± 0.5	Eu(III) luminescence	82
30-DTPA-enDTPA-en	0.8 ± 0.2	^{17}O Dy.I.S.	81
30-DTPA-enDTPA-en	1.2 ± 0.5	Eu(III) luminescence	82
DOTA	1.0 ± 0.3	^{17}O LIS	83
DOTA	1.2 ± 0.4	Eu(III) luminescence	84
DOTA	1.2	Eu(III) luminescence	75
DOTA	1.0 ± 0.1	Tb(III) luminescence	85
DOTA	1.2 ± 0.5	Eu(III) luminescence	86
DOTA	0.9 ± 0.5	Tb(III) luminescence	86
DOTA	0.98 ± 0.10	Eu(III) luminescence	343
DOTA	1.05 ± 0.11	Tb(III) luminescence	343
TCE-DOTA	1.06 ± 0.11	Eu(III) luminescence	343
TCE-DOTA	0.60 ± 0.06	Tb(III) luminescence	343
HP-DO3A	1.3 ± 0.1	Tb(III) luminescence	85
DO3A	1.9 ± 0.5	Eu(III) luminescence	79
DO3A	1.8 ± 0.2	Tb(III) luminescence	85
DO3A	1.80 ± 0.18	Eu(III) luminescence	343
DOTP	0.4 ± 0.5	Eu(III) luminescence	79
F-DOPTME	0	^{17}O Dy.I.S.	87
DOTBzP	0	Eu(III) luminescence	343
DOTBzP	0	Tb(III) luminescence	343
DOTMP	0.01	Eu(III) luminescence	343
DOTMP	0.05	Tb(III) luminescence	343
DOTMP-MBBzA	0.58 ± 0.06	Eu(III) luminescence	343
DOTMP-MBBzA	0	Tb(III) luminescence	343
TETA	0.6	Eu(III) luminescence	75
TTHA	0.2	Tb(III) luminescence	78
TTHA	0.2 ± 0.2	^{17}O Dy.I.S.	76

When the chemical shift data for the Ln(III) complexes of DOTBzP were plotted according to eqs 3 and 4, the data fell into two classes: the larger lanthanides, Ce(III) to Nd(III), lay on one line and the smaller ions, Eu(III) to Yb(III) lay on another. This was ascribed to a change in the coordination number at the metal center.[53] Examination of the ^{17}O LIS of water is a ready means of confirming the constancy of a hydration number, q, across the lanthanide series. Geraldes, Peters, and co-workers used this method to show that the Ln(III) complexes of DTPA and DTPA-BPA are all $q = 1$.[80,90,91]

A simple application of using LIS is the method described by Alpoim et al.[76] to determine the number of bound water molecules in a Dy(III) complex. They have shown that the dysprosium induced shift (Dy.I.S.) of the ^{17}O NMR water resonance in Dy(III) chelates is proportional to q. The utility of this method is that natural abundance ^{17}O is measured, there is no need for isotopic enrichment, and the measurements take just minutes. The drawback is sensitivity; millimolar solutions are required.

The LIS effect has an r^{-3} dependence from which structural information about the chelate can be extracted, eq 5.[15] The values of ϕ, θ, and r can be computed directly from crystallographic structures.

$$G = C\left(\frac{3\cos^2\phi - 1}{r^3}\right) + C\left(\frac{\sin^2\theta\cos^2 2\phi}{r^3}\right) \quad (5)$$

Alternately, the internal coordinates of a geometrical model of the complex can be adjusted until the best agreement is reached between the experimental and the calculated NMR shifts. Ytterbium(III) is often selected as a paramagnetic center since this ion induces shifts that are essentially pseudocontact. This avoids the need to dissect the LIS into $\Delta\omega_c$ and $\Delta\omega_p$ contributions.

Paramagnetic lanthanide ions also increase the longitudinal and transverse relaxation rates of ligand nuclei, lanthanide induced relaxation (LIR). This relaxation enhancement has an r^{-6} dependence, making relaxation data useful for obtaining metal−nuclei distances. For example, Nd(III) induced ^{13}C relaxation rate enhancements were used to obtain structural information on DTPA and DTPA-bisamide chelates of Nd(III).[80,90] For paramagnetic lanthanides other than Gd(III), the correlation time which determines nuclear relaxation is the longitudinal electronic relaxation time, T_{1e}, and the dipolar contribution to T_1 for a ^{13}C nucleus is described by eq 6. Here,

$$\frac{1}{T_1} = \frac{4}{3}\left(\frac{\mu_0}{4\pi}\right)^2\left(\frac{\mu_{eff}^2\gamma_I^2\mu_B^2 T_{1e}}{r^6}\right) \quad (6)$$

μ_{eff} is the effective magnetic moment, μ_B is the Bohr magneton, γ_I is the nuclear magnetogyric ratio (^{13}C in this case), $\mu_0/4\pi$ is the magnetic permeability of a vacuum, and r is the electron spin−nuclear spin distance.

Common NMR structure elucidation experiments, e.g., COSY, 1D-NOE, NOESY, have been used to determine solution structures and to confirm their agreement with solid state X-ray crystallographic results for lanthanide complexes. Two-dimensional exchange spectroscopy (EXSY) has proven to be very valuable in the study of the dynamics of conformational equilibria and has been applied to a variety of highly stable lanthanide complexes.[41,92−96] With EXSY, chemical exchange is probed using a standard NOESY pulse sequence, where exchange effects are monitored rather than distance effects. Shukla has ex-

Table 8. Kinetic Data for Rearrangements in Ln(III) Complexes

complex	$\Delta G^{\ddagger}$ (kJ mol^{-1})	$\Delta H^{\ddagger}$ (kJ mol^{-1})	$\Delta S^{\ddagger}$ (J mol^{-1} K^{-1})	k_{ex} (s^{-1})	dynamic process[a]	ref
Pr(DTPA)	56.5(3.6)	35.2(2.0)	−71.4(5.8)	265 (278 K)	A	92
Eu(DTPA)	55.4(4.6)	38.5(2.4)	−56.8(7.0)	360 (278 K)	A	92
Yb(DTPA)	49.4(10)	37.0(5.0)	−41.7(16)	4300 (278 K)	A	92
Nd(DTPA-BPA)	53(1)			350 (283 K)	A	80
Eu(DTPA-dienH^{+})	57.5(0.3)					41
La(DTPA-BPA)	71(1)	47(8)	−84(25)	0.7 (283 K)	B	80
Lu(DTPA-BPA)	67(1)	42(8)	−88(20)	2.4 (283 K)	B	80
La(DTPA-BGLUCA)	66	34	−116	2.7 (283 K)	B	100
La(DTPA-BENGALAA)	65	37	−100	0.7 (283 K)	B	100
Lu(DOTA)	65.9(1.2)	100.5(0.6)	116(2)	18 (298 K)	C	45
Yb(DOTA)	65.9(1.0)	82(12)	52(39)		C	93
La(DOTA)	60.7(1.2)	59.4(0.8)	−4.6(3.3)	23 (278 K)	D	103
La(DOTP)	101(11)				D	105
Lu(TETA)	63.7(7.5)	71.7(5.3)	27(8)	7 (278 K)	E	114

[a] A: exchange between wrapping isomers. B: racemization of terminal backbone nitrogens. C: enantiomerization. D: ring inversion. E: exchange between dodecahedral conformations of TETA.

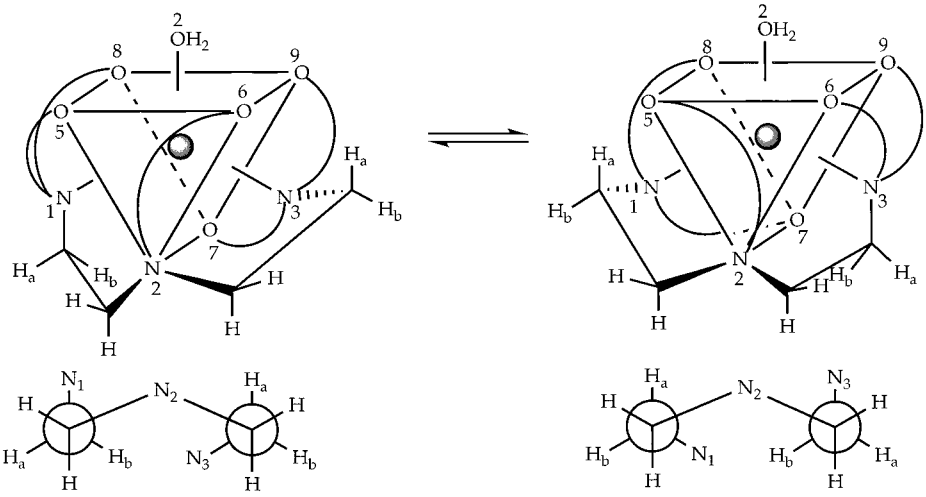

Figure 28. Rapid exchange interconversion between wrapping isomers of Ln(DTPA) results in a psuedo mirror plane, reducing the number of observed proton resonances by half.

ploited rotating-frame exchange spectroscopy (ROESY) to study the exchange dynamics of [Y(HP-DO3A)-(H_2O)].[97]

C. Solution Structures/Dynamics

1. DTPA

The ligation of Ln(III) ions by DTPA were deduced from 2D-EXSY spectroscopy (Pr(III), Eu(III), and Yb(III)) and LIR enhancements of the ^{13}C nuclei in the Nd(III) complex.[91,92] The solution structure was consistent with crystallographic results showing nonadentate coordination at the metal center involving three nitrogens and five monodentate carboxylate oxygens. Luminescence studies on the Eu(III) complex[77] and ^{17}O LIS data for a series of Ln(III) complexes[91] were consistent with a single coordinated water molecule as found in several crystal structures. At low temperatures, the proton NMR spectra for the Pr(III) and Eu(III) chelates exhibited 18 resonances corresponding to 18 nonexchangeable protons. These peaks shift and broaden with temperature until coalescing to nine resonances at 95 °C. At higher temperatures two chiral wrapping isomers exchange rapidly in solution, giving averaged signals for pairs of protons. Activation parameters for the exchange process were obtained for Pr(III), Eu(III), and Yb(III) (Table 8).[92] The major feature of the exchange process involves the shuffling of coordinated acetates accompanied by a flip of the backbone ethylenes between staggered conformations (see Figure 28). This results in a change in the helicity of the complex and leads to the equilibration of two of the acetate arms, which alternate coordination of position 7, and converts axial ethylenediamine protons to equatorial.

2. BOPTA

Uggeri et al. reported the X-ray structure, solution structure, and solution dynamics of Ln(III) complexes of BOPTA.[28] As with the DTPA complexes, BOPTA complexes can adopt two conformations depending upon the helical arrangement of the carboxylate groups around the Ln(III) center. For DTPA complexes this dynamic process involves the interconversion of enantiomers, while for complexes of BOPTA interconverting isomers of opposite helicity are not enantiomerically related. The benzyloxymethyl (BOM) substituent at one acetate group results in two chiral nitrogens upon chelation. This along with the two possible wrapping isomers and the presence of a stereogenic carbon (at the point of substitution) results in 16 possible stereoisomers for

Ln(III) complexes of BOPTA. The observed temperature dependence of the ^{13}C resonances for the La(III) and Lu(III) complexes were consistent with two (or more) couples of interconverting isomers. Activation parameters for exchange processes were not reported, but are expected to reflect the data previously observed for DTPA and DTPA-bisamide complexes. The exchange process involving inversion of the central nitrogen in BOPTA complexes is unusual. This process requires significant decoordination (octadentate to tridentate) of the ligand and is unlikely to be rapid enough to be observable by NMR.

3. EOB-DTPA

Schmitt−Willich et al. have recently reported on the solution behavior of Ln(III) complexes of EOB-DTPA (Chart 2).[98] For the drug substance, the ligand is prepared as the *S* enantiomer at the chiral carbon. The ethoxybenzyl (EOB) substituent in the diethylenetriamine backbone results in chirality at the central nitrogen upon chelation. The presence of two chiral centers (one of which is enantiomerically pure) and the possibility to form two wrappping isomers result in four possible diastereomers for the chelate. ^1H and ^{13}C NMR for the La(III) complex reveal two interconvertable isomers. In both the La(III) and Gd(III) complexes, these isomers exchange very slowly and are readily separated by HPLC. For the Gd(III) complex the equilibrium ratio of the two isomers is 65:35. NMR data collected for the La(III) complex established that the two observed isomers differ in the chirality of the central nitrogen. Similar solution behavior was observed for a DTPA substituted ligand analogous to the Y(III) chelate.[99]

4. DTPA-Bisamides

Upon chelation of a DTPA-bisamide ligand, the two terminal nitrogen atoms become chiral resulting in four diastereomers (see Figure 7). Two enantiomers (wrapping isomers) exist for each diastereomer, resulting in eight possible stereoisomers for their Ln(III) complexes. Geraldes and Peters reported a detailed NMR study on the La(III), Lu(III), and Nd(III) complexes of DTPA-B^{n}PA (Chart 4).[80,90] Consistent with X-ray structures of related Ln(III) complexes (R = Me, Bz, Et), they concluded that DTPA-B^{n}PA binds these Ln(III) cations in an octadentate fashion and that all of the complexes contain one inner sphere water molecule. Eight signals for the β- and γ-^{13}C nuclei of the propyl groups were observed for the Nd(III) complex at −30 °C, indicating that all four diastereomeric pairs of conformers were present in aqueous solution. Activation parameters for the exchange process occurring between the two wrapping isomers were determined for the Nd(III) complex. These are consistent with data reported for DTPA complexes and suggest that the barrier to the exchange is determined by the eclipsing of the ethylene bridges in the transition state, which is unchanged by replacement of carboxylates with amide groups. A racemization of the terminal N-atoms was also observed. The process involves inversion of the terminal backbone nitrogens. This requires partial decoordination of the ligand (octadentate to pentadentate), resulting in a high barrier to exchange. That a similar process was not observed in studies of DTPA complexes was attributed to differences between the coordination strength of carboxylate and amide donors. Activation parameters for the racemization of the terminal nitrogens in La(III) complexes of DTPA-BGLUCA and DTPA-BENGALAA (Chart 4) were reported and were found to be consistent with those reported for DTPA-B^{n}PA.[100] The complexity in the ^{13}C spectrum of the Lu(III) complex of DTPA-BMEA (Chart 4) was attributed to these types of exchange processes.[101] On the basis of the number of resonances observed, it was suggested that at least three unsymmetric conformers of the Lu(III) DTPA-BMEA complex were present in solution. Activation parameters are provided in Table 8.[80,100]

5. Cyclic DTPA-Bisamides

Their are four possible diastereomeric pairs (cis, trans, syn, and anti) for complexes of the linear DTPA-bisamides. The steric requirements of the tether reduce this to two diastereomers (cis and syn) for the cyclic complexes. The crystal structures of the Gd(III), Y(III), and La(III) complexes of 15-DTPA-EAM revealed binuclear structures with one bound water per metal ion and bridging ligands incapable of wrapping around the metal center.[37,38] Luminescence studies on the corresponding Eu(III) complex were suggestive of two bound waters at the metal center.[82] It was postulated that, as these studies are performed under highly dilute conditions (10 μM), a monomer is present in solution and that the ligand binds in a heptadentate fashion, leaving space for two water molecules. In contrast, Dy(III) induced ^{17}O shifts were consistent with one bound water.[81] Multinuclear NMR studies showed that with the smaller Ln(III) ions (Dy(III) to Lu(III)), 15-DTPA-EAM coordinated in an octadentate fashion and monomeric species predominated. ^{13}C NMR of the Lu(III) complex revealed the presence of one diastereomer in rapid exchange with its enantiomer. The ^1H NMR spectra of Ln(III) complexes of 18-DTPA-dien indicated two pairs of isomers.[41] Variable temperature NMR and 2D-EXSY established that one of the isomers (a dynamic isomer) underwent rapid exchange with its enantiomer, while the other isomer remained static. For these complexes two types of diastereomeric pairs were available, cis and syn. The syn enantiomers can undergo exchange by flip of the backbone ethylenes between staggered conformations and shuffling of the donor acetates and amides without changing the chirality of the terminal nitrogens. However, the cis enantiomers cannot undergo exchange without inversion of the terminal nitrogens, requiring partial decoordination of the complex. The static isomer for Ln(III) complexes of 18-DTPA-dien was concluded to comprise of the cis enantiomers, while the dynamic isomer was comprised of the syn enantiomers. For the Ln(III) (Dy(III) to Lu(III)) complexes of 15-DTPA-en only the dynamic syn enantiomers are seen.[81] Because the five atoms, −C−CO−N−C−, of each amide group are constrained to be planar and the tether between amide groups, an

ethylene bridge, is small, a cis configuration is sterically unfavorable for the 15-DTPA-en complexes. The ^{13}C NMR for lanthanide complexes of 30-DTPA-en-DTPA-en revealed several species present in solution. These were assigned to three isomeric pairs; syn−syn (dynamic−dynamic), syn−cis (dynamic−static), and cis−cis (static−static) configurations.

6. DOTA

Solution NMR studies support the presence of two slowly interconverting diastereomers for Ln(III) chelates of DOTA.[93,94,96,102,103] The population of each form is dependent upon the size of the Ln(III) cation, the temperature, and the concentration of added salt. The presence of two diastereomers was supported by luminescence studies of the Eu(III) complex.[104] The structural differences between the two isomers were determined by analysis of the LIS and fitting the NMR results to an axial symmetry model of the chelates based on published X-ray data. The LIS data suggested that the difference between the two isomers arose from the layout of the acetate arms. This was supported by COSY and EXSY experiments. The difference in the arrangement of the acetates gives rise to twisted CSAP (sometimes referred to as inverted CSAP) and CSAP geometries for the two isomers. This difference was described in terms of the relative orientation of the two square planes formed by the eight donor atoms, four nitrogens forming the basal plane, and four acetates forming the monocapped plane (Figure 29). The major isomer has a CSAP geometry with a twist angle between the two planes of ca. 40°. The minor isomer has an twisted CSAP geometry with a twist angle of ca. 30°. There are four stereoisomers, two pairs of enantiomers, which can interconvert in solution by either ring inversion (interconversion of ($\delta\delta\delta\delta$) and ($\lambda\lambda\lambda\lambda$) isomers) or acetate arm rotation (interconversion of Δ and Λ isomers). Either process alone results in exchange between CSAP and twisted CSAP geometries. Both processes combined result in an exchange between enantiomeric pairs as shown in Figure 29. Activation parameters for the exchange processes are provided in Table 8. The structure of the major isomer is consistent with the X-ray analysis of the Eu(III), Gd(III), Y(III), and Lu(III) complexes. The structure of the minor isomer is consistent with the X-ray structure of the La(III) complex.

7. α-Substituted DOTA Derivatives

The introduction of chiral centers of equal configuration (*RRRR* or *SSSS*) to all four acetate arms of DOTA (as with DOTMA and TCE-DOTA), or to one acetate arm of DOTA (as with DOTA-pNB), results in four possible diastereomers upon chelation (Chart 6). The solution structure of the Yb(III) complex of DOTMA, where the configuration at each chiral carbon is (*RRRR*), was reported by Brittain and Desreux.[104] The ^1H NMR spectrum indicated the presence of only two species in solution. This observation was supported by high-resolution luminescence of the Eu(III) complex which indicated two chemically distinct species were present in solution. Two solution isomers were observed for the (*RRRR*)

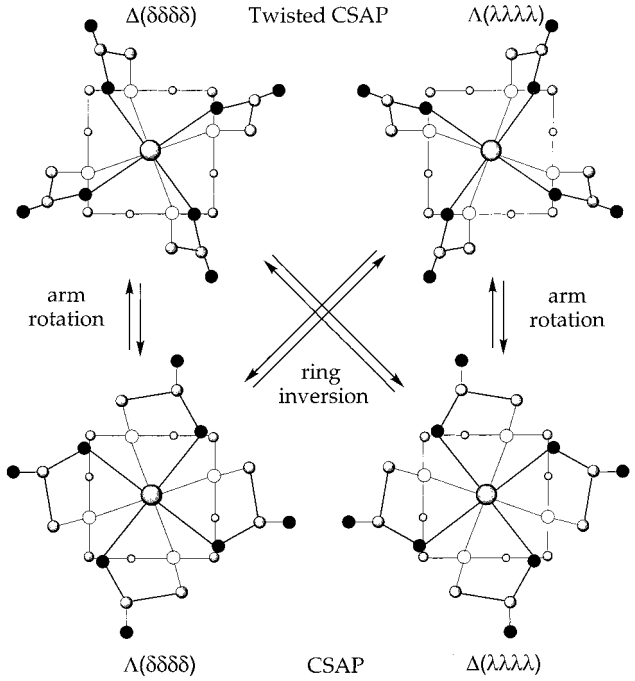

Figure 29. There are two diastereomeric conformations (CSAP and twisted CSAP) for lanthanide complexes of DOTA. Pairs of enantiomers exist for the major isomer (Δ-($\lambda\lambda\lambda\lambda$) and Λ($\delta\delta\delta\delta$)) and for the minor isomer (Δ($\delta\delta\delta\delta$) and Λ($\lambda\lambda\lambda\lambda$)) of $[Ln(DOTA)]^-$.

TCE-DOTA derivative reported by Howard et al.[50] ^1H EXSY established an exchange process between the two isomers that occurred through inversion of the macrocycle ring. Similar observations were made for the Ho(III) and Yb(III) complexes of DOTA-pNB.[95] As with the DOTA complexes, ring inversion results in an exchange between CSAP and twisted CSAP geometries which have the same helicity. Rearrangement of the acetate groups (not observed) would result in exchange between CSAP and twisted CSAP geometries of opposite helicity. The lack of such a dynamic process suggested that the configuration of the stereogenic center at carbon determines the least sterically hindered helical form of the complex. This view was supported by the solid state structures of the Eu(III) complexes (*RRRR*) and (*SSSS*) TCE-DOTA, which revealed a change in the helicity of the complex with the change in the configuration at the carbon center. In both enantiomers the substituent was equatorially positioned (pointing away from the coordination cage). The same observation was made for the Yb(III) complex of DOTA-pNB by analysis of the LIS data, showing that the substituent in both solution species is positioned equatorial from the chelate ring and away from the metal ion. The preference for a particular helicity reduces the number of diastereomers from four to two and is consistent with the NMR data reported for the DOTMA, TCE-DOTA, and DOTA-pNB complexes.

8. HP-DO3A

A number of different isomers are possible for Ln(III) complexes of HP-DO3A. The replacement of an acetate arm with a hydroxypropyl group gives rise to diastereomeric differentiation of the four expected isomers. In addition, the presence of a chiral carbon

Table 9. Rate Constants for HP-DO3A Dynamic Processes[a]

cross-peak	k_i (s^{-1})
ethylene (a)	118.37
ethylene (b)	91.70
ethylene (c)	104.16
hydroxypropyl	33.16
acetate arm (1)	21.13
acetate arm (2)	21.99

[a] For ethylene and acetate assignments, see Figure 30.

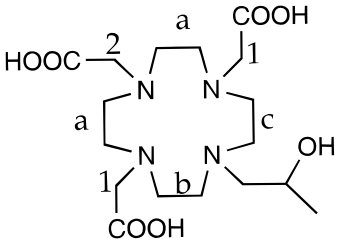

Figure 30. HP-DO3A labeled to show the groups involved in dynamic processes (Table 9).

center in the hydroxypropyl arm doubles the number of possible stereoisomers to eight (four pairs of enantiomers). ROESY analysis of the exchange dynamics for the Y(III) complex of HP-DO3A was reported by Shukla.[97] The presence of the hydroxypropyl arm introduced a site of asymmetry that enabled the chemical shift separation of the acetate arms and ethylene groups. Rearrangement of the acetate groups and inversion of the macrocycle were both observed. Exchange rates were determined using the cross-peak decay between the geminal spin pairs as a function of mixing time. These results showed that exchange of the ethylene groups in the ring is faster than exchange for the pendant arms and exchange for the hydroxypropyl arm is faster than for acetate arms (Table 9 and Figure 30). While resolution was too poor to confirm the presence of multiple diastereomers by counting peaks, the observation of the exchange processes confirmed the presence of multiple species. Two of these diastereomers, found in the crystal structures of the Y(III) and Gd(III) complexes, interconvert by ring inversion. In solution, the presence of diastereomers of opposite helicity was suggested by the observation of an exchange process involving rearrangement of the acetate arms.

9. DOTP

The ^{1}H and ^{13}C NMR spectra of the La(III) and Lu(III) complexes of DOTP (Chart 8) were consistent with a very rigid chelate structure with very long-lived metal−nitrogen and metal−oxygen bonds.[105] The tetraazacyclododecane ring was locked into a single conformation at room temperature. The barrier to inversion, 101 ± 11 kJ mol^{-1}, was considerably higher than that reported for DOTA systems. Unlike the DOTA systems, no fluxional behavior was observed for the phosphonate arms in these complexes. LIS data for ^{1}H, ^{31}P, and ^{13}C nuclei for the entire lanthanide series were reported by Geraldes et al. Analysis of the LIS data for a series of Ln(III) complexes was consistent with eight-coordinate metal ions in an isostructural series.[105,106] The average ionic form of Ln(III) complexes of DOTP at pH = 7.4 is H[Ln(III)(DOTP)].$^{4-}$[107] The highly charged complexes readily form tight ion-paired complexes with alkali and alkaline earth cations. This was exploited in the use of the Tm(III) complex as an in vivo shift reagent for ^{23}Na NMR.[108−111]

10. Phosphinates and Phosphonate Esters

As with DOTA complexes, the Ln(III) complexes of the analogous phosphonate esters and phosphinates have clockwise and counterclockwise wrapping isomers. In addition, coordination of the pendant arm results in an asymmetric center at each phosphorus. Six diastereomers are possible, *RRRR*, *RRRS*, *RRSS*, *RSRS*, *RSSS*, and *SSSS*, each with two possible wrapping isomers resulting six enantiomeric pairs (Δ*RRRR* and Λ*SSSS* are enantiomers).[112] ^{19}F NMR spectra for the Ln(III) complexes of the fluorinated phosphonate ester, F-DOTPME (Chart 8), (Ln = La, Gd, Eu, Dy, Tm, and Yb) revealed up to 16 resolved ^{19}F resonances, consistent with formation of all six possible diastereomers.[87] In contrast, the ^{1}H NMR spectra for the Y(III), Yb(III), and Eu(III) complexes of the tetraphosphinate DOTBzP showed only one species present in solution, with no fluxional behavior observed over a temperature range of 5−80 °C.[52,113] Comparison with Yb(III) data from the corresponding DOTA complex suggested that the DOTBzP complex shares the same twisted square antiprismatic structure found in the minor isomer of the DOTA complex. This is consistent with crystal structure data in which the geometry about the metal centers is twisted CSAP (twist angle ca. 29°). The structure for the Y(III) complex exhibits both *RRRR* and *SSSS* conformations at the stereogenic phosphorus centers in a 1:1 ratio of enantiomers of opposite helicity. Analysis of the ^{31}P LIS for Ln(III) complexes of DOTBzP showed a discontinuity in the structures occurring at Pr(III) (vide supra).[53] This is consistent with crystallographic data which showed a change in coordination number between the heavy and light lanthanide complexes of DOTBzP. The solution properties of the phosphinate complexes and phosphonate ester complexes are very different. While the tetra(benzylphosphinate) complex formed one enantiomeric pair of rigid diastereomers in solution, the F-DOTME complexes formed all of the possible diastereomers.

11. TETA

The solution structure and dynamics of Ln(III) TETA complexes were studied by variable temperature ^{13}C and ^{1}H NMR.[114] A conformational analysis of the Yb(III) complex of TETA using LIS data showed reasonable agreement with the crystal structure of the Tb(III) complex. A temperature dependence in the ^{1}H NMR spectra of the Yb(III) complex and the ^{13}C spectra of the Lu(III) complex was interpreted as arising from an exchange between two equivalent dodecahedral geometries. In a dodecahedral geometry, the Ln(III) complexes contain two different groups of donor atoms (high and low). The exchange was consistent with a dynamic process in which the high and low groups are continuously

moving up and down. Unlike the inversion of ring conformation in DOTA complexes, which required no substantial motion in the ligating atoms, the donor groups for the TETA complexes were rapidly exchanging between two different locations. The heavier lanthanide complexes Eu(III) to Lu(III) behaved similarly. The spectra for the lighter and larger Pr(III) ion were much more complex, indicative of a highly asymmetric structure. Kinetic parameters for the dynamic process in the Lu(III) complex are given in Table 8.

12. TTHA

The La(III), Lu(III), and Y(III) complexes of TTHA were studied by ^{1}H and ^{13}C NMR.[115] ^{13}C data for the La(III) complex showed all of the carboxylate carbon resonances shifted downfield from the free ligand, suggesting that all four amine nitrogens and all six carboxylate oxygens are bound to the metal center. This is consistent with the solid state structure reported for the La(III) complex. The spectra for the Lu(III) and Y(III) complexes were complicated by fluxional processes consistent with multiple 1:1 species present in solution. Absorption spectroscopy for the Eu(III) complex also suggested the presence of two distinct 1:1 species.[116] Monomeric and dimeric X-ray structures of the Nd(III) complex, which differ in coordination number, were reported.[60,62] The f−f transitions in the two crystals were compared to a solution of the Nd(III) complex to determine the solution ratio of monomer to dimer. The results were consistent with a 4:1 ratio of monomeric to dimeric species in solution. Analogous monomeric and dimeric structures were reported for Gd(III) and account for the two distinct species observed for solutions of the Eu(III) complex.

The solution structures of these selected lanthanide complexes generally agree with their solid state structures. Studies of exchange processes in these systems provide a rich description of the solution behavior of these complexes. The occurrence of CSAP and twisted CSAP isomers appears to be a general phenomenon of Ln(III) complexes of DOTA derivatives that naturally results from rotation of the nitrogen donor atoms upon ring inversion (Figure 31). A similar interconversion between gauche conformations in DTPA derivatives also gives rise to multiple isomers in these systems. Another common feature among DOTA and DTPA derivatives is the influence that substituents can have upon the conformational solution equilibria. Several examples have shown that the chiral configuration of a substituent will determine the overall helicity of the complex. A well-placed substituent can reduce the symmetry in these complexes and allowed otherwise unobservable exchange processes to be investigated. For example, with [Y(HPDO3A)(H_2O)] the differentiation of each pendant arm and ethylene group allows the dynamics of each to be monitored separately. For the Gd(III) complex of EOB-DTPA, the exchange between diastereomers which differ only in the chirality of the central backbone nitrogen could be monitored by HPLC.

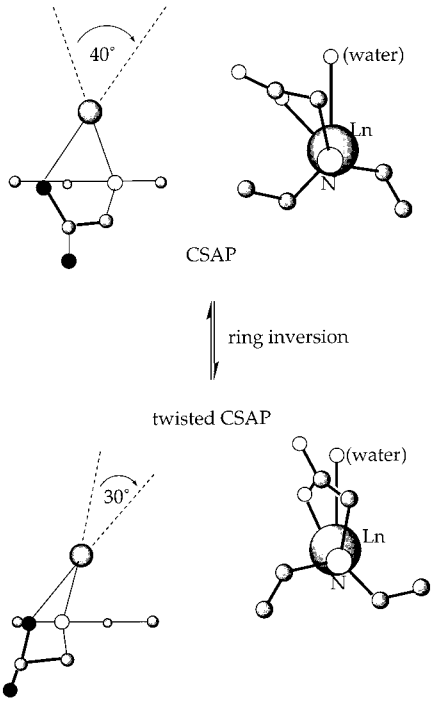

Figure 31. Two positions for the acetate arms of DOTA-type complexes results from the twisting of the macrocycle nitrogens upon ring inversion. On the right, this is viewed looking down the Ln−N bond. On the left, this is viewed looking down the Ln−water bond at one edge of the macrocycle.

D. Gadolinium(III) Chelate Stabilty

It is clear that the integrity of the gadolinium(III) complex must be maintained in vivo in order to create a safe and efficacious MRI agent. Dissociation of Gd(III) from an MRI contrast agent is undesirable, as both the free metal and unchelated ligands are generally more toxic than the complex itself. Free Gd(III) is known to bind with some avidity to serum proteins; eventually much of the released metal comes to reside in the bone, where it becomes tightly and irreversibly associated. Detection of significant amounts of Gd(III), usually by either ICP or gamma counting (in the case of Gd-153 or Gd-159 labeled complexes) in skeletal tissue is the hallmark of gadolinium(III) dissociation from a chelate.[117−119]

The exact prediction of in vivo stability on the basis of fundamental physical properties remains an uncertain science. However a number of significant studies have been published during the past decade which shed light on relevant physical properties, such as solution thermodynamics and dissociation kinetics. This section will focus on compounds for which data have been published since the previous review.[1] An emphasis is placed on clinically relevant chelate systems and those for which combinations of in vitro and in vivo biodistribution data are available.

E. Solution Equilibria and Contrast Agent Dissociation in Vivo

The solution equilibria behavior of gadolinium(III) complexes should be considered in the context of MRI contrast agent medicinal chemistry along with phar-

Table 10. Stability Constants, LD_{50}, and Gd(III) Bone Uptake Data for Selected Complexes

ligand	LD_{50}[f]	%ID[n]/gram	log K_{GdL}	log K^*_{GdL} (pH 7.4)	log K_{sel}	log K_{CaL}	log K_{CuL}	log K_{ZnL}
EDTA	0.3[m]	0.80	17.7[b]	14.70	4.23[m]	10.61[l]	18.78[l]	16.5
			17.37[l]	14.8[b]				
DTPA	5.6[m]	0.005	22.46[l]	17.70	7.04[m]	10.75[l]	21.38[l]	18.29[l]
DTPA-BMA	14.8[m]	0.03	16.85[m]	14.90	9.04	7.17[m]	13.03[m]	12.04[m]
DTPA-BMEA			16.84[b]					
DTPA-BP	2.8[m]		16.83[m]		5.32[m]			
DOTA	11[d]	NDR[o]	25.3[b]	18.33[d]	8.3[a]	17.23[e]	22.63[e]	21.05[e]
			24.6[h]	18.6[b]				
			24.0[i]					
			22.1[k]					
DO3A	7−9[a]	0.0080	21.0[b]	14.97[d]	4.13[a]	11.74[d]	22.87[d]	19.26[d]
				14.5[b]				
DO3MA			25.3[c]		8.3[a]			
HP-DO3A	12[e]	NDR[o]	23.8[b]	17.21[d]	6.95[a]	14.83[d]	22.84[d]	19.37[d]
				17.1[b]				
BOPTA			22.59[j]					

[a] Reference 123, 25.0 °C, μ = 0.1 M $(CH_3)_4NCl$. [b] Reference 47. [c] Reference 51. [d] Reference 124. [e] Reference 125. [f] Intravenous LD_{50} in mice, mmol kg^{-1}. [g] Reference 126. [h] Reference 127. [i] Reference 128. [j] Reference 28. [k] Reference 130. [l] Reference 129. [m] Reference 122. [n] Mean % ID/g in femur at 14 days, estimated from ref 121. [o] NDR = no detectable radioactivity.

macokinetics, protein binding, elimination, and safety. Equilibria between gadolinium(III) and other competing endogenous metals and anions can potentially contribute to the dissociation of gadolinium(III) from the complex, an event which removes the critical magnetic core of the drug. By design, the magnitude of the thermodynamic stability constant K_{GdL}, defined in eq 7,[120] is large for all of the clinically viable

$$M + L = ML \qquad K_{ML} = \frac{[ML]}{[M][L]} \tag{7}$$

contrast agents, ranging from $10^{16.85}$ for [Gd(DTPA-BMA)] to $10^{25.6}$ for [Gd(DOTA)] (Table 10). Clearly, the equilibrium in eq 7 lies heavily to the side of the complex, GdL, and little, if any, free metal is present at equilibrium under conditions where eq 7 is valid.

The coordination chemist will appreciate the fact that protons will compete for the ligand L as the pH is lowered; this competition must be taken into account if one is to understand the solution equilibria at physiological pH. This is critical for the multidentate, multiprotic ligands which are being discussed in this review. Given the protonation constants of the ligands and the formal stability constant K_{ML}, the conditional (or pH dependent) stability constant K^*_{ML} can be calculated using eq 8. The conditional stability constant K^*_{ML} is often used to compare the relative thermodynamic stability of different chelates at pH 7.4. Table 10 also reports the conditional stability constants for the series of clinically relevant contrast agents as well as $[Gd(EDTA)(H_2O)_n]^-$.

$$K^*_{ML} = \frac{K_{ML}}{(1 + K_1[H^+] + K_1K_2[H^+]^2 + ... + K_1K_2K_n[H^+]^n)} \tag{8}$$

where K_1, K_2, K_3, ... K_n are the stepwise protonation constants of the ligand.

Given that there is a difference in the relative thermodynamic stability of these compounds at physiological pH, how do these data correlate with observed in vivo results, particularly the deposition of dissociated gadolinium(III) in the skeleton? To investigate this question, Wedeking et al.[121] have measured the %ID (initial dose)/gram found in the femur at 7 days postinjection (mouse) for a series of clinically relevant extracellular contrast agents (Table 10) with similar pharmacokinetic and elimination characteristics. $[Gd(EDTA)(H_2O)_n]^-$ was not an approved contrast agent, but was included for comparison purposes.

When comparing the complex stability in Table 10 to the amount of gadolinium(III) found in the rodent skeleton at 7 days, it is immediately striking that while thermodynamic (K_{ML}) and conditional stability constants (K^*_{ML}) values for $[Gd(EDTA)(H_2O)_n]^-$ and [Gd(DTPA-BMA)(H_2O)] are relatively similar (for example, K^*_{GdL} = 14.9 and 14.7, respectively, for L = EDTA and L = DTPA-BMA), the amount of Gd(III) deposited in the mouse at 7 days is rather significant (~0.8%ID/gram) for $[Gd(EDTA)(H_2O)_n]^-$ and small for [Gd(DTPA-BMA)(H_2O)] (~0.03%ID/gram).[121] Likewise, the amount of Gd(III) found in the bone for $[Gd(DO3A)(H_2O)_n]$ is surprisingly small given the rather low conditional stability constant. Thus, it is clear that thermodynamics, i.e., the gadolinium(III) stability constant alone, is not sufficient to explain in vivo stability trends.

Cacheris et al. evaluated the relationship between thermodynamics and toxicity for a series of gadolinium(III) complexes and also concluded thermodynamic stability of the Gd(III) complexes in itself was insufficient to correlate observed acute toxicity (not bone deposition) for a series of Gd-153 labeled DTPA derivatives examined in rodents. In their study, the authors assumed that acute toxicity was related to the dissociation of gadolinium(III). Consideration of the relative affinity of the ligands for Gd^{3+} as well as biologically relevant cations such as Ca^{2+}, Zn^{2+}, and Cu^{2+} led the authors to propose the use of a "selectivity" factor, log K_{sel}, to accommodate the biological data. Table 10 shows the observed LD_{50} in mice,[122−125] stability constants for the ligands with Gd(III), Ca(II), Cu(II), and Zn(II),[28,47,51,126−130] as well as a selectivity factor, log K_{sel}, which was calculated using eq 9. This factor takes into account the ligand

equilibria for H^+, Gd^{3+}, Ca^{2+}, Zn^{2+}, and Cu^{2+}. At equilibrium, a ligand with a higher selectivity factor will bind Gd(III) more strongly in the presence of the competing metal ions (Ca(II), Cu(II), Zn(II)) than a ligand with a lower selectivity factor.

$$K_{sel} = K_{ML}(\alpha_H^{-1} + \alpha_{CaL}^{-1} + \alpha_{CuL}^{-1} + \alpha_{ZnL}^{-1})^{-1} \quad (9)$$

where the α's are defined below

$$\alpha_H^{-1} = 1 + K_1[H^+] + K_1K_2[H^+]^2 + K_1K_2K_3[H^+]^3 + ...K_1K_2K_3K_n[H^+]^n \quad (10)$$

$$\alpha_{CaL}^{-1} = K_{CaL}[Ca^{2+}] \quad (11)$$

$$\alpha_{CuL}^{-1} = K_{CuL}[Cu^{2+}] \quad (12)$$

$$\alpha_{ZnL}^{-1} = K_{ZnL}[Zn^{2+}] \quad (13)$$

Examination of Table 10 reveals that the compound with the highest selectivity factor, GdDTPA-BMA, also has the highest LD_{50}. Cacheris and coworkers suggested that an increase in selectivity for Gd(III) over endogenous cations substantially contributes to the high LD_{50} (indicating a lack of acute toxicity) for DTPA-BMA, and they calculate that all four complexes become toxic to 50% of the mice when approximately 13−15 μM Gd(III) is released. On the basis of these calculations, [Gd(DTPA-BMA)(H_2O)] is expected to release half of its Gd(III) as compared with $[Gd(DTPA)(H_2O)]^{2-}$. However, the studies of Wedeking[121] and others[131,132] contradict this prediction, and consistently indicate that less Gd(III) is dissociated from DTPA than from DTPA-BMA as measured by skeletal uptake or by transmetalation.

It is also noteworthy that the selectivity arguments failed for the Gd(III) complex of the macrocyclic polyaminocarboxylate ligand DOTA, presumably because of the kinetic inertness of the macrocyclic complex. This result highlights a key point: the thermodynamic selectivity index can be considered only for those complexes which have sufficiently fast dissociation and substitution kinetics such that transmetalation occurs during the time in which the gadolinium(III) complex remains in vivo.

F. Kinetic Inertness and in Vivo Dissociation of Gadolinium(III) Complexes

As noted above, dissociation and transmetalation kinetics play a key role in determining the fate of a complexed Gd(III) ion in vivo.[133] While fast kinetics are characteristic of metal complexes derived from acyclic ligands, an accumulated body of literature has shown that macrocylic complexes tend to be significantly more inert.[113,130,134−136] This is clearly the case for the polyaminocarboxylate analogues of DOTA, which form Gd(III) complexes that are exceptionally inert as well as thermodynamically stable.[137,138] These properties were exploited in the design of [Gd(HP-DO3A)(H_2O)], which is a commercially available neutral macrocyclic extracellular agent (see ProHance, Charts 1 and 6).

Table 11. Acid Dissociation Rate Constants, k_{obs}, ($[H^+]$ = 0.1 M)

ligand	Log K_{GdL}	%ID/g @ 24 h	k_{obs} (10^3 s^{-1})	$t_{1/2}$ (h)
EDTA	17.70		140000[f]	
DTPA-BMA	16.85[b]		> 20	0.18[e]
DTPA	22.2	0.3[e]	1.2	
DO3A	21.0[g]		2.37 (2)[b]	
NP-DO3A	16.0		> 20	
HP-DO3A	23.8[h]		0.064 (9)[b]	
HE- DO3A	22.3[h]		0.466[c]	
HIP-DO3A	23.9[h]		0.0582[c]	
DOTA	25.3[g]		0.021	60.2[d]
			0.0032 (3)[d]	
BOPTA	22.59[i]	0.22[e]		
DTPA-BMEA	16.84[a]			
DOTBzP		<0.05[e]	0.0239 (2)[d]	8.1[d]
DOTMP		0.08[e]	0.0104 (1)[d]	18.5[d]
DOTBuP			0.0369 (6)[d]	5.2[d]
DOTMP-MBBzA		<0.05[e]	0.00430 (8)[d]	44.9[d]
DOTMP-MBuA			0.00130 (2)[d]	153[d]
DOTBuP-MMA		0.09[e]	0.00410 (9)[d]	47[d]
DOTPP			0.0777 (6)[d]	2.5[d]

[a] Reference 126. [b] Reference 134, 25 °C, μ = 1.0 M NaCl. [c] Reference 138, Supporting Information. [d] Reference 113. [e] Reference 139. [f] Reference 121. [g] Reference 47. [h] Reference 138. [i] Reference 28.

As noted in Table 10, small but measurable differences in in vivo Gd(III) dissociation are observed for this class of complex, which have similar pharmacokinetic characteristics. To explain these variations, the Tweedle group explored the use of acid-catalyzed dissociation rates as a predictor for in vivo loss of gadolinium(III).[121] Table 11 lists acid-catalyzed dissociation constants for a series of macrocyclic and acyclic gadolinium(III) complexes. Wedeking et al. report that a good correlation exists between the acid dissociation constant determined in 0.1 M HCl and the amount of Gd(III) deposited in the bone at 7 days for the first nine entries in Table 10. Parker and coworkers have also reported a correlation between the acid-catalyzed dissociation rate and in vivo loss of Gd(III) for the series of phosphinate compounds shown in Chart 10.[113,139] These data are consistent with the accumulated body of research which has established that the macrocyclic gadolinium(III) complexes discussed here, such as GdDOTA (Chart 1), are remarkably kinetically inert.

For relatively inert complexes, such as the macrocyclic agents, transmetalation is not anticipated to be an important mechanism for release of Gd(III), and acid-catalyzed dissociation should be minimal in the extracellular environment. It is not surprising that acute toxicity could result from one or more other pharmacological effects besides gadolinium(III) release. It is an important scientific goal to minimize the in vivo dissociation of gadolinium(III) from contrast agents; however, the notion that acute toxicity results predominantly from Gd(III) release is probably an oversimplification.

G. New Compounds

1. Stability Constants

The hypothesis that a high thermodynamic selectivity of a ligand system for Gd(III) over endogenous

Chart 10

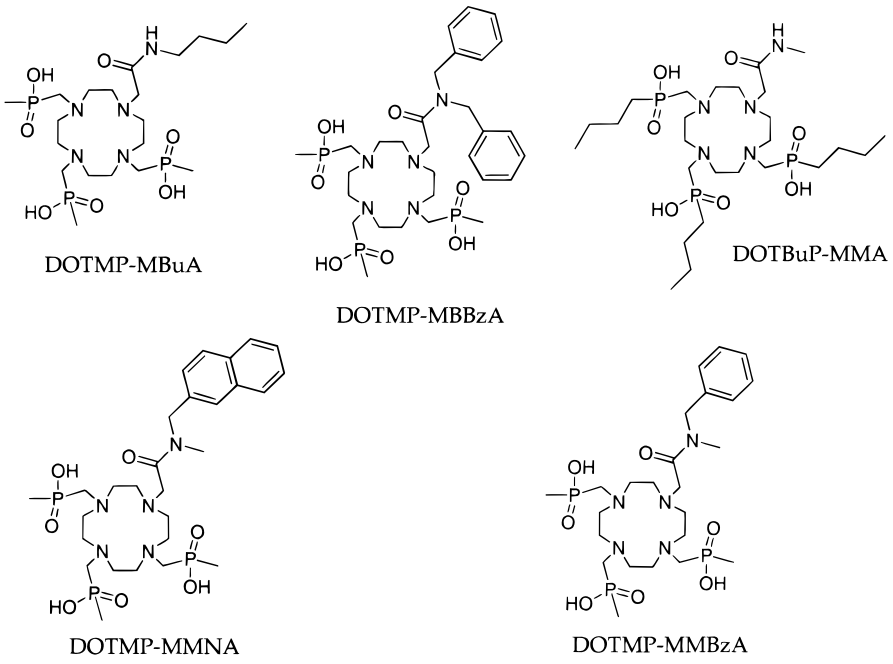

ions may enhance the safety of MRI contrast agents has resulted in fundamental research efforts directed at understanding how to modulate selectivity. Consequently, a number of papers have appeared which detail the synthesis and solution equilibria of acyclic ligand systems with Gd(III), Ca(II), Cu(II), and Zn(II) (see Table 12).[123,140−144] The effect of various donor groups on metal ion selectivity is of particular relevance to the design of new contrast agents, as exemplified by the study of Paul-Roth and Raymond comparing the effect of amide vs carboxylate substitution.[145] In that report, the authors studied the effect of the amide substitution for acetate on Gd/Ca selectivity using two diethylenetriamine derivatives: DTPA-BMA, a diethylenetriaminepentaacetic acid diamide ligand, and DTTA-BM, a diethylenetriaminetriacetic acid ligand. The contribution of amide substitution to stability was found to produce selectivity for Gd(III) over Ca(II) by approximately 3.4 log units per amide group. The selectivity should be quantified by the decrease in free metal ion concentration under specified conditions and not the formation constant, because ligands have different proton basicity as well as different metal ion stability constants. Paul-Roth and Raymond used the difference in pM value, (ΔpM), as a measure of the metal ion free energy. The pM value of a complex specifies the degree of metal chelation at a given pH and is defined as −log[free metal ion] under stated conditions of total metal, total ligand, pH, and ionic strength.[146] The pM value incorporates the protonation competition effect and is useful to directly compare the relative affinities of different ligand systems for a given metal ion.

The contribution of various neutral donors to the stability of lanthanide chelation is summarized in Figure 32 (after Caravan et al.[147] and Thompson et al.[148]). The term Δlog *K* here refers to a free energy difference in binding after taking into account the difference in ligand basicity. The neutral donors which give the most increase in stability are alchoholic oxygen, pyridyl nitrogen, and amide oxygen.

The relatively low pK_a of the hydroxypyridinone functional group (Chart 9) has been exploited in the design of new contrast agents. The HOPO ligands coordinate in a hexadentate fashion to Gd(III). In these complexes, the gadolinium ion is eight-coordinate with two coordinated waters. The Gd(III) complex was found to be more stable than DTPA at pH 7.4 and to be more selective than DTPA for Gd/Ca.[64]

A significant amount of fundamental macrocyclic chemistry has been reported during the last 10 years.[28,47,49,51,107,122,126,132,140,144,145,149−155] Table 12 shows the solution equilibrium data collected for these compounds (see Charts 11−13 for ligands). There are large discrepancies in the reported values for the stability constant of some macrocyclic compounds, particularly $[Gd(DOTA)(H_2O)]^-$. These problems arise from two sources: (1) the relatively high pK_1 of the ligand, which is strongly depressed in sodium electrolyte due to cation binding,[47] and (2) the slow kinetics of the macrocyclic systems.[134] A number of competition methods have been used to determine the stability constants, including the use of competing ligands—arzenazo dye or DTPA, and metals such as Eu(III).[156,157] The latter appears to be a powerful technique, as it combines the use of a well-characterized competing ligand (DTPA) with sensitive, direct quantification of the different Eu(III) species using luminescence techniques.

Macrocyles containing amide donors have also been prepared and charcterized[49,158] and are of particular interest as a similar structure has recently been incorporated into a new macromolecular dendrimer-based agent, Gadomer 17 (see section V). One disadvantage of chelates containing amide donors is the fact that the water exchange rate is slow relative to the acetate analogues, resulting in exchange-limited relaxivity. This will be further discussed in sections IV and V.

Table 12. Stability Constants for Various Cyclic and Acyclic Gd(III) Complexes

ligand	ligand denticity	log K_{GdL}	log K_{GdL*}	pM	ΔH (kJ/mol)	ΔS (J K^{-1} mol^{-1})	ref
DTPA	8	22.46			−32.6	321	126
DTPA-BMEA	8	16.84[a]			−27.5	231	126
					−25.3[a]	238[a]	
DTPA-BMMEA	8	17.68[a]			−35.3	220	126
DTPA-BHMEA	8	17.49[a]			−35.1	217	126
DTPA-BMA	8	16.85		15.83			145
DTTA-BM	6	13.12		9.08			145
DTTA-HP	8	23.65					149
DOTA-MPA	8	20.1	16.2				158
DO3A−L2	8	25.9					49
DO3A−L1	8	26.4					49
DTPA-BGLUCA	8	16.54	15.7				132
BOPTA	8	22.59					28
DOTA	8	25.3					47
DO3MA	7	25.3					51
DO3A	7	21.1	14.5				47
DOTP	8	28.8					107
HP-DO3A	8	23.8	17.1				138
HIP-DO3A	8	23.9	16.7				138
HE-DO3A	8	22.3	16.7				138
DTPA-EAM	8	11.15					144
DTPA-PAM	8	14.49					144
DTPA-BAM	8	15.39					144
DTPA-cis$^{C=C}$BAM	8	15.56					144
DTPA-PenBAM	8	15.94					144
DTPA-OAM	8	17.44					144
NOTA	6	13.7					155
DETA	6	15.1					155
Me-DETA	6	14.7					155
Me_2−DETA	6	10.4					155
PC2A	6	16.6					152
BP2A	6	14.5					152
N_3O_6−L1	9	16.27					153
N_3O_5−L1	8	11.49					129
N_3O_6−L2	9	18.07					149
N_3O_5−L2	8	17.23					129
ODOTRA	7	21.6					154
TTAHA	10	19.00					150
PEDTA	6	15.56					150

[a] Reference 140.

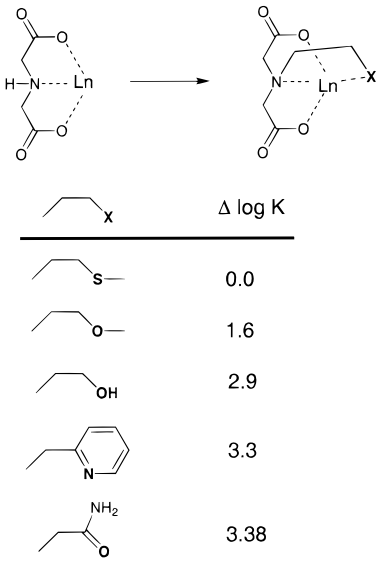

Figure 32. Relative affinity of different donor atoms for Ln(III) ions.

Phosphinate derivatives of macrocyclic chelates have been explored in detail by Parker and Sherry.[52,107,112,113,159−164] Many of these complexes have high thermodynamic stability to compliment their kinetic inertness.

2. Kinetic Inertness

Phosphinate derivatives of the tetraazacyclododecane ring system are quite inert to acid dissociation. Table 11 shows some data obtained for a series of functionalized phosphinate derivatives. The data show that the triphosphinate monoamide macrocycles are more inert to acid dissociation than the tetraphosphinate analogues (see Charts 8 and 10 for ligand structures).

In principle, rigid acyclic ligand systems, as exemplified by the classic *trans*-cyclohexylethylendiaminetetraacetic acid (CDTA) ligand, also provide enhanced kinetic inertness relative to flexible parent ligands. For example, Choppin reported the acid dependent dissociation constant of $[Eu(EDTA)(H_2O)_n]^-$ to be 230 M^{-1} s^{-1} as compared with 6.3 M^{-1} s^{-1} for $[Ce(CDTA)(H_2O)_n]^-$, indicating that substantial differences in dissociation rates can be expected.[165] Similarly, for a series of Y(III) complexes of eight-coordinate DTPA-type ligands which included cyclohexyl and benzyl moieties in the backbone, the observed acid-catalyzed

Chart 11

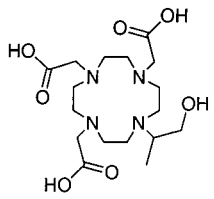

HIP-DO3A

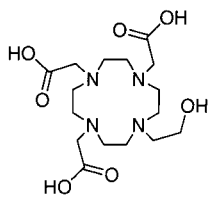

HE-DO3A

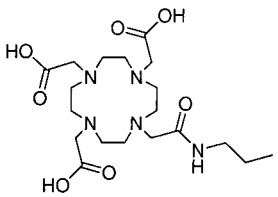

DO3A-MPA

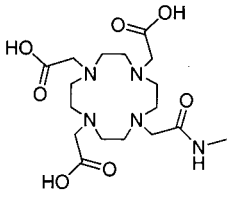

DO3A-MMA

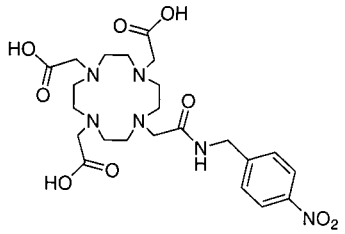

DO3A-MNBA

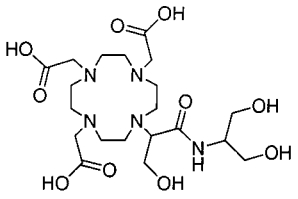

DO3A-L4

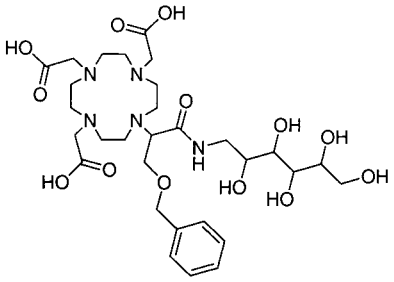

DO3A-L1

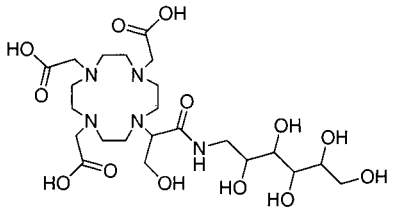

DO3A-L3

Chart 12

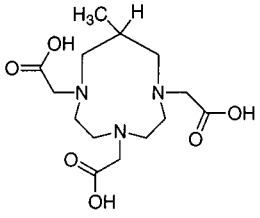

MeDETA

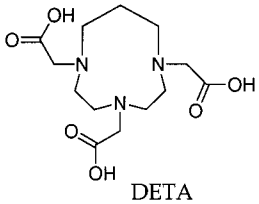

DETA

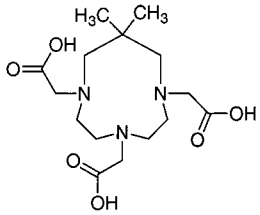

Me_2DETA

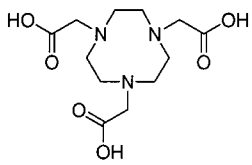

NOTA

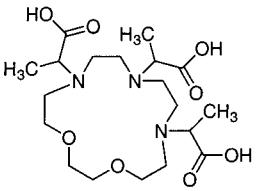

N_3O_5-L1

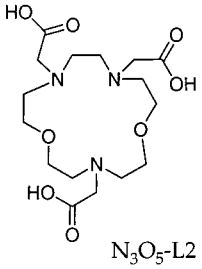

N_3O_5-L2

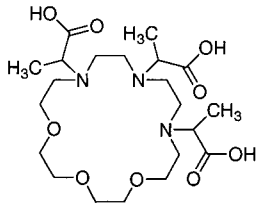

N_3O_6-L1

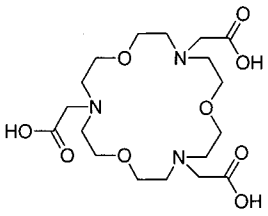

N_3O_6-L2

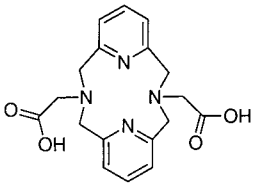

BP2A

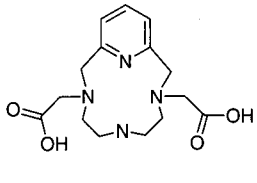

PC2A

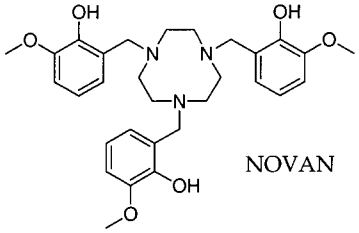

NOVAN

dissociation rate constants varied by up to 3 orders of magnitude.[166] Too much emphasis should not be placed on acid-catalyzed dissociation; it was noted in this report that the compound with the slowest observed acid dissociation rate actually had the highest loss of radioactive Y(III) in vivo. Although the principles are general, much of this work has not yet been extended to include studies with gadolinium(III).

Chart 13

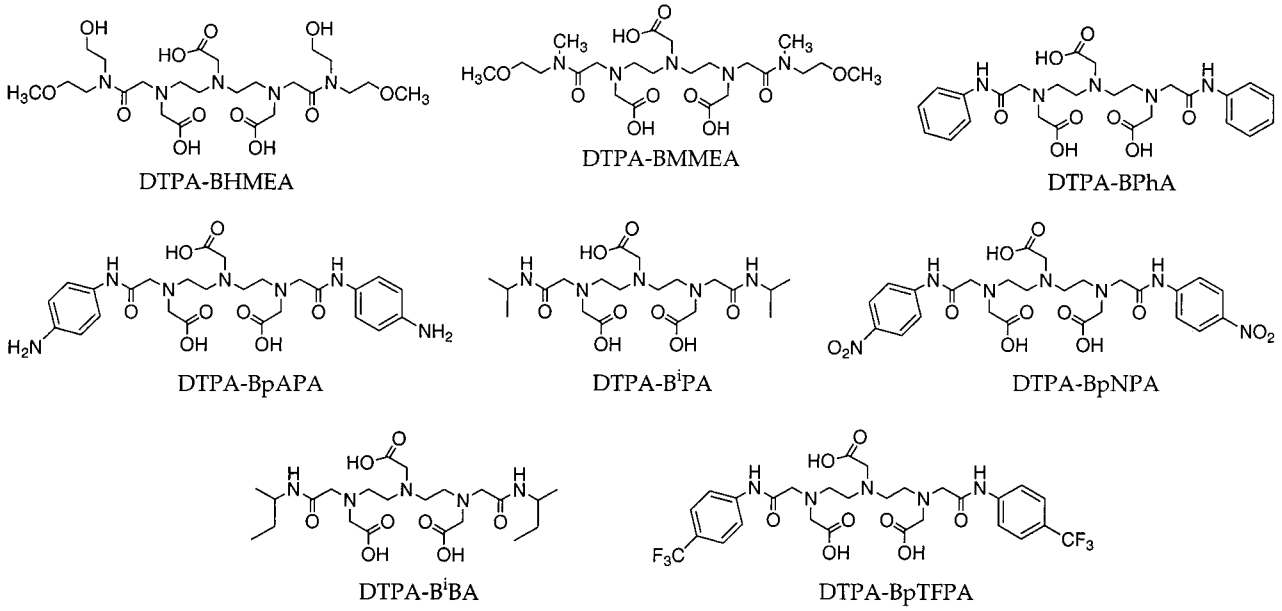

H. Summary/Future Directions

Data accumulated over the past 10 years indicate that all of the chelates utilized in the commercially available products are remarkably stable with respect to dissociation in vivo. Chemical factors which contribute to the stability include the multidentate nature of the ligand systems, high thermodynamic stability, and in some cases, remarkable kinetic inertness. In examples where significant dissociation is evident, such as the noncommercial but well-studied $[Gd(EDTA)(H_2O)_n]^-$, multiple solvent coordination sites accessible to various competing anions undoubtedly contribute to the loss of gadolinium(III). Given the interest in imaging low-concentration receptors, a significant challenge for coordination chemists in the future is to balance the need for higher relaxivity with acceptable stability.

III. Relaxation Theory

A. Introduction

Relaxation theory was discussed in detail in the previous review,[1] but will be reintroduced because it is essential to a discussion of gadolinium(III)-based contrast agents. The presence of a gadolinium(III) complex will increase the longitudinal and transverse relaxation rates, $1/T_1$ and $1/T_2$, respectively, of solvent nuclei. Diamagnetic and paramagnetic relaxation rates are additive and given by eq 14 where $(1/T_i)_{obs}$

$$(1/T_i)_{obs} = (1/T_i)_d + (1/T_i)_p \qquad i = 1, 2 \quad (14)$$

is the observed solvent relaxation rate and the subscripts "*d*" and "*p*" refer to diamagnetic and paramagnetic, respectively. The paramagnetic contribution is dependent on the concentration of paramagnetic species. Relaxivity, r_i, is defined as the slope of the concentration dependence, eq 15. Thus a plot

$$(1/T_i)_{obs} = (1/T_i)_d + r_i[Gd] \qquad i = 1, 2 \quad (15)$$

of $(1/T_i)_{obs}$ versus concentration would give the relaxivity as the slope. Relaxivity is normally expressed in units of $mM^{-1}\ s^{-1}$; however, molal concentrations should be used when dealing with nondilute systems (see section VI).

The origin of paramagnetic relaxation enhancement is generally divided into two components, inner-sphere and outer-sphere, eq 16. Inner-sphere relaxation refers to relaxation enhancement of a solvent molecule directly coordinated to the paramagnetic ion, and outer-sphere relaxation refers to relaxation enhancement of solvent molecules in the second coordination sphere and beyond (i.e., bulk solvent). This separation is used in an attempt to explain observed relaxivities in terms of existing theories. As in the previous review, the emphasis will be on the longitudinal relaxation rate $(1/T_1)$ enhancement of water hydrogen atoms since this is the effect which is of most interest in MRI.

$$(1/T_i)_p = (1/T_i)_{inner-sphere} + (1/T_i)_{outer-sphere} \qquad i = 1, 2 \quad (16)$$

B. Inner-Sphere Relaxation

The equations relating the lifetime, chemical shift, and relaxation rates of solvent molecules in the inner-sphere to NMR observables are given[167,168] in eqs 17−19.

$$\frac{1}{T_1^{IS}} = \frac{qP_m}{T_{1m} + \tau_m} \quad (17)$$

$$\frac{1}{T_2^{IS}} = qP_m \frac{1}{\tau_m}\left[\frac{T_{2m}^{-1}(\tau_m^{-1} + T_{2m}^{-1}) + \Delta\omega_m^2}{(\tau_m^{-1} + T_{2m}^{-1})^2 + \Delta\omega_m^2}\right] \quad (18)$$

$$\Delta\omega_{obs}^{IS} = qP_m\left[\frac{\Delta\omega_m}{(1+\tau_m T_{2m}^{-1})^2+\tau_m^2\Delta\omega_m^2}\right] \quad (19)$$

The IS superscript refers to inner-sphere, P_m is the mole fraction of bound solvent nuclei, q is the number of bound water (or solvent) nuclei per metal ion (i.e., the hydration number), τ_m is the lifetime of the solvent molecule in the complex (τ_m is the reciprocal of the solvent exchange rate, k_{ex}). The "m" subscript refers to the shift or relaxation rate of the solvent molecule in the inner-sphere. $\Delta\omega$ refers to the chemical shift difference between the paramagnetic complex and a diamagnetic reference.

From eq 17, one sees that if the water exchange rate is fast enough such that $\tau_m \ll T_{1m}$, then the relaxation rate enhancement experienced by the bulk solvent will depend on the relaxation rate enhancement for the coordinated solvent molecule ($1/T_{1m}$). The approach generally used to calculate the bound relaxation rates is through the Solomon−Bloembergen−Morgan equations outlined below. Further details can be obtained from the review by Kowalewski and co-workers,[169] or by consulting the books by Bertini and co-workers.[2,170]

$$\frac{1}{T_{im}} = \frac{1}{T_i^{DD}} + \frac{1}{T_i^{SC}} \qquad i = 1, 2 \quad (20)$$

$$\frac{1}{T_1^{DD}} = \frac{2}{15}\frac{\gamma_I^2 g^2 \mu_B^2 S(S+1)}{r^6}\left[\frac{3\tau_{c1}}{(1+\omega_I^2\tau_{c1}^2)} + \frac{7\tau_{c2}}{(1+\omega_s^2\tau_{c2}^2)}\right] \quad (21)$$

$$\frac{1}{T_1^{SC}} = \frac{2}{3}S(S+1)\left(\frac{A}{\hbar}\right)^2\left[\frac{\tau_{e2}}{(1+\omega_s^2\tau_{e2}^2)}\right] \quad (22)$$

$$\frac{1}{T_2^{DD}} = \frac{1}{15}\frac{\gamma_I^2 g^2 \mu_B^2 S(S+1)}{r^6}\left[\frac{3\tau_{c1}}{(1+\omega_I^2\tau_{c1}^2)} + \frac{13\tau_{c2}}{(1+\omega_s^2\tau_{c2}^2)} + 4\tau_{c1}\right] \quad (23)$$

$$\frac{1}{T_2^{SC}} = \frac{1}{3}S(S+1)\left(\frac{A}{\hbar}\right)^2\left[\frac{\tau_{e2}}{(1+\omega_s^2\tau_{e2}^2)} + \tau_{e1}\right] \quad (24)$$

$$\frac{1}{\tau_{ci}} = \frac{1}{T_{ie}} + \frac{1}{\tau_m} + \frac{1}{\tau_R} \qquad i = 1, 2 \quad (25)$$

$$\frac{1}{\tau_{ei}} = \frac{1}{T_{ie}} + \frac{1}{\tau_m} \qquad i = 1, 2 \quad (26)$$

For protons, the two relaxation mechanisms operative are the dipole−dipole (DD) mechanism and the scalar (SC) or contact mechanism. The correlation times that define dipole−dipole and scalar relaxation are τ_{ci} and τ_{ei}, respectively. At high field strengths with slowly rotating molecules the Curie spin relaxation mechanism may become important, but it is negligible at the low fields used in MRI (typically up to 1.5 T). For deuteron or ^{17}O relaxation, quadrupolar mechanisms must also be considered. Equations 21−24 apply to ions with $S > {}^1/_2$ such as Gd(III) ($S = {}^7/_2$). Here, γ_I is the nuclear gyromagnetic ratio, g is the electronic g factor, μ_B is the Bohr magneton, r is the electron spin−solvent nuclear spin distance, ω_s and ω_I are the electron and nuclear Larmor precession frequencies, respectively, and $A/\hbar$ is the electron − nuclear hyperfine coupling constant. These equations describe relaxation as a function of magnetic field (recall that nuclear or electron Larmor frequency is related to magnetic field, B, by the gyromagnetic ratio, γ, $\omega = \gamma B$). In each equation there is a characteristic correlation time, which is related to the different dynamic processes occurring on the molecular level. τ_R is the rotational correlation time related to the reorientation of the metal ion−solvent nucleus vector. T_{1e} and T_{2e} are the electronic longitudinal and transverse relaxation times for the metal ion, sometimes referred to as τ_{s1} and τ_{s2}.

To make matters more complex, the electronic relaxation rates themselves are field dependent. For Gd(III), the electronic relaxation rate is usually ascribed to a transient zero field splitting (ZFS) brought about by solvent collisions or molecular vibrations. This is described by an equation such as eq 27 where the constant B is related to the magnitude of the transient ZFS and τ_v is a correlation time for the modulation of this transient ZFS. Sometimes one sees B written as ${}^1/_5\tau_{s0}$ where τ_{s0} refers to the electronic relaxation time at zero field. Other workers use $B = (1/25)\Delta^2[4S(S+1) - 3]\tau_v$, where Δ is the trace of the ZFS tensor. For T_{2e} an analogous equation exists, where there is also a field independent term, eq 28. The validity of these expressions will be discussed further.

$$\frac{1}{T_{1e}} = B\left[\frac{1}{1+\omega_s^2\tau_v^2} + \frac{4}{1+4\omega_s^2\tau_v^2}\right] \quad (27)$$

$$\frac{1}{T_{2e}} = B\left[\frac{5}{1+\omega_s^2\tau_v^2} + \frac{2}{1+4\omega_s^2\tau_v^2} + 3\right]$$

$$B = \frac{1}{10\tau_{s0}} = \frac{\Delta^2}{50}[4S(S+1) - 3]\tau_v \quad (28)$$

At this point it may be useful to calculate some proton $1/T_1$ relaxation rates as a function of field to show the interplay between the various parameters. In eq 21, the two terms inside the square bracket (the "3 term" and the "7 term") have field dependence. The "3 term" is a function of the nuclear precession frequency while the "7 term" is a function of the electron precession frequency. Since the magnetogyric ratio is much larger for an electron than for a proton ($\gamma_s/\gamma_H = 658$), $\omega_s^2\tau_{c2}^2$ will become much greater than 1 at a much lower magnetic field than $\omega_I^2\tau_{c2}^2$.

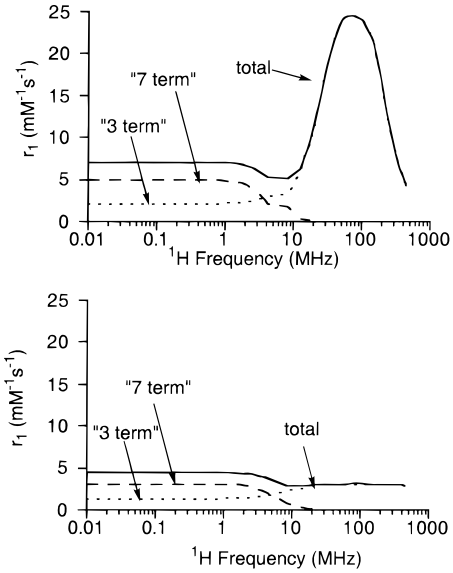

Figure 33. Simulated inner-sphere relaxivities. Top: $\tau_R = 1$ ns. Bottom: $\tau_R = 0.1$ ns. See text for other parameters.

At the field where $\omega_s^2\tau_{c2}^2$ becomes greater than 1, the "7 term" disperses away to approach zero. This is shown in Figure 33. In Figure 33 (top), where the rotational correlation time is lengthened (and hence τ_{c1} as well), the "3 term" dispersion can also be observed. It interesting to note how increasing the overall correlation times, τ_{ci}, increases the bound relaxation rate ($1/T_{1m}$). The relaxation enhancement will approach a maximum as the inverse of the correlation time, $1/\tau_{ci}$, approaches the Larmor precession frequency, ω_I.

Nuclear magnetic relaxation dispersion (NMRD), or the measurement of relaxation rates as a function of magnetic field, is widely used for characterizing contrast agents. Most often reported are proton $1/T_1$ rates for water in the presence of a Gd(III) chelate. The inner-sphere relaxation rate is described by eqs 17, 21, and 22. Because of the ionic nature of bonding in Gd(III) compounds, and the fact that the water proton is separated from the Gd(III) ion by two bonds, the hyperfine coupling constant, $A/\hbar$, is quite small. Thus the scalar mechanism, eq 22, is not very efficient; furthermore because of its $1/\omega_s^2$ dependence it has dispersed at frequencies below 10 MHz. $1/T_1^{IS}$ is determined by $1/T_1^{DD}$ (eq 21) and τ_m (eq 17). The variables in eqs 17 and 21 are: τ_m, τ_R, q, r, T_{1e}, and T_{2e}. The electronic relaxation times, T_{1e} and T_{2e}, are defined by Δ^2 and τ_v. An understanding of how these parameters influence the appearance of the NMRD curve is essential to optimizing relaxivity for a given field strength.

1. Hydration Number and Electron–Nuclear Spin Distance

From eq 17, it is clear that increasing the hydration number, q, will increase the inner-sphere relaxivity. However an increase in q is often accompanied by a decrease in thermodynamic stability and/or kinetic inertness. In attempting to understand the magnitude of relaxivity of a given compound, it is imperative to know its hydration number. Methods for determining q have been outlined in section II.

Table 13. Lanthanide(III)−Oxygen and −Deuterium Distances in Solution

complex	CN	r_{Ln-O} (Å)	r_{Ln-D} (Å)	method
$[Nd(H_2O)_9]^{3+}$	9	2.50	3.14	ND[a]
$[Sm(H_2O)_{8.5}]^{3+}$	8.5	2.46	3.11	ND[a]
$[Dy(H_2O)_8]^{3+}$	8	2.50	3.03	ND[a]
$[Yb(H_2O)_8]^{3+}$	8	2.50	2.98	ND[a]
$Gd^{3+}_{(aq)}$	7.6	2.43		XAFS[b]
$Gd^{3+}_{(aq)}$	8.0	2.37		XRD[c]
$Gd^{3+}_{(aq)}$	8.7	2.41		XAFS[d]
$[Gd(DTPA)(H_2O)]^{2-}$	9	2.490		XAFS[d]
$[Gd(DOTA)(H_2O)]^{2-}$	9	2.447		XAFS[d]

[a] ND = neutron diffraction, ref 171. [b] XAFS = X-ray absorption fine structure, ref 174. [c] XRD = X-ray diffraction, ref 175. [d] Reference 173.

The distance between the water proton and the unpaired electron spin, r, is a difficult parameter to measure and to control. Because of the $1/r^6$ dependence, a decrease of about 0.2 Å would result in a 50% increase in relaxivity according to eq 8. The Gd(III) water oxygen distance ranges from 2.41 to 2.50 Å for monomeric complexes in the solid state (vide supra). Merbach and co-workers [171,172] performed neutron diffraction first-order difference studies on the lanthanide aqua ions Nd^{3+}, Sm^{3+}, Dy^{3+}, and Yb^{3+} using the isotope substitution technique in D_2O. They concluded that Nd^{3+} was nine-coordinate, Sm^{3+} had a coordination number of 8.5 (i.e., there was a dynamic CN9−CN8 equilibrium), and Dy^{3+} and Yb^{3+} were eight-coordinate. The Ln−O and Ln−D distances are given in Table 13. The distances are shorter for the smaller (heavier) ions. This is a consequence of charge-to-radius ratio, but also of differing coordination number. For Gd^{3+}, one would expect a decrease in the Gd−O distance by decreasing the overall CN. Gadolinium−oxygen distances in solution can also be measured by X-ray measurements—X-ray absorption fine structure (XAFS) on relatively dilute solutions[173,174] and by X-ray diffraction (XRD) on more concentrated solutions.[175] It is unlikely that the change from solid state to solution would change the Gd−O bond distance, and this has been verified[173] for $[Gd(DTPA)(H_2O)]^{2-}$ and $[Gd(DOTA)(H_2O)]^{-}$.

Although Gd−O distances are relatively well defined, Gd−H distances are not. This is because the angle between the plane of the water molecule and the Gd−O vector is unknown; neutron diffraction studies, both in the solid and solution state, demonstrate that this angle can be quite varied for aqua complexes. Gd−H distances could, in principle, be measured by solution neutron diffraction. Clarkson et al.[176] used electron spin−echo envelope modulation (ESEEM) spectroscopy to examine Gd(III) complexes of TTHA, DTPA, and EDTA in deuterium oxide solution. The authors report a Gd−D distance of 2.7 Å for the coordinated water distance. This seems very short in light of the neutron diffraction studies.

Electron delocalization onto the ligand to shorten r is not a possibility for Gd(III) complexes. The bonding in Gd(III) complexes is predominantly ionic in nature, and this is reflected in the low $A/\hbar$ values for $H_2{}^{17}O$ coordinated to Gd^{3+} compared with transition metal ions. [170]

2. Rotation

Rotation is perhaps the most critical variable in these equations. It was recognized early[1] that the rotational correlation time of small Gd(III) chelates was the dominant contributor to the effective correlation time τ_{ci}. Strategies to slow rotation in order to improve relaxivity have had varying degrees of success (vide infra). Figure 33 shows calculated r_1^{IS} NMRD curves for two values of τ_R with the other parameters in eqs 17 and 21 being fixed[177] at values reported for $[Gd(DTPA)(H_2O)]^-$. The top NMRD curve is for a rotational correlation time of 1 ns and the bottom for 0.1 ns.

Rotational correlation times can be estimated in a number of ways. Equation 29 can be used for spherical molecules if a good estimate of the radius, a, and the viscosity, η, are known. The problem here is the value of a and also that, in microheterogeneous solutions, the microviscosity may differ from the measured macroscopic viscosity.

$$\tau_R = 4\pi a^3 \eta / 3kT \tag{29}$$

Other magnetic resonance techniques could be employed. Clarkson and co-workers have substituted the vanadyl ion, VO^{2+}, for Gd(III) in a variety of chelates.[178,179] The line shapes observed in the EPR spectra of VO^{2+} containing chelates are very sensitive to rotation. Simulation of the spectrum can afford a τ_R for the vanadyl ion. The problem with this technique is obvious: VO^{2+} is not Gd^{3+}. However, EPR is a very sensitive technique which can allow observation of vanadyl at physiological concentrations (sub-millimolar). Furthermore, the simulation of vanadyl EPR line shapes can distinguish between isotropic and anisotropic motion. In principle, a nitroxide spin label could be incorporated into the ligand, and similar measurements be carried out on a diamagnetic analogue of the chelate. To our knowledge, this approach has not been reported.

Merbach and co-workers often use $H_2{}^{17}O$ T_1 measurements to ascertain τ_R. ^{17}O is a quadrupolar nucleus that is dominantly relaxed via the quadrupolar relaxation mechanism (eq 30)[180] as well as by

$$\frac{1}{T_{q1}} = \frac{3\pi^2}{10}\frac{2I+3}{I^2(2I-1)}\chi^2(1+\eta^2/3)\left[\frac{0.2\tau_R}{1+\omega_I^2\tau_R^2} + \frac{0.8\tau_R}{1+4\omega_I^2\tau_R^2}\right] \tag{30}$$

dipolar relaxation in the presence of Gd(III). Here I is the nuclear spin, χ^2 is the quadrupolar coupling constant, and η is an asymmetry parameter. Gd(III) is not an efficient T_1 relaxation agent for ^{17}O. A small effect is observed, and another unknown is introduced, the $\chi^2(1+\eta^2/3)$ term. In terms of the quadrupolar coupling constant, the value for acidified water is often used. Yet there is no reason to believe that the quadrupolar coupling constant for an oxygen atom in a water molecule directly coordinated to a (+3) metal ion should be the same as that of an oxygen atom in acidified water. If the $\chi^2(1+\eta^2/3)$ term was known for a series of Gd(III) chelates (perhaps from NQR), then this method possesses some advantages. First, the measurement is being made on the Gd(III) complex—there are no metal ion substitutions. In addition, the rotation rate of the Gd(III)$-^{17}O$ vector is being probed, which is directly analogous to that of the Gd(III)$-^1H$ vector in ^1H NMRD.

Carbon-13 relaxation measurements have been made on carbon atoms in the ligand.[100,181] This technique employs a diamagnetic surrogate for Gd(III) such as Y(III), La(III), or Lu(III). The primary drawback here is the inherent insensitivity of ^{13}C NMR. High concentrations or ^{13}C labeling must be employed. High concentrations often preclude working at physiological conditions, while ^{13}C labeling may introduce synthetic challenges.

Recently, Vander Elst et al.[182] have advocated the use of deuterium labeling of the chelate and determining τ_R on a diamagnetic analogue of the Gd(III) complex. The problems here are the same as for ^{13}C: low sensitivity (although the T_1 values are shorter, leading to quicker measurements) and the synthetic challenge of deuterium labeling. In their study, [182] Vander Elst et al. labeled the α-acetate carbons of DTPA by refluxing the ligand overnight in a deuterated K_2CO_3 solution. This is not an alternative for chelates with chemically sensitive functional groups.

Fluorescence polarization spectroscopy[183] is another method of determining τ_R. This method requires the chelate to contain a fluorophore which fluoresces anisotropically and possesses a fluorescent lifetime of the same order of magnitude as τ_R. The problem here is introduction of a suitable fluorophore.

3. Water Exchange

The rate of water exchange between an inner-sphere water molecule and the bulk can usually be estimated by ^{17}O NMR by measuring the transverse relaxation rate of water in the presence and absence of a Gd(III) chelate. Merbach and co-workers[184] have shown that outer-sphere contributions to observed ^{17}O relaxation rates for Gd(III) complexes which contain inner-sphere water molecules are negligible; the observed relaxation rate is the inner-sphere relaxation rate. Because of the time scales involved and the relatively small values of chemical shifts reported for Gd(III)-aqua oxygen atoms, eq 18 reduces to eq 31. Since the oxygen is directly coordinated to the gadolinium(III) ion, $1/T_{2m}$ is dominated by the scalar term, which at high fields reduces to eq 32. A plot of $(1/T_2)_p$ vs reciprocal temperature has

$$\left(\frac{1}{T_2}\right)_p = \frac{1}{T_2^{IS}} = qP_m\left[\frac{1}{\tau_m + T_{2m}}\right] \tag{31}$$

$$\frac{1}{T_{2m}} = \frac{1}{T_2^{SC}} = \frac{1}{3}S(S+1)\left(\frac{A}{\hbar}\right)^2\left(\frac{1}{T_{1e}} + \frac{1}{\tau_m}\right)^{-1} \tag{32}$$

the form of Figure 34. It is useful to obtain data at at least two magnetic fields since $1/T_{1e}$ is field dependent, but $1/\tau_m$ is not. For very fast exchange rates, $T_{2m} \ll \tau_m$, and the $1/\tau_m$ side of the curve may not be observed. Under these conditions the residency

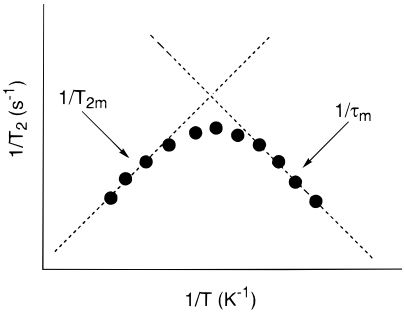

Figure 34. Contributions to the ^{17}O transverse relaxation rate for water coordinated to Gd(III). The circles represent the observed effect, and the dashed lines represent the contributions of $1/T_{2m}$ and $1/\tau_m$.

time cannot be estimated from ^{17}O relaxation measurements alone; some knowledge of T_{1e} is required.

Under neutral pH conditions, the water exchange rate and the proton exchange rate are usually equal. Determining proton exchange rates by NMR is more difficult since dipolar relaxation and outer-sphere relaxation also contribute to $(1/T_2)_p$. Aime et al. have shown that measuring relaxivity as a function of pH can be a good indicator of changes in proton residency time since this is an acid- or base-catalyzed event.[185]

4. Electronic Relaxation

T_{1e} and T_{2e} are the most difficult parameters to determine independently because of their field dependence. Equations 27 and 28 are valid only in the limit (extreme narrowing) $\omega_s^2\tau_v^2 \ll 1$.[2] This represents a monoexponential electronic relaxation process. Outside the extreme narrowing condition, electronic relaxation for an $S = {}^7/_2$ ion (e.g., Gd^{3+}) becomes multiexponential.[186] It has been proposed that at higher frequencies (fields) electronic relaxation can be described by an "average" monoexponential[2] which has the form of eqs 27 and 28. Strandberg and Westlund[186] have derived closed analytical expressions for electronic relaxation under nonextreme narrowing conditions.

The groups of Sharp,[187−195] Westlund,[196,197] Bertini,[2,198] and Kowalewski[169,199,200] have shown that when the energy of the ZFS interaction is larger than that of Zeeman energy, the SBM equations are no longer valid (the so-called low-field region). Physically, in the Zeeman (SBM) limit, the electron spin precesses about the direction of the external magnetic field axis (i.e., in the laboratory reference frame). In the ZFS limit the electron spin precesses about the principal axis of the ZFS tensor (i.e., in the molecular frame). Under these conditions (ZFS limit), nuclear relaxation is strongly dependent upon the angle, θ, between the electron spin−nuclear spin vector and the principal axis of the ZFS tensor. It is also dependent upon the symmetry of the molecule; rhombicity in the ZFS can greatly diminish nuclear relaxation. Qualitatively, the magnetic field dispersion profiles of nuclear relaxation generated using low-field theories look similar to those generated using SBM.

Electronic relaxation parameters of small molecules are often estimated by fitting NMRD curves to the SBM equations from ^1H frequencies ranging from 0.01 to 50 MHz and higher. At some point the ZFS energy will become larger than the Zeeman energy, and the SBM equations will become invalid. Low-field NMRD data fit to the SBM equations may well be "fit", but the parameters obtained may be physically meaningless.

5. Influence of Various Parameters on Inner-Sphere Relaxivity

Relaxivity will reach a maximum when the correlation time τ_{c1} is the inverse of the proton Larmor frequency. For a 0.5 T imaging spectrometer (21 MHz ^1H frequency), the optimum τ_{c1} is 7.4 ns; while for a 1.5 T magnet (64.5 MHz), the optimum τ_{c1} is 2.5 ns. Since τ_m enters into both eqs 17 and 21, there is a trade-off. From eq 17, one wants $\tau_m \ll T_{1m}$; however, if τ_m is too short, it will begin to influence T_{1m}. The optimum value for τ_m is about 10 ns. In Figure 35, the influence of T_{1e}, τ_R, and τ_m on relaxivity at two common imaging fields is displayed. At these field strengths, the "7 term" has dispersed such that T_{2e} is unimportant. These results are simulated with $q = 1$ and $r = 3.1$ Å. Doubling q would double r_1^{IS} and decreasing r would increase r_1^{IS} in an obvious manner. There are two points of interest here. The first is that the maximum relaxivity attainable will decrease with increasing field strength. The second is that as one parameter begins to be optimized, the other parameters become more critical; the slope about the relaxivity maximum is very large. A decline in maximum relaxivity with increasing field strength is offset by an increase in resolution and sensitivity at higher field. Also, T_{1e} is getting longer as field strength increases. At 0.5 T, T_{1e} may be a limiting factor, but at 1.5 T it may have lengthened to the point where it does not influence r_1. At higher fields, contrast agent design need depend on only τ_m and τ_R. The approved contrast agents lie somewhere on the front of these plots; τ_R is on the order of 0.1 ns. It is clear from Figure 35 that there is room for improvement.

6. Some Caveats Concerning SBM

Most of the preceding discussion has been based upon the Solomon−Bloembergen−Morgan equations. The validity of the description of electronic relaxation has been questioned above. A second point not addressed is that of anisotropic rotation. Strategies to increase τ_R include incorporation of a Gd(III) chelate into a polymer, dendrimer, or binding to a macromolecule. Under these circumstances there may be fast internal motion (e.g., side chain rotation) coupled with the overall rotation of the macromolecule. It can be shown that the correlation function that defines relaxation is a function of the overall motion of the macromolecule and the internal motion. This may be approximated using the model free approach of Lipari and Szabo[201] whereby a second spectral density term is added to account for the fast motion. The degree to which fast motion limits relaxation is given by an order parameter.

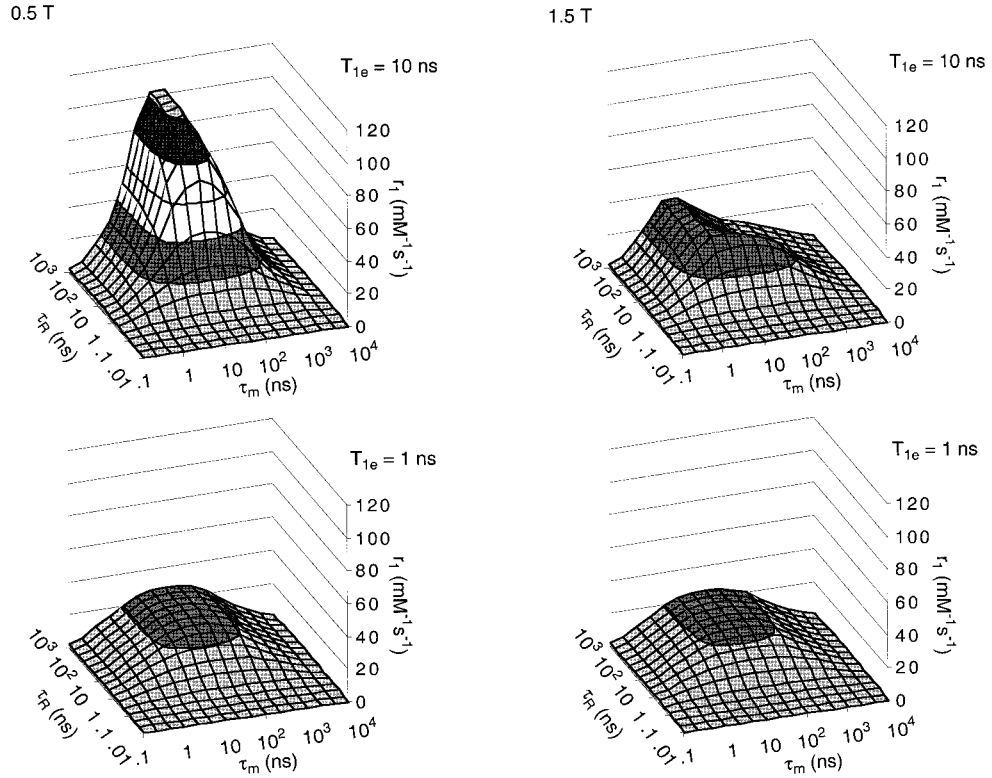

Figure 35. Inner-sphere relaxivities calculated as a function of τ_m and τ_R for various values of T_{1e} at 0.5 T (~21 MHz) and 1.5 T (~64.5 MHz).

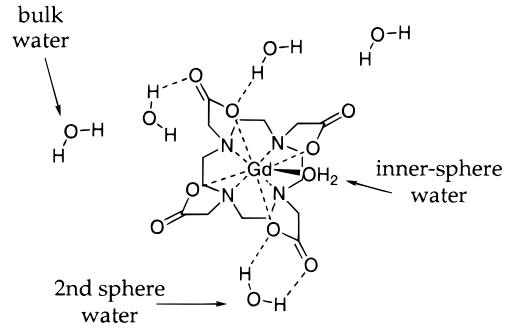

Figure 36. Three classes of water: inner-sphere (directly coordinated to Gd(III)), second-sphere (H-bonded to the complex), and bulk water.

C. Outer-Sphere Relaxation

Coordinatively saturated Gd(III) complexes also enhance relaxivity. This occurs by two mechanisms: second-sphere relaxation and outer-sphere relaxation. Second-sphere relaxation occurs when water molecules in the second coordination sphere (H-bonded to lone pairs on the carboxylate oxygen atoms), see Figure 36, are relaxed via a dipolar mechanism. This can also be described by eqs 17 and 21 where the relevant parameters are usually denoted with a prime, q', r', etc. This is difficult to quantify since the number of second-sphere water molecules is unknown, the Gd−H distance is unknown, and τ_m is very short and the likely limiting parameter in determining T_{1m}.

Outer-sphere relaxation arises from the translational diffusion of water molecules near the Gd(III) complex. Water molecules and the Gd(III) complex are often treated as hard spheres,[202,203] and the outer-sphere relaxation rates are described by eqs 33 and 34

$$\frac{1}{T_1^{OS}} = C[3j(\omega_I) + 7j(\omega_S)] \quad (33)$$

$$\frac{1}{T_2^{OS}} = C[2 + 1.5j(\omega_I) + 6.5j(\omega_S)] \quad (34)$$

$$C = \left(\frac{32\pi}{405}\right)\gamma_I^2\gamma_S^2\hbar^2 S(S+1)\frac{N_A M}{1000aD}$$

$$j(\omega) = \mathrm{Re}\{[1 + {}^1/_4[i\omega\tau_D + (\tau_D/T_{1e})]^{1/2}]/[1 + [i\omega\tau_D + (\tau_D/T_{1e})]^{1/2} + {}^4/_9[i\omega\tau_D + (\tau_D/T_{1e})] + {}^1/_9[i\omega\tau_D + (\tau_D/T_{1e})]^{3/2}]\}$$

where N_A is Avogadro's number, M is the concentration of the complex, a is the distance of closest approach of the water molecule and the complex, D is the sum of the diffusion constants of water and the complex, and τ_D is a diffusional correlation time given by $\tau_D = a^2/D$.

Separation of the two contributions in a $q = 0$ chelate is not obvious. An approach often taken in determining the inner-sphere relaxivity is to subtract the relaxivity of a $q = 0$ complex such as $[Gd(TTHA)]^{3-}$ or $[Gd(TETA)]^-$ from the observed r_1 and hope that this a reasonable estimation of outer-sphere plus second-sphere relaxivity.[77,204] Often the second-sphere contribution is ignored and the observed r_1 fit to the sum of eqs 17 and 33.

D. Data Fitting of NMRD Curves

It is apparent from the previous discussion of the complexity of the parameters determining proton

Table 14. Kinetic Parameters for Water Exchange at Various Gd(III) Complexes

ligand	k_{ex}^{25} (10^6 s^{-1})	τ_m^{37} (ns)	$\Delta H^{\ddagger}$ (kJ mol^{-1})	$\Delta S^{\ddagger}$ (J K^{-1} mol^{-1})	$\Delta V^{\ddagger}$ (cm^3 mol^{-1})	ref
aqua	804	0.94	15.3	−23.1	−3.3	177
DTPA	3.30	130	51.6	53	12.5	177
EOB-DTPA	3.60	124	49.1	45.2	12.3	215
MP-2269	4.20	102	51.6	55.8		220
COPTA	3.40					228
DTPA-N′-MA	1.90	230	50.6	40.2	10.6	215
DTPA-N-MA	1.30	346	48.6	35.7	12.7	215
DTPA-BMA	0.45	1000	47.6	22.9	7.3	177
DTPA-BMEA	0.39	1130	49.8	27	7.4	217
DTPA-BPDA	0.36	1400	41	−1.1	6.7	100
DTPA-BGLUCA	0.38	1200	47.6	21.7	6.8	100
DTPA-BENGALAA	0.22	2252	42.5	0	5.6	100
DOTA	4.10	108	49.8	48.5	10.5	177
DO3A-MNBA	1.60	317	40.9	11.1	7.7	212
$(DO3A)_2L2$	1.00	602	30	−29	0.5	177
$(DO3A)_2L6$	1.50	376	34.2	−11.7		213
$(DO3A)_2L7$	1.40	377	38.5	1.7	2.3	177
DO3A	6.25	77	44	33		225
PCTP-[13]	125	3	58	105		231
PCTA-[12]	14	34	45	43		225
PCTP-[12]	170	5	14	−40		225
EGTA	31	16	42.7	42	10.5	215
PDTA	100	8	11	−54.6	−1.5	207
taci	11	34	59.8	−89	−12.7	217

relaxation as a function of magnetic field. Assuming that SBM equations are valid and that there is no second-sphere relaxation and that outer-sphere relaxation can be described by eq 20, there are still eight parameters to be fit: τ_m, τ_R, τ_v, Δ^2, q, r, D, and a. Fitting a rather featureless curve like the NMRD profile of $[Gd(DTPA)(H_2O)]^{2-}$ to eight parameters is meaningless. Often what one sees is that certain parameters are arbitrarily fixed and a limited number fit. Unfortunately ranges of values or values with errors representing a 95% confidence limit are rarely given so that it is difficult for the reader to ascertain which parameters strongly influence the fit. For example, values of τ_m may vary over 3 orders of magnitude and still produce an identical NMRD curve for a small molecule, whereas τ_R may be limited to values within a factor of 2. Only when several of these parameters can be determined independently can any credence be given to the result of an NMRD fit.[205] Operating on this principle, the next section will discuss the relaxivities and relevant physical parameters for small molecule Gd(III) chelates.

IV. Physical Properties of Small Molecule Gadolinium Complexes

A. Water Exchange

It had been assumed that water exchange rates for Gd(III) complexes were very fast, on the order of 10^9 s^{-1}, similar to that of $[Gd(H_2O)_8]^{3+}$.[206] In 1993 Micskei et al.[184] showed that the water exchange rates for $[Gd(DTPA)(H_2O)]^{2-}$ and $[Gd(DOTA)(H_2O)]^{-}$ (Chart 1) were lower by about 3 orders of magnitude compared with the Gd^{3+} aqua ion. The Merbach group has since shown that Gd(III) water exchange rates can vary over 4 orders of magnitude.[100,177,184,207−220] Recently a tripositive europium complex was shown to have an exceedingly slow water exchange rate in a water−acetonitrile mixture.[221] If the analogous Gd(III) complex has a similar rate (which is likely), then the rate of water exchange would vary by almost 7 orders of magnitude for known complexes! In Table 14 the water exchange rates, water residency times, activation parameters, and volumes of activation determined from ^{17}O NMR are given for a host of Gd(III) complexes.

Table 15. Kinetic Parameters for Water Exchange at Ln(III)-DTPA-BMA Complexes[222]

Ln(III)	k_{ex}^{25} (10^6 s^{-1})	τ_m^{37} (ns)	$\Delta H^{\ddagger}$ (kJ mol^{-1})	$\Delta S^{\ddagger}$ (J K^{-1} mol^{-1})	$\Delta V^{\ddagger}$ (cm^3 mol^{-1})
Nd	0.53	922	43.4	10.2	−0.8
Eu	0.66	676	49.2	31.5	8.5
Gd	0.45	1000	47.6	22.9	7.3
Tb	1.61	272	50.3	42.6	9.8
Dy	3.53	127	48.9	44.4	7.3
Ho	5.98	69	54.2	66.6	9.4

The complexes clinically available are all nine-coordinate, with the polyaminopolycarboxylato ligand providing eight donors, and a water molecule occupying the ninth coordination site. These complexes all have large positive values of $\Delta V^{\ddagger}$ which is indicative of a dissociative mechanism. This is also suggested by the positive entropies of activation for these complexes, $\Delta S^{\ddagger}$.

There are two studies[222,223] on the effect of varying the lanthanide ion on the water exchange rate, and these are summarized in Tables 15 and 16. In the case of DTPA-BMA (Chart 4), water exchange at Nd(III) is the slowest and the volume of activation suggests an interchange, I, process (Table 15). The exchange rate increases by a factor of 10 on going from Nd(III) to Ho(III). In the PDTA system, where $q = 2$, the exchange rate decreases from Gd(III) to Yb(III) by almost 2 orders of magnitude. The mechanism also appears to change as $\Delta V^{\ddagger}$ is negative from Gd(III) to Tm(III) but positive for Yb(III). This suggests a change from an I_A (or A) mechanism for the gadolinium complex to an I_D (or D) mechanism

Table 16. Kinetic Parameters for Water Exchange at Ln(III)-PDTA Complexes[223]

Ln(III)	k_{ex}^{25} (10^6 s^{-1})	τ_m^{37} (ns)	$\Delta H^{\ddagger}$ (kJ mol^{-1})	$\Delta S^{\ddagger}$ (J K^{-1} mol^{-1})	$\Delta V^{\ddagger}$ (cm^3 mol^{-1})
Gd	100	8	11	−54.6	−1.5
Tb	24	30	19	−47.6	−7.6
Dy	6.6	100	24.2	−33.1	−5.5
Er	0.56	890	42.1	6.3	−6.5
Tm	0.35	1340	46	15.5	−1.2
Yb	0.28	2000	34.8	−23.6	7.4
Er(EDTA)	9.8	69	22.7	34.8	ND

for the ytterbium complex. The results are summarized in Table 16.

It is clear that changing the size of the ion can dramatically alter k_{ex}. This is not neccessarily true for altering substituents on a given ligand. The kinetic parameters for Gd(III) complexes of DTPA, COPTA, MP-2269, and EOB-DTPA (Chart 2) are all very similar. Likewise the various bisamides of DTPA all have similar kinetic parameters. This suggests that the water exchange rates for these types of chelates incorporated into macromolecules will not vary significantly, and in some instances this has been shown (see section V).

Coincidentally, $[Gd(DOTA)(H_2O)]^-$ has very similar water exchange parameters to $[Gd(DTPA)(H_2O)]^{2-}$. Replacement of one carboxylato donor by an amide donor results in a decrease in the exchange rate by a factor of 3−4.[224] The bisamides of DTPA have exchange rates which are slower still. The effect of this is that for compounds such as $[Gd(DTPA\text{-}BMA)(H_2O)]^-$ τ_m is of the same magnitude as T_{1m}. Since $r_1 \alpha 1/(T_{1m} + \tau_m)$, the relaxivity of these compounds can become limited by the slow water exchange rate. This is especially true in instances when T_{1m} can be shortened by slowing down the tumbling time of the molecule. The Eu(III) complex of the tetraamide DOTAM (Chart 14) has the slowest water exchange rate reported to date for a lanthanide. The complex $[Gd(DTMA)(H_2O)]^{3+}$ is another instance of a tetraamide ligand with an exceedingly slow water exchange rate.[185] Indeed, the relaxivity of this $q = 1$ complex is more consistent with a $q = 0$ complex at neutral pH, since for relaxivity purposes it is exchange inert.

A few other ligand systems have been studied. The $[Gd(EGTA)(H_2O)]^-$ complex exchanges faster than $[Gd(DTPA)(H_2O)]^{2-}$, dispelling simple-minded notions that complex charge dictates water exchange dynamics.[214] The pyridine-based macrocycles have different dynamic properties as well.[225,226] There is clearly room for more study to delineate the factors which influence water exchange at Gd(III).

B. Proton Exchange

Water exchange measurements give a lower limit for proton exchange, $\tau_m^O \geq \tau_m^H$. Proton exchange of a bound water molecule with the bulk is likely to be acid- or base-catalyzed as it is for proton transfer in pure water. One way to observe this is to measure proton relaxivity as a function of pH. This is best observed at low temperatures where τ_R will be longer, making T_{1m} comparable to τ_m. Aime and co-workers have observed this phenomenon for a bisamide derivative of DTPA with gadolinium(III)[227] and with the complex $[Gd(DTMA)(H_2O)]^{3+}$ noted above.[185] This may be a more widespread phenomenon, but not readily observable in chelates with shorter water residency times since $\tau_m \ll T_{1m}$. A recent report on the $[Gd(COPTA)(H_2O)]^{2-}$ complex supports this hypothesis.[228]

C. Electronic Relaxation

Electronic relaxation parameters for a selection of Gd(III) complexes (see Charts 14−16 for additional ligand structures) are listed in Table 17. The NMRD literature tends to use τ_{s0} while the EPR literature usually refers to Δ^2. Both are listed in the table with the conversion factor being given in eqs 27 and 28. A selection of EPR line widths are given in Table 18 to give a sense of T_{2e} at a given field strength.

Most of the information on electronic relaxation is indirect, coming from NMRD studies.[28,53,95,100,160,177,204,225,228−239] These data must be viewed with caution in light of the previous discussion on the uncertainty of the contribution of outer-sphere relaxation, the magnitude of r, the validity of the Bloembergen−Morgan equations describing the field dependence of T_{1e} and T_{2e} (especially at low fields), and of the large number of parameters used in fitting the data. Some generalizations can be made. DOTA-type chelates and monoamide or monohydroxyl derivatives of DOTA all have longer τ_{s0} (smaller Δ^2) values than all other Gd(III) compounds studied. Physically this translates to a higher low-field (0.01 MHz) relaxivity, and this is shown in Figure 37 along with the NMRD profiles of $[Gd(DTPA)(H_2O)]^{2-}$ and $[Gd(DTPA\text{-}BMA)(H_2O)]$. Interestingly, symmetric phosphonate, phosphinate, and phosphonic ester derivatives of DOTA do not show this effect (long τ_{s0}), suggesting that there may be another effect besides molecular symmetry which influences low-field relaxivity.

X-band line widths range from 90 to over 1200 G which is indicative of the disparate relaxation behavior of the Gd(III) ion in different environments.[237] The X-band data seem to correlate with low field relaxivity. As expected from Bloembergen−Morgan, Gd(III) EPR line widths decrease with increasing field strength, Table 18. It is interesting perhaps that the great difference in low-field electronic relaxation rate between $[Gd(DOTA)(H_2O)]^-$ and $[Gd(DTPA)(H_2O)]^{2-}$ is not nearly as marked at high field. At X-band $1/T_{2e}$ is 6−7 times faster for $[Gd(DTPA)(H_2O)]^{2-}$, but only twice as fast at Q-band, and at the highest field (5 T), only one-third as fast.

Subtle changes in solvation can have a dramatic effect on electronic relaxation. Sur and Bryant[240] showed that the addition of nitrite to a gadolinium chloride solution causes a marked decrease in X-band line width. The authors showed that this was consistent with the formation of a second-sphere nitrite complex. Addition of carbonate ion had the opposite effect.

Shukla et al.[241] carried out a pulsed EPR study at X-band over the temperature range 18−100 K and

Table 17. Electronic, Rotation, Gd(III)−H Distances, and Hydration Numbers for a Selection of Gd(III) Complexes

ligand	temp (°C)	τ_v (ps)	τ_R (ps)	τ_{s0} (ps)	Δ^2 (10^{19} s^{-2})	r	q	o.s. model	method	ref
aqua	25	7.3	41	96	11.90	3.13	1	fit	NMRD/O-17	177
DOTA	37	65	56	650	0.20	3.13	1.15	TTHA	NMRD	160
	5	9	100	430	2.15	3.13	1.15	TTHA	NMRD	160
	25	11	77	473	1.60	3.13	1	fit	NMRD/O-17	177
DOTA-pNB	39	4.9	58	497	3.42	3.02	1	fit	NMRD	95
DOTA-pNB	25	7.4	81	420	2.68	3.02	1	fit	NMRD	95
DOTA-pNB	10	15	113	271	2.05	3.02	1	fit	NMRD	95
DO3A	25	14	66	129	4.6	3.15	2	fit	NMRD	225
$(DO3A)_2L6$	25	19	171	258	1.70	3.13	1	fit	NMRD/O-17	177
$(DO3A)_2L7$	25	15	106	265	2.10	3.13	1	fit	NMRD/O-17	177
DOTEP	35	20	72	86	4.84	3.26	1	fit	NMRD	235
	25	27	107	92	3.35	3.26	1	fit	NMRD	235
	5	33	189	96	2.63	3.26	1	fit	NMRD	235
	37	18	65	49	9.45	3.13	0.7	TTHA	NMRD	160
	37	15	57	41	13.55	3.13	0.8	TTHA	NMRD	160
	5	33	180	120	2.10	3.13	0.7	TTHA	NMRD	160
	5	26	160	100	3.21	3.13	0.8	TTHA	NMRD	160
DOTPME	37	11	53	86	8.81	3.13	0.6	TTHA	NMRD	160
	37	10	43	80	10.42	3.13	0.7	TTHA	NMRD	160
	5	8.4	140	150	6.61	3.13	0.7	TTHA	NMRD	160
	5	8.4	120	140	7.09	3.13	0.8	TTHA	NMRD	160
DOTPMB	37	9.4	130	67	13.23	3.13	0.2	TTHA	NMRD	160
	37	8.2	82	41	24.79	3.13	0.3	TTHA	NMRD	160
	5	11	160	480	1.58	3.13	0.2	TTHA	NMRD	160
	5	17	110	330	1.49	3.13	0.3	TTHA	NMRD	160
DOTMP-MMBzA	37	9	61	91	10.18	3.4	1	fit	NMRD	230
DOTMP-MMBzA	25	18	100	122	3.79	3.4	1	fit	NMRD	230
DOTMP-MMNA	37	8.4	60	113	8.78	3.44	1	fit	NMRD	230
DOTMP-MMNA	25	16	91	124	4.20	3.44	1	fit	NMRD	230
DOTMP-MMNA	5	24	190	118	2.94	3.44	1	fit	NMRD	230
DTPA	25	25	58	72	4.60	3.13	1	fit	NMRD/O-17	177
EOB-DTPA	25	4	178	91	23	NA	1	NA	O-17	215
COPTA	25	25	80	83	4	2.96	1	fit	NMRD	228
BOPTA	25	26	88	76	4.22	2.96	1	fit	NMRD	28
DTPA-N′-MA	25	3.1	155	87	31	NA	1	NA	O-17	215
DTPA-N-MA	25	3	143	107	26	NA	1	NA	O-17	215
DTPA-N-MBA	25	17	98	70	7.00	3.10	1	TTHA	NMRD	238
DTPA-BMA	25	25	66	81	4.10	3.13	1	fit	NMRD/O-17	177
	35	15	58	72	7.72	3.1	1	fit	NMRD	234
	25	17	72	65	7.54	3.1	1	fit	NMRD	234
	5	21	107	89	4.46	3.1	1	fit	NMRD	234
	37	13	77	50	12.82	3.1	1	TTHA	NMRD	204
	5	2.4	>100	15	231.48	3.1	1	TTHA	NMRD	204
DTPA-BPDA	25	15	162	116	4.8	3.1	1	fit	NMRD/O-17	100
DTPA-BGLUCA	25	14	183	94	6.3	3.1	1	fit	NMRD/O-17	100
DTPA-BENGALAA	25	16	265	98	5.3	3.1	1	fit	NMRD/O-17	100
DTPA-BPhA	25	19	80	93	4.72	3.14	1	NG	NMRD	232
DTPA-B^{n}PA	37	26	81	57	5.62	3.1	1	TTHA	NMRD	204
DTPA-BBuA	37	25	93	53	6.29	3.1	1	TTHA	NMRD	204
DTPA-BMEA	37	21	88	53	7.49	3.1	1	TTHA	NMRD	204
DTPA-BHpA	37	60	120	85	1.63	3.1	1	TTHA	NMRD	204
DTPA-BMPEA	37	32	86	57	4.57	3.1	1	TTHA	NMRD	204
DTPA-BDHEA	37	46	84	76	2.38	3.1	1	TTHA	NMRD	204
DTPA-B^{n}PA	5	11.4	223	12	60.92	3.1	1	TTHA	NMRD	204
DTPA-BBuA	5	20	66	12	34.72	3.1	1	TTHA	NMRD	204
DTPA-BMEA	5	9	28	9	102.88	3.1	1	TTHA	NMRD	204
DTPA-BHpA	5	60	240	270	0.51	3.1	1	TTHA	NMRD	204
DTPA-BMPEA	5	2.4	56	1.9	1827.49	3.1	1	TTHA	NMRD	204
DTPA-BDHEA	5	20	22	0.8	520.83	3.1	1	TTHA	NMRD	204
PC2A	37	23	40	96	3.77	3.06	3.3	BPO4A	NMRD	229
	25	27	54	93	3.32	3.06	3.3	BPO4A	NMRD	229
	15	14	79	75	7.94	3.06	3.3	BPO4A	NMRD	229
	5	27	96	71	4.35	3.06	3.3	BPO4A	NMRD	229
PCTA-[12]	37	15	44	87	6.39	3.06	2.4	BPO4A	NMRD	229
	25	21	60	104	3.82	3.06	2.4	BPO4A	NMRD	229
	15	19	80	85	5.16	3.06	2.4	BPO4A	NMRD	229
	5	24	106	87	3.99	3.06	2.4	BPO4A	NMRD	229
PCTA-[12]	25	28	70	106	2.8	3.1	2	fit	NMRD	225
PCTP-[12]	25	19	106	56	7.8	3.06	1	fit	NMRD	225
PCTA-[13]	25	32	NG	141	1.85	3.2	1	fit	NMRD	255
PCTP-[13]	25	31	102	90	3	3	1	DOTP	NMRD	231
BP2A	37	19	47	119	3.69	3.06	3.5	BPO4A	NMRD	229
	25	42	64	140	1.42	3.06	3.5	BPO4A	NMRD	229
	15	37	87	104	2.17	3.06	3.5	BPO4A	NMRD	229
	5	35	102	89	2.68	3.06	3.5	BPO4A	NMRD	229

Table 17 (Continued)

ligand	temp (°C)	τ_v (ps)	τ_R (ps)	τ_{s0} (ps)	Δ^2 (10^{19} s^{-2})	r	q	o.s. model	method	ref
NOVAN	35	41	166	105	1.94	3.1	4	TTHA	NMRD	237
NOVAN	5	31	143	80	3.36	3.1	4	TTHA	NMRD	237
Tx	37	46	120	140	1.29	3.13	3.5	TTHA	NMRD	236
Tx	25	62	160	145	0.93	3.13	3.5	TTHA	NMRD	236
Tx	5	42	295	130	1.53	3.13	3.5	TTHA	NMRD	236
N_6–L1	39	9.1	87	46	19.91	2.91	3	fit	NMRD	239
N_6–L1	25	13	105	59	10.86	2.91	3	fit	NMRD	239
N_6–L1	4	21	192	73	5.44	2.91	3	fit	NMRD	239

[a] NA = not applicable; ND = not determined; NG = not stated; o.s. = outer-sphere.

Chart 14

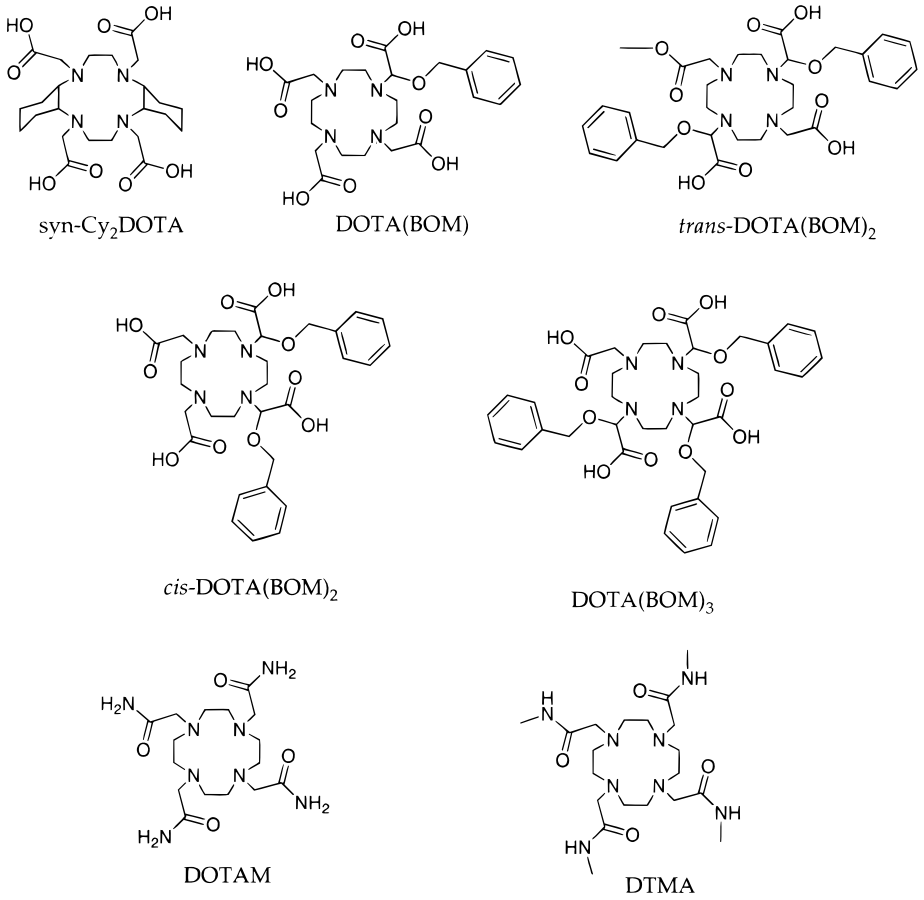

Table 18. EPR Line Widths for Selected Gd(III) Complexes at Three Magnetic Fields

ligand	X-band (0.34 T) line width (G)	Q-band (1.2 T) line width (G)	2 mm (5.0 T) line width (G)
DTPA[a]	604	103	16.1
DOTA[a]	91	57	11.7
DTPA-BMA[a]	428	75	18.0
DOTP[b]	531		
aqua	527,[a] 492[c]	195	52.5
aqua + CO_3^{2-}	890[c]		
aqua + NO_2^-	173[c]		

[a] Reference 177. [b] Reference 237. [c] Reference 240.

measured T_{1e} using an inversion recovery method. The results correlate roughly with the low-field (0.01−0.1 MHz) r_1 values for these complexes. It would appear that increasing structural rigidity slows down the longitudinal electronic relaxation rate, at least at very low temperatures (Table 19). This is likely an effect of minimizing the static ZFS. It would be interesting to estimate the T_{1e} values at a higher field by ^{17}O NMR to determine whether this trend still holds.

Merbach and co-workers performed several variable field EPR studies in conjunction with ^{17}O NMR measurements and sometimes ^1H NMRD. They find that $1/T_{2e}$ as determined by line width measurements can be well described by the semiempirical expression in eq 35.[242] Longitudinal ($1/T_{1e}$) values are inferred

$$\frac{1}{T_{2e}} = \Delta^2\tau_v\left[\frac{5.26}{1 + 0.372\omega_s^2\tau_v^2} + \frac{7.18}{1 + 1.24\omega_s\tau_v}\right] \quad (35)$$

from ^{17}O NMR transverse relaxation rates via eq 32, and from ^1H NMRD via eq 8. The field dependence of $1/T_{1e}$ is given by eq 27. All the relaxation data are then fitted simultaneously.[177] This is a usefull method since it allows the field dependence of $1/T_{ie}$ to be probed over a broad field range. At high fields it was

Chart 15

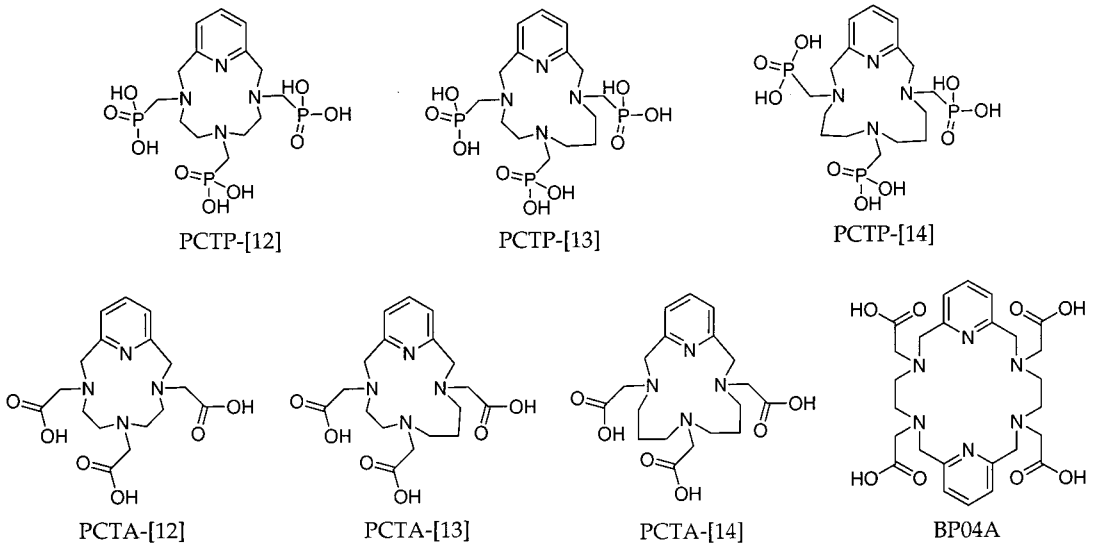

Chart 16

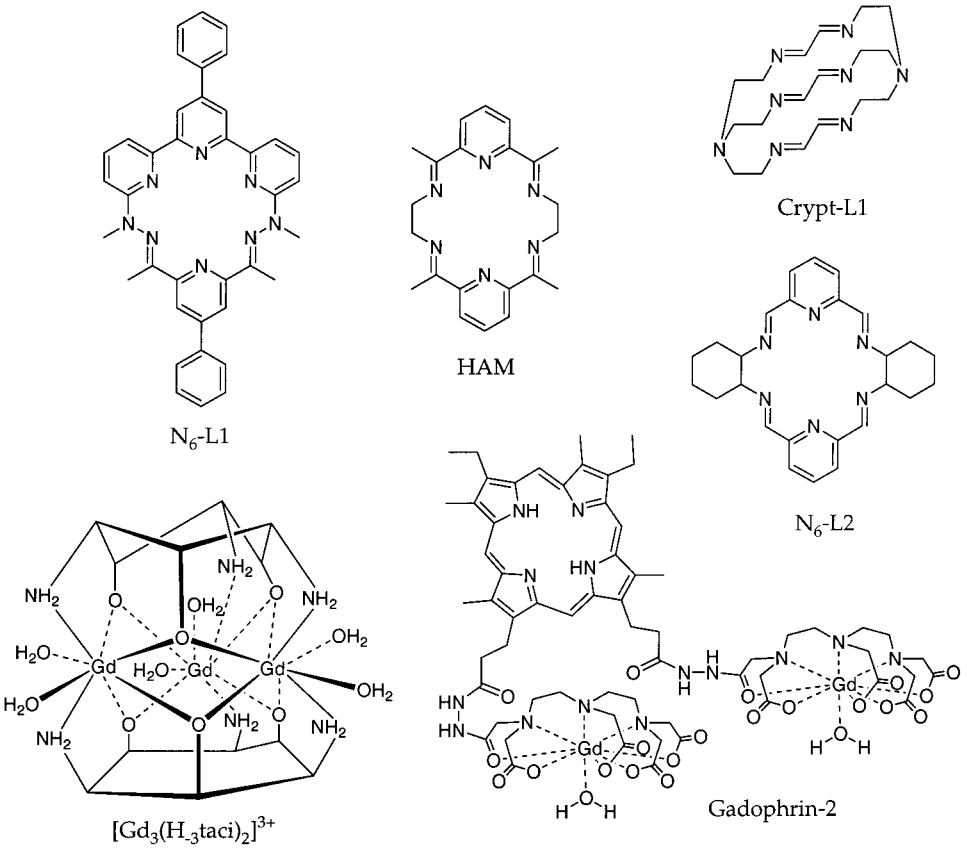

Table 19. Directly Measured T_{1e} Values (X-band) for Four Gd(III) Complexes at Low Temperature[241]

ligand	T_{1e} at 17.9 K (μs)	T_{1e} at 100 K (μs)
DTPA	58.5	0.81
DOTA	56.8	1.27
Cy_2DOTA	82.0	1.37
DOTMA	90.2	1.34

sometimes necessary to include a second relaxation mechanism, which the Lausanne group ascribed to a spin rotation mechanism which is field independent. This is perhaps not surprising given that $1/T_{1e}$ is predicted to decrease with the square of the field and these ^{17}O NMR measurements were made at 14.1 T. Since relaxation times are much longer at high fields (approaching microseconds), the advent of pulsed high-field EPR may illuminate the mechanisms underlying electronic relaxation of Gd(III) complexes.

Merbach and co-workers have also examined several systems in which there exist more than one Gd(III) ion. These are the dimers[177] $[Gd_2(DO3A)_2L6(H_2O)_2]$ and $[Gd_2(DO3A)_2L7(H_2O)_2]$ and the trinuclear $[Gd_3(H_{-3}taci)_2(H_2O)_6]^{3+}$ complex (Charts 16 and 17).[217] Here a dipolar coupling relaxation mechanism was

Chart 17

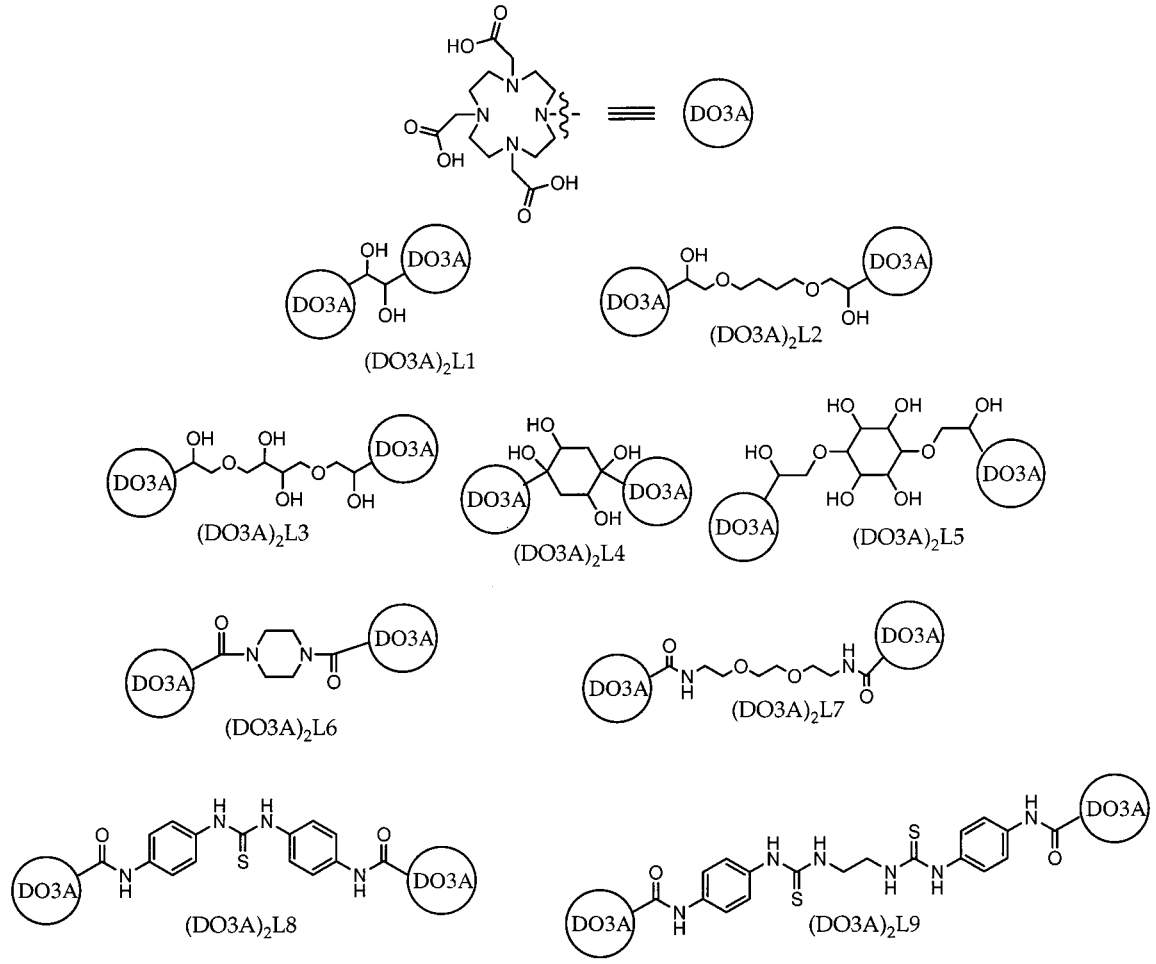

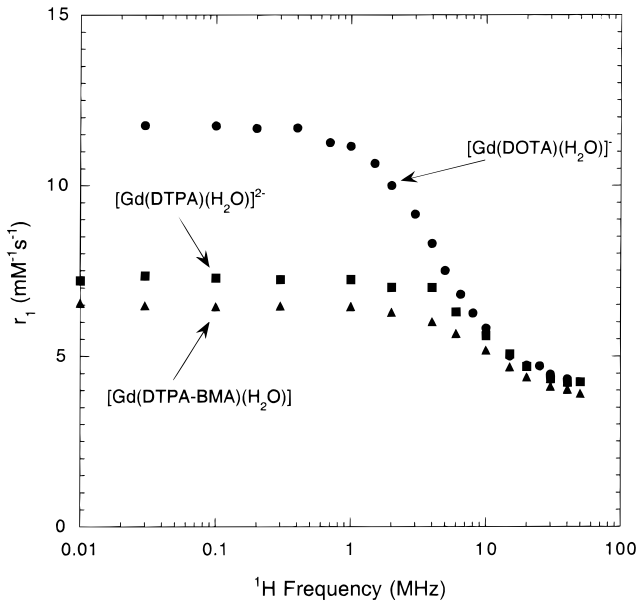

Figure 37. NMRD curves for three clinically approved gadolinium(III) chelates at 25 °C.

invoked to account for the relaxation of one Gd(III) ion by another. The taci system is of particular interest because of the close proximity of the Gd(III) ions, 3.7 Å. There is very little magnetic exchange in this system, $J = -0.092$ cm^{-1}, and the electronic relaxation could be accounted for by a dipolar mechanism modulated on a vibrational time scale. However this mechanism only dominated at high magnetic fields; the consequence for contrast agent design is that aggregation of Gd(III) centers in a multimeric environment is unlikely to limit ^{1}H relaxivity.

D. Relaxivity

The relaxivity of these low molecular weight species is dominated by rotation, especially at ^{1}H Larmor frequencies greater than 10 MHz. Most of the 20 MHz relaxivities can be accounted for by assuming an approximately equal contribution to outer- and second-sphere relaxivity with the inner-sphere relaxivity determined by a fast rotational rate. As noted in the previous section, electronic relaxation can influence low field (<1 MHz) relaxivities; however, the similarity in relaxivity at 20 MHz for [Gd(DOTA)(H$_2$O)]$^-$, [Gd(DTPA)(H$_2$O)]$^{2-}$, and [Gd(DTPA-BMA)(H$_2$O)] can be attributed to the similar rotational correlation times of the three complexes. In Tables 20 and 21, relaxivities are collected for a variety of gadolinium(III) chelates.[23,28,33−35,40,49,51,64,65,85,87,144,150,152,159,160,162,185,204,225−227,231,239,243−264] Tweedle and co-workers[265] have shown that relaxivity per gadolinium(III) correlates well with molecular weight for a series of monomeric and multimeric gadolinium(III) chelates (Charts 17−19) and this is shown in Figure 38 (data in Table 21). For spheroidal molecules, increases in relaxivity increase approxi-

Table 20. Relaxivities for Various Gd(III) Complexes

compound	r_1 ($mM^{-1}\,s^{-1}$)	r_2 ($mM^{-1}\,s^{-1}$)	^{1}H freq (MHz)	temp (°C)	pH[a]	ref
		DTPA Derivatives				
DTPA	4.3		20	25	7.4	253
DTPA	3.8		20	25		241
BOPTA	5.2		20	25	7.4	253
EOB	5.3		20	37		260
MP-2269	6.2		20	40		258
B-21326/7	6.78	7.77	20	39	7.0	246
MS-325	6.6		20	37	7.4	301
DTPA-L1	3.7		20			252
BOPTA	4.39	5.56	20	39	7.4	28
		DOTA Derivatives				
DOTA	4.2		20	25	7.4	253
DOTA	3.56	4.75	20	39	7.3	49
DOTA	4.8		20	40		257
DOTA	3.5		20	25		241
syn-Cy_2DOTA	4.5		20	25		241
DOTMA	3.8		20	25		241
DOTA-pNB	5.4		20	25		95
DOTA(BOM)	5.4		20	25	7.4	243
cis-$DOTA(BOM)_2$	6.8		20	25	7.4	243
trans-$DOTA(BOM)_2$	6.5		20	25	7.4	243
$DOTA(BOM)_3$	7.5		20	25	7.4	243
DOTA(BOM)	5.4		20	25	7.4	253
cis-$DOTA(BOM)_2$	5.7		20	25	7.4	253
trans-$DOTA(BOM)_2$	5.8		20	25	7.4	253
$DOTA(BOM)_3$	6.7		20	25	7.4	253
		DTPA-Monoamides				
DTPA-MpNPA	5.08		20	25		261
		DTPA-Bisamides				
DTPA-BMA	4.58		20	5		177
DTPA-BMA	4.39		20	25		177
DTPA-BMA	3.96		20	35		177
DTPA-BMEA	4.7		20	40		259
DTPA-BPA	4.66		20	25		261
DTPA-BPA	4.86			25		33
DTPA-BpAPA	4.12		20	25		261
DTPA-BpNPA	3.78		20	25		261
DTPA-BpTFPA	3.71		20	25		261
DTPA-B^{i}PA	4.27			25		33
DTPA-B^{i}BA	5.09			25		33
DTPA-BMMEA	4.1		20	40		259
DTPA-BHMEA	4.2		20	40		259
DTPA-BBA	4.50			25		33
DTPA-BBA	4.8		20	25	7	227
DTPA-BBA	6.5		20	25	12	227
DTPA-BBA	4.08	6.01	20	37	7	34
		DTPA Cyclic Amides				
DTPA-*cis*-BAM	3.2		20	40		144
DTPA-PenAM	3.6		20	40		144
DTPA-OAM	4.2		20	40		144
16-DTPA-PN	2.8		64	24		40
16-DTPA-PN	3.7		250	24		40
17-DTPA-BN	2.5		64	24		40
17-DTPA-BN	3.4		250	24		40
16-DTPA-PN−OH	3.5	4.4	250	23		39
		DO3A Derivatives				
HP-DO3A	3.7		20	40		257
HP-DO3A	3.65		20	40		85
HP-DO3A	3.7		20	40		51
DO3MA	4.4		20	40		51
DO3A	4.8		20	40		51
DO3A−L2	4.49	5.99	20	39	7.3	49
DO3A−L1	4.03	5.35	20	39	7.3	49
DO3A−L4	5.19	7.29	20	39	7.3	49
DO3A−L3	4.33	6.36	20	39	7.3	49
		$q = 0$ Compounds				
DOTPMB	2.8					160
BPO4A	1.71	1.74	40	25	7	229
BPO4A	1.66	1.83	40	25	12	229
DOTPMe	2.09	2.34	64	25		162
DOTMP-MBBzA	3.09		20	25		256
DOTMP-MPA	3.08		20	25		256
$CF_3CH_2PO_3$DOTA	2.5		40	25	6.8	87
DOTEP	5.1		40	25	7	159

Table 20 (Continued)

compound	r_1 ($mM^{-1}\,s^{-1}$)	r_2 ($mM^{-1}\,s^{-1}$)	^1H freq (MHz)	temp (°C)	pH[a]	ref
			Pyridine Containing Macrocycles			
PCTP-[13]	7.7		20	25	7.5	231
PCTA-[13]	6.3		20	25		255
PCTA-[12]	6.9		20	25		225
PCTP-[12]	7.5		20	25		225
PC2A	7.5	8.3	40	25	7	229
PCTA-[12]	5.42	6.52	40	25	7	229
BP2A	8.27	8.63	40	25	7	229
PC2A	3.7	3.9	40	25	12	229
PCTA-[12]	3.43	3.11	40	25	12	229
BP2A	4.51	4.91	40	25	12	229
PCTA-[12]	6.9		20	25	7	226
PCTA-[13]	6.3		20	25	7	226
PCTA-[14]	5.9		20	25	7	226
			Other Macrocyclics			
Tx	18		50	25		236
Tx	5.3		50	25	P_i	236
Tx	19.0		20	25		65
Tx	16.9		50	25		65
Tx	5.3		50	20	P_i	65
HAM	9.7		300	25	7.4	266
HAM	9.7		20	30	7.4	266
N_6−L1	12.8		20	25	6	239
N_6−L1	~2		20	25	12	239
N_6−L2	11.0		20	37	6	248
N_6−L2	4.7		20	37	P_i	248
Crypt-L1	5.8		10	25	6	251
Crypt-L1	3.5		10	25	9	251
			Other Acyclics			
TTAHA	9.5	10.5	300	25	7.4	150
PEDTA	8.8	9.6	300	25	7.4	150
EDMP	11.1	15.9	10	37	7	249
Phos-L1	10.0	14.3	10	37	7	249
DTPMP	8.6	11.8	10	37	7	249
HOPO	10.5		20	37		64

[a] P_i = phosphate buffer. If a pH is not specified, the compound was often dissolved in water or saline solution.

Table 21. Relaxivities (20 MHz, 40 °C) and Molecular Weights for Multimeric Gd(III) Complexes[265]

ligand	MW (Da)	r_1 ($mM^{-1}\,s^{-1}$)	ligand	MW (Da)	r_1 ($mM^{-1}\,s^{-1}$)
HP-DO3A	588	3.7	$(DO3A)_3L2$	2259	8.5
DO3A-MA	585	3.5	$(DO3A)_3L1$	2285	8.8
DO3A-PA	647	4.1	$(DO3A)_4L4$	2417	8.4
$(DO3A)_2L2$	1231	5.1	$(DO3A)_4L1$	2229	8.5
$(DO3A)_2L5$	1257	5.4	$(DO3A)_4L2$	2461	9.6
$(DO3A)_2L3$	1103	6.4	$(DO3A)_4L3$	2501	9.8
$(DO3A)_2L4$	1201	6.6	$(DO3A)_4L5$	2597	10.2
$(DO3A)_2L8$	1367	6.2	$(DO3A)_6L1$	4390	11.2
$(DO3A)_2L9$	1469	6.9	$(DO3A)_8L1$	4998	13

mately with increasing molecular weight. It should be noted that it is the rotational correlation time of the Gd(III)−H vector which determines relaxation and this rotational correlation time may be much shorter than one computed using eq 29 for the molecule as a whole.

Figure 38 is comprised of monomers, dimers, trimers, tetramers, a hexamer, and an octamer. It has been recognized that rigidity plays a role in determining the relaxivity of multimeric gadolinium(III) chelates.[265] For instance, the relaxivity of dimer $[Gd_2(DO3A)_2L4]$ is 6.6 $mM^{-1}\,s^{-1}$ while that of $[Gd_2(DO3A)_2L5]$ is 5.4 $mM^{-1}\,s^{-1}$. Both compounds have identical chelate structures and almost identical molecular weight, but $[Gd_2(DO3A)_2L4]$ has a much less flexible linker between the two gadolinium(III) chelates. Even for compounds with molecular weights

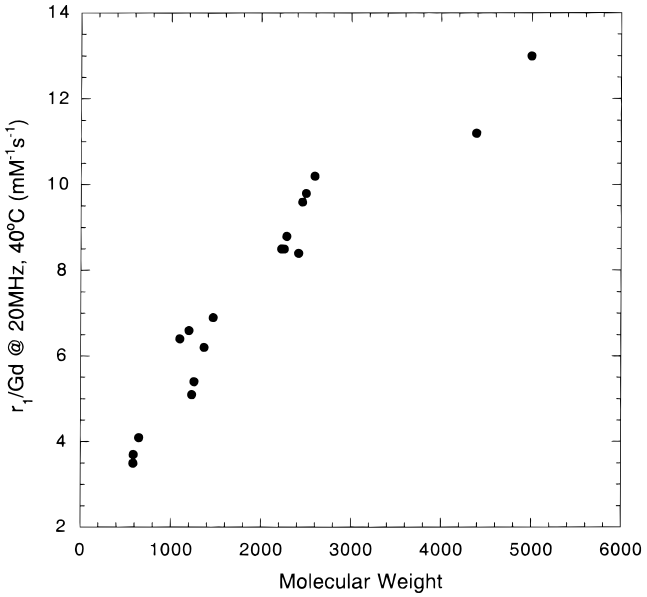

Figure 38. Relaxivity per Gd(III) vs molecular weight for various Gd(III) multimeric complexes.

in the 3000 Da range, the difference in rotational correlation times between rigid and "floppy" multimers is not likely to be large. The effect of internal motion becomes dramatic for polymeric conjugates.

The hydration number plays an important role in determining relaxivity. Notable examples of thermodynamically stable/kinetically inert complexes with

Chart 18

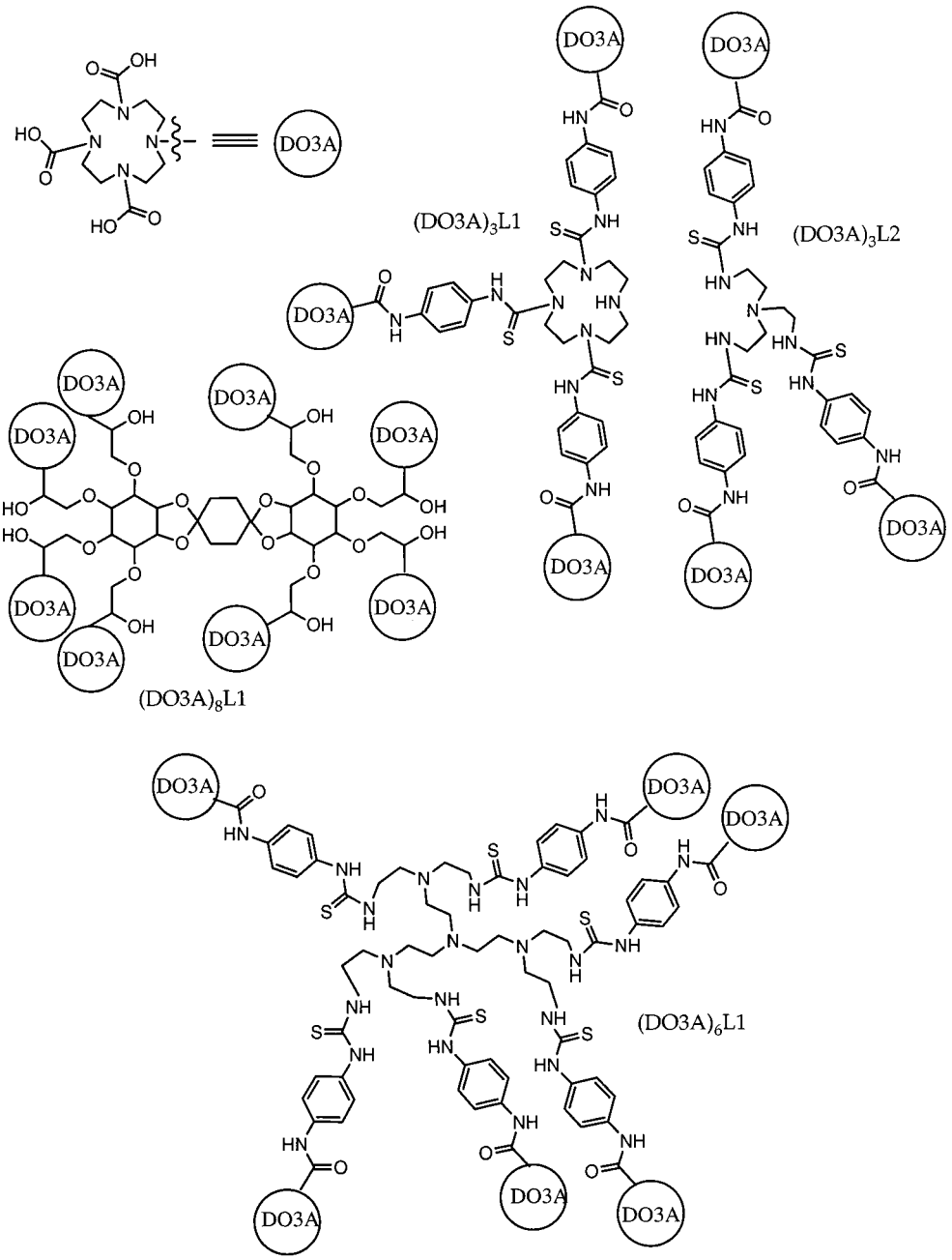

$q > 1$ are $[Gd(TX)(H_2O)_3]^{2+}$, $[Gd(HOPO)(H_2O)_2]$, $[Gd(DO3A)(H_2O)_2]$, $[Gd(HAM)(H_2O)_3]^{3+}$, and $[Gd(N_6\text{-L1})(H_2O)_3]^{3+}$.[64,85,236,239,244,266] These complexes (Charts 7, 9, 16 and Scheme 1) represent dramatic improvements in small molecule contrast agent design. One hurdle that remains in these systems is the coordination of endogenous anions, a factor that is generally not a problem for $q = 1$ complexes.[267] In Table 20 there are some values reported in the presence and absence of phosphate buffer (P_i). Lower relaxivity in the presence of phosphate is an indicator of ternary complex formation which decreases q and lowers relaxivity. Bicarbonate is another endogenous anion present in rather large concentration in vivo which is known to coordinate to [Gd(DO3A)] and reduce relaxivity.[44]

Relaxivities tend to increase at lower temperatures for low molecular weight chelates. This is a consequence of slower molecular tumbling rates. Exceptions can occur for molecules with long water residency times. Activation energies for rotation tend to be in the 20 kJ mol^{-1} range[177] while the energy barrier to water exchange is usually about 50 kJ mol^{-1}. Thus τ_m increases faster than τ_R with decreasing temperature, and this may bring about the limiting condtion $\tau_m > T_{1m}$.

E. Outer- and Second-Sphere Relaxivity

Outer-sphere relaxivity can vary from complex to complex. It is often assumed that the relaxivity exhibited by $q = 0$ complexes can be described by Freed's equation (eq 33) for outer-sphere relaxation. While the NMRD curves of complexes such as $[Gd(TETA)]^-$ and $[Gd(TTHA)]^{3-}$ (Charts 7 and 9) can be modeled by eq 33, it does not neccessarily follow that the values for τ_{s0}, τ_v, a (distance of closest

Chart 19

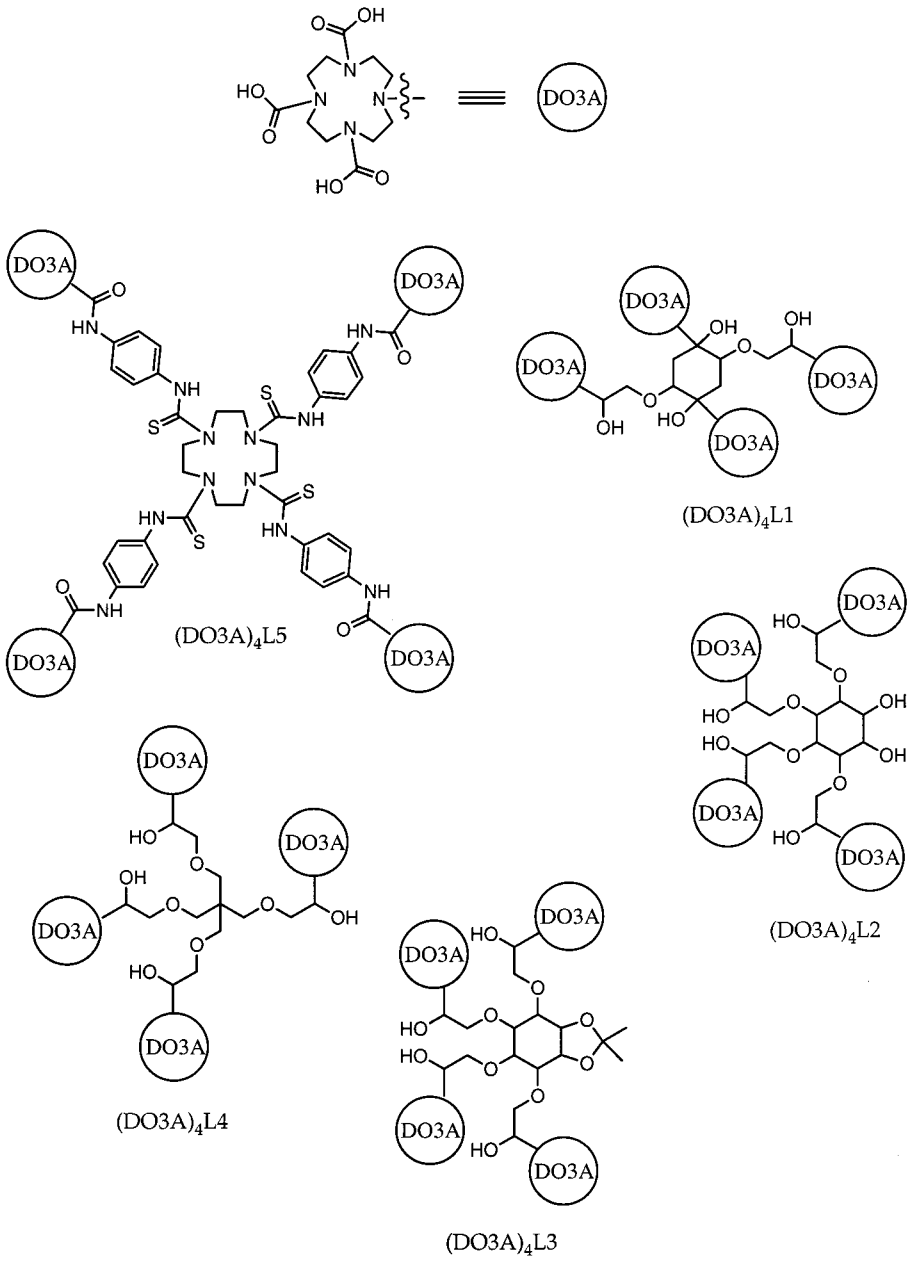

approach), and *D* (diffusion constant) are physically meaningful. As in the preceding section, electronic relaxation may not be well described by the BM equation in the low-field limit. There is also the question of second-sphere relaxivity.

The NMRD curves of $[Gd(TTHA)]^{3-}$ and $[Gd(DOTP)]^{5-}$ are shown in Figure 39. Both ions are $q = 0$ and are of similar size. The increased relaxivity for $[Gd(DOTP)]^{5-}$ (Chart 8) cannot be due to pure outer-sphere relaxation alone. This is likely because of second-sphere relaxivity. This is not surprising considering that lanthanide complexes of DOTP have been used as shift reagents for sodium and other metal ions.[112]

The existence of a second coordination sphere is well established for such species as the aqua complexes of tripositive ions. Neutron diffraction, X-ray diffraction, and LAXS (large angle X-ray scattering) studies of tripositive ions such as $Cr^{3+}_{(aq)}$, $Al^{3+}_{(aq)}$, $Ga^{3+}_{(aq)}$, $In^{3+}_{(aq)}$, and $Rh^{3+}_{(aq)}$ show well-defined second-sphere structure in solution.[268] Bleuzen et al.[269] estimated a residency time of 128 ps at 25 °C for a water molecule in the second sphere of the $Cr^{3+}_{(aq)}$ ion from both ^{17}O NMR relaxation and molecular dynamics. This is long enough to cause a relaxivity enhancement via an SBM dipolar mechanism.

Chen et al. have used VO^{2+} EPR of various polyaminocarboxylates to study second-sphere hydration.[178,179] They determine τ_R and τ_v from EPR solution simulations at various temperatures. From the τ_R data, the hydrodynamic radius is determined, and the distance of closest approach, *a*, is estimated. Fitting the NMRD curves of $[VO(EDTA)]^{2-}$ and other complexes to only the outer-sphere equation gave values for *a* that are physically too small, leading to the conclusion that a second-sphere process was also contributing to the observed r_1. The authors went on to study $[Gd(TTHA)]^{3-}$ assuming that it had a similar

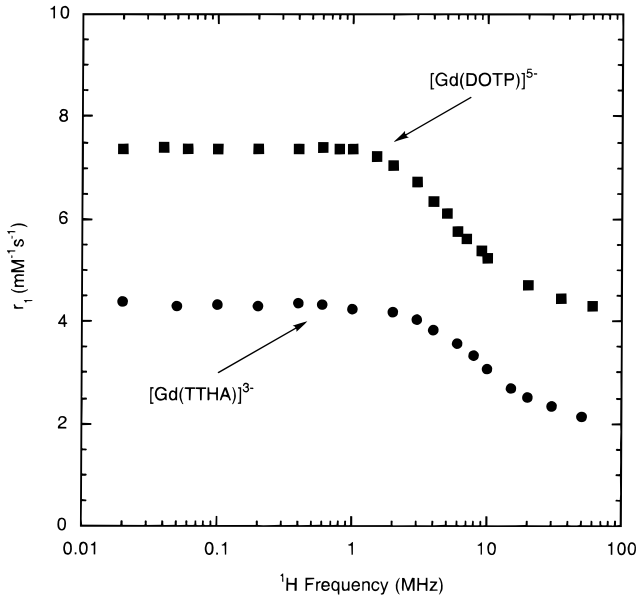

Figure 39. NMRD curves for two $q = 0$ complexes, $[Gd(DOTP)]^{5-}$ and $[Gd(TTHA)]^{3-}$ at 25 °C, showing that all "outer-sphere" complexes are not created equal.

rotational correlation time as $[VO(TTHA)]^{4-}$ and a similar value for a. This lead to a description in which the second-sphere mechanism contributed between 20 and 25% of the observed relaxivity. NMRD curves of $[Gd(DTPA)]^{2-}$ and $[Gd(EOB\text{-}DTPA)]^{2-}$ were also trisected into inner-, second-, and outer-sphere contributions, but the large number of parameters and assumptions makes the analysis statistically questionable.

F. Methods of Improving Relaxivity

The obvious way to ameliorate relaxivity is to increase τ_R, and this will be discussed in depth in the next two sections. It is likely that rigidity will play a role in optimizing τ_R as a function of molecular weight. The limitations of slow water exchange on relaxation have been recognized, and there is a growing body of evidence to aid in optimizing τ_m. Increasing the hydration number poses some interesting challenges to maintain thermodynamic stability/kinetic inertness and, at the same time, be resistant to formation of ternary complexes with endogenous ligands such as phosphate and carbonate. However increasing q offers a large reward in terms of relaxivity. Outer-sphere relaxation is still a misunderstood entity receiving little attention.

Although a large body of data has been accumulated since the previous review, most of this centers around polyaminopolycarboxylate ligands. This bias is understandable considering the composition of the clinically available complexes coupled with the need for thermodynamically stable complexes. It would behove the coordination chemist to examine the physical properties of Gd(III) complexes with a variety of donor atoms in order to ascertain the factors which influence water exchange, electronic relaxation, and outer-sphere relaxation.

V. Macromolecular Conjugates

A. Introduction

The conjugation of low molecular weight chelates such as GdDTPA or GdDOTA to macromolecules alters the biophysical and pharmacological properties of low molecular weight agents.[270] From the biophysical perspective, the conjugation of gadolinium(III) chelates to polymeric materials was anticipated to increase the rotational correlation time and, hence, to improve the relaxivity per gadolinium atom. Combined with tissue-specific targeting moieties, polymeric conjugates were also envisioned to provide MRI with the ability to image low-concentration receptors by delivering a large payload of gadolinium(III) chelates. High molecular weight conjugates are retained in the vascular space by virtue of molecular size and thus facilitate blood pool imaging. However the goal of imaging receptors using MRI in the clinic has been elusive.[271]

The most common approaches which have been used to prepare macromolecular structures containing gadolinium(III) chelates involve conjugation of functionalized chelates to polymers, dendrimers, or biological molecules. In addition, macromolecules with multiple ligands have been prepared by polymerization. The intent of this portion of the review is to survey the synthesis and chemical structure of representative macromolecular conjugates as well as to survey their biophysical properties.

B. General Conjugation Methods

Conjugation methods for linking chelates to macromolecules are well established in the literature.[272] Typical chemistries include the functionalization of primary amines using acylation, alkylation, ureas or thiourea formation, and reductive amination. The majority of papers have been published using commercially available reagents, such as DTPA itself or DTPA-dianhydride, to functionalize macromolecules. Reaction of these reagents with a reactive primary amine on the macromolecule generates an amide bond using one of the DTPA carboxylates (see for example, Figure 40). While still an eight-coordinate ligand, the donor set has been modified as compared with DTPA itself: one acetate donor has been replaced with an amide oxygen. Because the substitution of an amide for a carboxylate has significant relaxivity implications, the tables will explicitly note the chemical structure of the ligand donor set (for example, DTPA vs DTTA-MA, diethylenetriamine tetraacetic acid monoamide).

C. Synthetic Linear Polymers

Polylysine is commercially available in a variety of molecular weight ranges and has been derivatized with gadolinium chelates.[273−277] The reactive epsilon amino groups of the lysine backbone are typically modified with acyclic and macrocyclic polyaminocarboxylate derivatives as shown in Figure 40. Conjugates containing up to 70 Gd(IIII) chelates have been reported (Table 22). Polylysine has also been co-

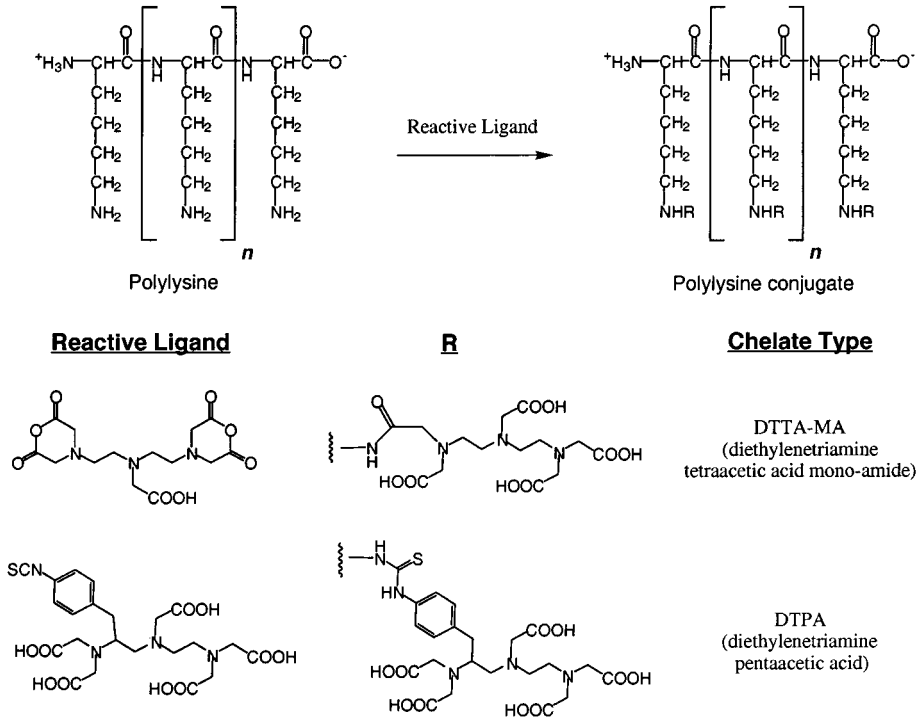

Figure 40. Chemical structure of polylysine and representative chelate conjugates.

Table 22. Synthetic Polymer-Based Macromolecular Contrast Agents

macromolecular contrast agent	chelate type	MW (Da)	no. Gd(III)	% Gd content	ion r_1 (mM^{-1} s^{-1})[a,b]	mol. r_1 (mM^{-1} s^{-1})[a]	freq (MHz)	T (°C)	ref
polylysine-GdDTPA	Gd-DTTA-MA	48 700	60−70		13.1	850	20	39	273
PL-GdDTPA	Gd-DTTA-MA	50 000			10.8		10	37	274
PL-GdDTPA	Gd-DTTA-MA	238 100			11.74		100	37	275
PL-GdDTPA	Gd-DTTA-MA	89 900			11.58		100	37	275
PL-GdDTPA	Gd-DTTA-MA	56 000			10.56		100	37	275
PL-GdDTPA	Gd-DTTA-MA	7 700			11.67		100	37	275
PL-GdDOTA	Gd-DO3A-MA	65 000			13.03		10	37	274
MPEG- PL-GdDTPA	Gd-DTTA-MA	320 000	110	5.5	18	2000−2500	20	37	277, 278
Gd-DTPA-PEG I-polylysine	Gd-DTTA-MA	10 800	6−7	9.64	6.0	39	20	37	276
Gd-DTPA-PEG II-polylysine	Gd-DTTA-MA	13 600	8−9	9.85	6.0	51	20	37	276
Gd-DTPA-PEG III-polylysine	Gd-DTTA-MA	18 500	9−10	7.75	6.0	57	20	37	276
Gd-DTPA-PEG IV-polylysine	Gd-DTTA-MA	21 900	11−12	8.42	6.0	69	20	37	276
Gd-DTPA-PEG V-polylysine	Gd-DTTA-MA	31 500	7−8	3.73	6.0	45	20	37	276
Gd-DTPA-PEG VI-polylysine	Gd-DTTA-MA	39 600	9−10	3.93	6.0	57	20	37	276
Gd-DTPA-PEG VII-polylysine	Gd-DTTA-MA	83 400	35−36	6.65	6.0	213	20	37	276
(DTPA-BA)-PEG	triacetate bisamide	20 000			6.13		20	37	281
(DTPA-BA) α,ω alkyldiamine $(CH_2)_n$, where $n = 4$	triacetate bisamide	8 000		26.2	8*		20	35	280
(DTPA-BA) α,ω alkyldiamine $(CH_2)_n$, where $n = 5$	triacetate bisamide	8 300		25.6	9*		20	35	280
(DTPA-BA) α,ω alkyldiamine $(CH_2)_n$, where $n = 6$	triacetate bisamide	19 400		21.75	10*		20	35	280
(DTPA-BA) α,ω alkyldiamine $(CH_2)_n$, where $n = 10$	triacetate bisamide	10 300		19.92	15*		20	35	280
(DTPA-BA) α,ω alkyldiamine $(CH_2)_n$, where $n = 12$	triacetate bisamide	15 700		20.06	18*		20	35	280

[a] Water. [b] Asterisk (*) indicates values estimated from NMRD curve.

modified with PEG to modulate the pharmacokinetic properties of the agents.[278,279] The relaxivity of polylysine derivatives range from 15 to 20 mM^{-1} s^{-1} at 20 MHz (Table 22), lower than anticipated for a truly immobilized monoamide DTPA chelate. This is likely because of the flexible nature of the linear polymeric backbone and the epsilon amino side chain.

A series of linear copolymers of bisamide chelates linked by α,ω-alkyldiamides with a varying number (n) of methylenes[280] or poly(ethylene glycol) (PEG) diamines [219] have been prepared. These compounds differ from those described above in that the chelates are incorporated directly into the polymeric chain instead of being conjugated to an existing polymer. An example synthetic route and structure of one representative copolymer incorporating poly(ethylene glycol) units are shown in Figure 41.

Variable temperature EPR, variable temperature, pressure, multiple field ^{17}O NMR, and variable temperature NMRD studies were reported for the linear

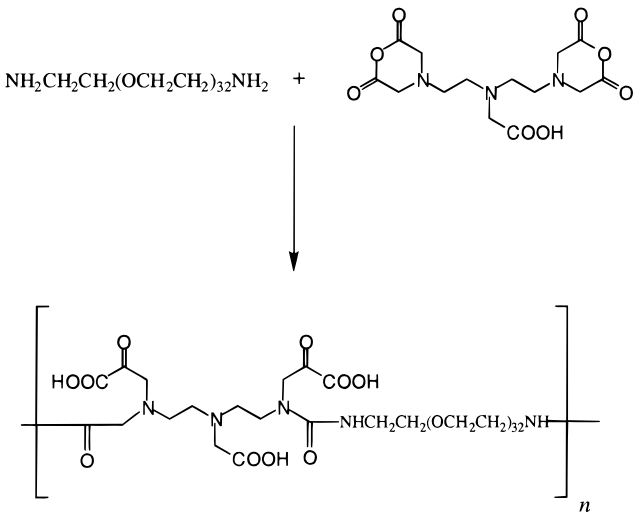

[α-ω-poly(ethyleneglycol)diamine]-DTPA copolymer)

Figure 41. Chemical synthesis and structure of a linear DTPA derivative copolymer: [α-*ω*-poly(ethyleneglycol)-diamine]-DTPA copolymer.

Gd(DTPA-bisamide)-poly(ethylene glycol) copolymer.[219] This work demonstrated for the first time that the water exchange rate ($k_{ex}^{298} = 4.8 \times 10^5\ s^{-1}$) and mechanism (dissociatively activated) were identical for the polymer and the corresponding small molecule chelate. As a result of the slow water exchange and relatively fast rotational correlation time, the relaxivities for this polymer were low and independent of temperature at all field strengths.

Relaxivity studies were also reported for the related series of copolymers which were prepared from DTPA dianhydride and α,*ω*-alkyldiamines without the poly(ethylene glycol) spacers.[280] Contrary to expectations, r_1 was higher than the PEG containing copolymers and increased with increasing *n*, the number of methylene units between each chelate. This was explained by postulating the presence of intramolecular aggregates which made the linear polymers less rodlike and more globular, thereby increasing the rotational correlation time. Again, the water exchange rate of the monomer was identical to that of the polymer, indicating that the relaxivity of these compounds was limited by a slow water exchange rate (τ_m limited).[281] Toth et al.[281] showed that the relaxivity differences between polymers with varying *n* could be explained by fitting the ^{17}O longitudinal relaxation rates to a Lipari-Szabo model to separate local fast motions within the polymer from the global tumbling time of the entire molecule. The local motional rates and the extent to which they contributed to relaxivity were found to be similar (as in the case of the PEG-based copolymers); however, the slower global motion of the larger polymers accounted for the difference in observed relaxivity.

D. Synthetic Dendrimer-Based Agents

Dendrimers are three-dimensional, oligomeric structures prepared by reiterative reaction sequences starting from smaller "core" molecules, as shown schematically in Figure 42. The highly branched, nearly monodisperse structure of dendrimers have led to a number of interesting molecular attributes for this relatively new class of macromolecule. Several excellent reviews describing the evolution of dendrimer chemistry have appeared.[282,283]

A number of workers have explored the potential use of conjugated dendrimers as a new class of macromolecular MRI agents. The potential advantages of Gd(III) chelate dendrimer conjugates include the fact that dendrimers, such as the Starburst polyamidoamine (PAMAM) dendrimers (Figure 42), have uniform surface chemistry and minimal molecular weight distribution and shape variation. In contrast to linear polymers, dendrimers have a relatively rigid structure and the overall tumbling of the molecule contributes to the rotational correla-

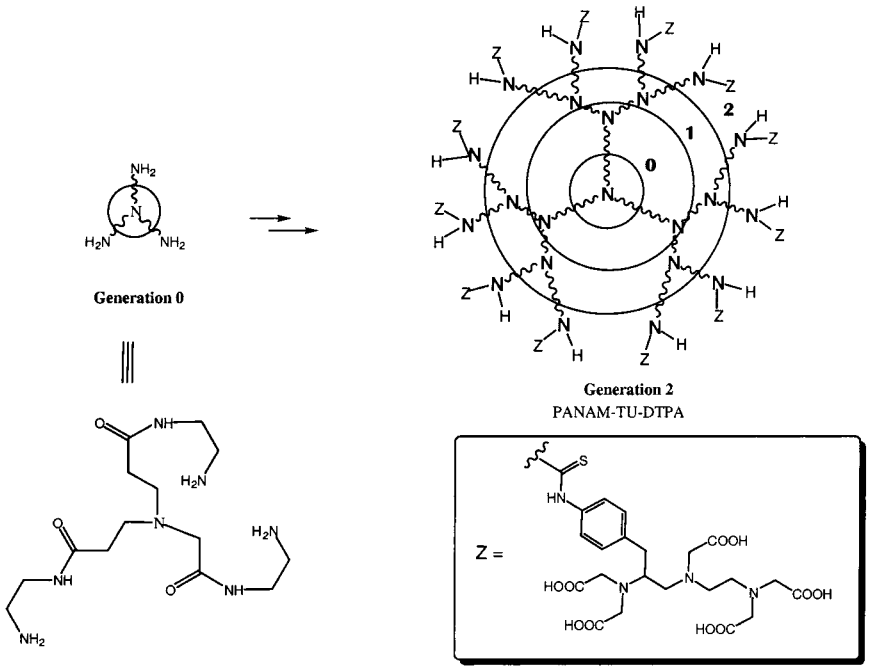

Figure 42. Schematic drawing of a generation 2 PAMAM thiourea DTPA dendrimer.

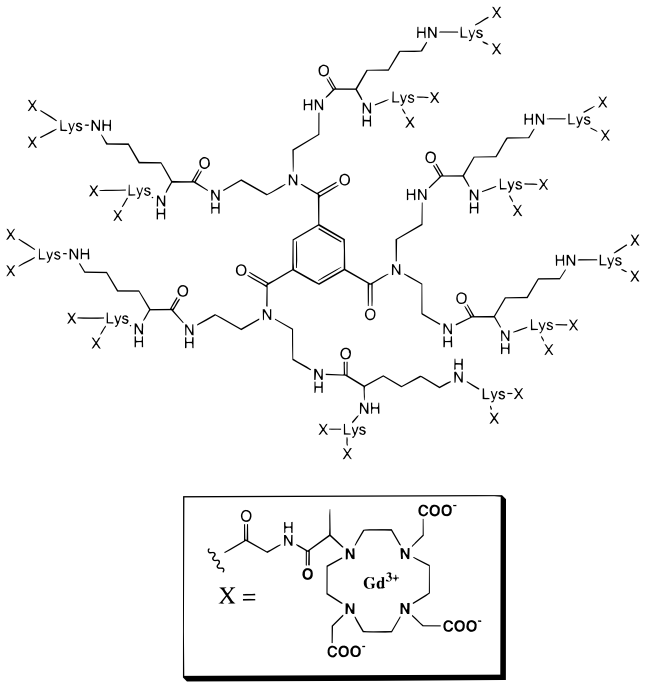

Figure 43. Chemical structure of Gadomer 17.

tion time. The rotational correlation times of the carbon atoms in PAMAM-type dendrimers was measured by ^{13}C NMR. These studies found that the correlation time of the internal carbons increased by several orders of magnitude between generation 0 and 10, and doubled for carbons on the surface.[284] Provided chelates can be attached in a manner which limits rapid rotation of the chelate itself, the relaxivity should benefit from conjugation to a dendrimeric structure.

A dendrimer-based MRI agent was prepared by linking p-NCS-Bz-DTPA to a G = 2 and G = 6 PAMAM Starburst dendrimer (Figure 42). The resulting G = 2 and G = 6 conjugates of DTPA contained, on average, 11 and 170 chelates, respectively. This work has recently been extended to include larger dendrimers (up to G = 9) and DOTA chelates, which appear to provide materials with the largest number of Gd(III) ions per macromolecule yet reported.[285]

Margerum and co-workers have employed an analogous approach to link the macrocyclic monoamide chelate DO3A-monoamide to PAMAM dendrimers of generation 2−5.[286] In addition, these authors report the incorporation of PEG subunits, which have a pronounced effect on the pharacokinetic properties.

Schering AG has reported the preparation and characterization of two types of dendrimer-based MRI agents: GdDTPA-cascade-24-polymer[287−289] and Gadomer 17.[290,291] GdDTPA-cascade-24-polymer is a PAMAM dendrimer which has been functionalized with 24 Gd-DTPA chelates, whereas Gadomer 17 is derived from a lysine-functionalized 1,3,5-benzene tricarboxylic acid core (Figure 43). Comparisons of the pharmacokinetics of GdDTPA-cascade-24-polymer with Gd-DTPA-polylysine in the rat indicate that the dendrimer-based agents are eliminated much more readily than the linear polylysine polymer, presumably due to the globular nature of the dendrimer.[292]

The reported relaxivity values of the dendrimer conjugates range from ∼14 mM^{-1} s^{-1} to 36 mM^{-1} s^{-1} at 25 MHz, 37 °C depending on the nature of the chelate and the dendrimer structure. These values are higher than those observed for the linear analogues for two reasons. First, most of the linear polymer work has been reported using mono- or diamide polyaminocarboxylate derivatives, both of which are now known to have relaxivities limited by slow water exchange. Second, the dendrimers are inherently more rigid than their linear analogues, leading to fewer degress of freedom for the conjugated gadolinium chelate.

Tóth and Merbach have reported an ^{17}O NMR and NMRD study of a series of functionalized PAMAM dendrimers.[212] Importantly, these experiments demonstrated for the first time that the attachment of the macrocyclic DO3A-monoamide chelate to the dendrimer did not significantly influence water exchange on the complex. The water exchange and relaxivity results of this study are summarized in Table 23. The NMRD profiles of the dendritic contrast agents G_3Gd_{52} and G_3Gd_{23} showed a high-field peak characteristic of contrast agents with long rotational correlation times. However, the relaxivity improvement at 20 MHz is relatively modest as compared with that reported by Weiner et al. for the DTPA and DOTA functionalized PAMAM dendrimers.[285,293] Given the discussion in section IV, one can appreciate that the relaxivity of the DO3A-monoamide chelates studied by Tóth and Merbach is limited by the long water residency time (τ_m) of the mono amide ligand system. These results have important implications for the design of optimized macromolecular contrast agents.

E. Naturally Occurring Polymers (Proteins, Polysaccharides, and Nucleic Acids)

A significant amount of exploratory research has been performed using Gd-DTPA derivatives of human or bovine serum albumin (HSA or BSA).[294] Because of the intravascular retention of the macromolecule, Gd-DTPA-BSA/HSA is used as a "gold standard" blood pool agent and has been used to demonstrate the benefits of MR angiography.[295] Conjugates containing up to about 30 ligands are readily formed by the reaction of DTPA-dianhydride with BSA or HSA in buffered aqueous solution.

Dextran has also been explored as a scaffold for the attachment of various chelates.[296,297] As with polylysine, dextrans are available in a variety of molecular weight ranges and can be modified to include chelating agents.[298−302] Of relevance to potential human use is the fact that dextrans have been successfully employed as plasma volume expanders.[303]

Dextran-based macromolecular contrast agents have been investigated as blood pool MRI contrast agents. An example of well-studied macrocyclic conjugates is CMD-A2-Gd-DOTA, shown in Figure 44.[300] This macromolecular contrast agent is prepared by a three-step modification of dextran by alkylation

Table 23. Dendrimeric Macromolecular Contrast Agents

macromolecular contrast agent	dendrimer type	chelate	MW (Da)	no. of Gd(III)	ion r_1 ($mM^{-1}\,s^{-1}$)	mol. r_1 ($mM^{-1}\,s^{-1}$)	freq (MHz)	T (°C)	ref
G_9(N[CS]N-bz−GdDTPA)$_{1331}$	PANAM	Gd-DOTA	1 600 000	1 331	36	47 916	25	23	285
G_7(N[CS]N-bz−GdDTPA)$_{383}$	PANAM	Gd-DOTA	375 000	383	34	13 022	25	23	285
G_6(N[CS]N-bz−GdDTPA)$_{170}$	PANAM	Gd-DTPA	139 000	170	34	5 800	25	20	293
G_6(N[CS]N-bz−GdDTPA)$_{170}$	PANAM	Gd-DTPA	139 000	170	34	5 800	25	35	293
G_6(N[CS]N-bz−GdDTPA)$_{170}$	PANAM	Gd-DTPA	139 000	170	23.1	3 900	10	20	293
G_6(N[CS]N-bz−GdDTPA)$_{170}$	PANAM	Gd-DTPA	139 000	170	23.5	4 000	10	35	293
G_2(N[CS]N-bz−GdDTPA)$_{11}$	PANAM	Gd-DTPA	8 508	11	21.3	234	25	20	293
G_2(N[CS]N-bz−GdDTPA)$_{11}$	PANAM	Gd-DTPA	8 508	11	16.7	184	10	20	293
G_5(N[CS]N-bz−GdDO3A)$_{57}$	PAMAM	Gd-DO3A- MA	61 775	57	18.8	1 072	25	37	286
G_4(N[CS]N-bz−GdDO3A)$_{38}$	PAMAM	Gd-DO3A- MA	37 420	38	16.9	642	20	37	286
G_3(N[CS]N-bz−GdDO3A)$_{24}$	PAMAM	Gd-DO3A- MA	22 074	24	14.8	355	25	37	286
G_4(N[CS]N-bz−GdDO3A)$_{11}$	PAMAM	Gd-DO3A- MA	18 385	11	16.0	176	25	37	286
G_3(N[CS]N-bz−GdDO3A)$_{13}$	PAMAM	Gd-DO3A- MA	14 319	13	12.3	160	20	37	286
G_3(N[CS]N-bz−GdDO3A)$_{10}$(PEG_{5000})$_{12}$	PAMAM	Gd-DO3A- MA	69 352	10	13.8	138	20	37	286
G_3(N[CS]N-bz−GdDO3A)$_{15}$(PEG_{2000})$_9$	PAMAM	Gd-DO3A- MA	33 330	15	13.7	205	20	37	286
G_2(N[CS]N-bz−GdDO3A)$_9$(PEG_{5000})$_3$	PAMAM	Gd-DO3A- MA	23 760	9	12.4	112	20	37	286
G_2(N[CS]N-bz−GdDO3A)$_5$(PEG_{2000})$_7$	PAMAM	Gd-DO3A- MA	20 587	5	11.0	55	20	37	286
Gd-DTPA-cascade-polymer	PAMAM	Gd-DTPA	<30 000	24	11.9	289	20	40	292
Gadomer 17	polyamide	Gd-DO3A- MA	17 453	24	15.2[a]	365	64.5	37	291
Gadomer 17	polyamide	Gd-DO3A- MA	17 453	24	18.7[a]	449	20	39	291
Gadomer 17	polyamide	Gd-DO3A- MA	17 453	24	17.3	415	20	39	291

[a] In plasma.

Table 24. Natural Polymer-Based Macromolecular Contrast Agents

macromolecular contrast agent	chelate type	MW (Da)	no. of Gd(III)	% Gd	ion r_1 ($mM^{-1}\,s^{-1}$)[a]	mol. r_1 ($mM^{-1}\,s^{-1}$)[a]	freq (MHz)	T (°C)	ref
albumin-GdDTPA	Gd-DTTA-MA	90 000	90		14	420	10	25	274
CMD-A2-DOTA-Gd	Gd-DO3A-MA	52 100			10.59		20	37	296
dextran-alanine-GdDTPA	Gd-DTTA-MA			1.7	9.4		10	37	
dextran-alanine-GdDTPA	Gd-DTTA-MA			2.2	8.7		10	37	
dextran-alanine-GdDTPA	Gd-DTTA-MA			3.4	8.7		10	37	
CMD-Gd-DTPA (carboxymethyldextran-GdDTPA, carbamate linked)	Gd-DTTA-MA	28 000			7.8		20	37	297
CMD-Gd-DTPA (carboxymethyldextran-GdDTPA, carboxymethyl linked)	Gd-DTTA-MA	39 900			9.8				299
CMD-Gd-DTPA	Gd-DTTA-MA	66 000			7.62		20	37[b]	301
CMD$_n$-Gd−DTPA where $n = 2$	Gd-DTTA-MA				9.4		20	37	302
CMD$_n$-Gd−DTPA where $n = 3$	Gd-DTTA-MA				9.5		20	37	302
CMD$_n$-Gd−DTPA where $n = 4$	Gd-DTTA-MA				9.4		20	37	302
CMD$_n$-Gd−DTPA where $n = 6$	Gd-DTTA-MA				8.9		20	37	302

[a] Water. [b] Plasma.

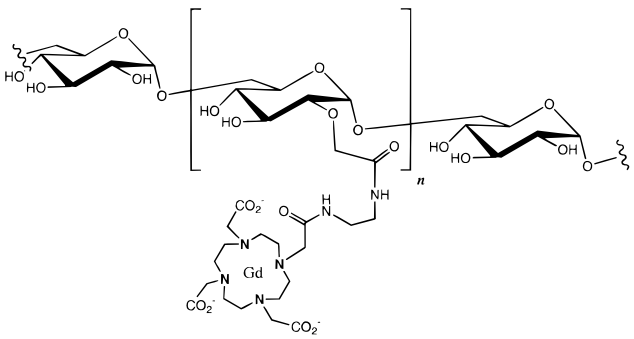

Figure 44. Chemical structure of CMD-A2-Gd-DOTA, a modified dextran polymer.

with chloroacetic acid, the introduction of an ethylenediamine spacer, followed by EDCI-mediated coupling of DOTA. The resulting conjugate has been investigated as an intravascular MR contrast agent for myocardial perfusion [296]

The relaxivity properties of CMD-A2-Gd-DOTA and related derivatives are shown in Table 24. The derivatives have modest 20 MHz relaxivity values (6−11 $mM^{-1}\,s^{-1}$ at 37 °C). Interestingly, the relaxivity data for a series of compounds differing by the number of methylene units linking the chelate to the dextran backbone are essentially identical. In addition, there was little dependence on molecular weight.

F. Targeted Agents

Conceptually, antibodies or other tissue-specific molecules may be combined with paramagnetic centers to provide disease-specific MRI agents. The challenge with regard to delivering sufficient quantity of paramagnetic label is substantial.[271] However, a number of interesting reports have appeared describing the preparation and characterization of targeted agents which contain a significant number of gadolinium atoms.

Curtet and co-workers have described the improved conjugation of polylysine-gadolinium chelates to anticarcinoembryonic antigen (CEA) monoclonal antibodies.[304] In this example, paramagnetic loading as high

Table 25. Targeted Macromolecular Contrast Agents

macromolecular contrast agent	conjugate	chelate type	target	MW (Da)	ion r_1 (mM^{-1} s^{-1})[a]	mol r_1 (mM^{-1} s^{-1})[a]	freq (MHz)	T (°C)	no. of Gd(III)	ref
Gd−PL-DTPA-HSA	HSA	DTTA-MA	vascular	140 000	∼10.8[b]		10	37	60−90	274
Gd−PL-DOTA-HSA	HSA	DO3A-MA	vascular	140 000	∼13.0[b]		10	37	60−90	274
f-PANAM-TU-DTPA	folic acid	DTPA	folate receptor	NR	NR	NR[c]	NR[c]	NR[c]	NR[c]	306
PL-Gd-DTPA$_{24-28}$−anti CEA	anti-CEA Fab(ab′)$_2$	DTTA-MA	Colorectal carcinoma	113 000	14.5	348−406	20	39	24−28 per antibody	304
PL-Gd-DOTA$_{24-28}$−anti CEA	anti-CEA Fab(ab′)$_2$	DO3A-MA	Colorectal carcinoma	114 000	16	384−448	20	39	24−28 per antibody	304

[a] Water. [b] Molar relaxivity of the polymeric chelate (reported to be essentially identical to that of the HSA conjugate). [c] NR = not reported.

as 24 to 28 metal ions per antibody was obtained without sacrificing immunoreactivity (80−85%) for conjugates PL-Gd-DTPA$_{24-28}$F(ab′)$_2$ and PL-Gd-DOTA$_{24-28}$F(ab′). The bipohysical data for these conjugates are listed in Table 25. The relatively low relaxivity for the antibody conjugates (r_1 = 13 to 16 mM^{-1} s^{-1}) is thought to be a consequence of fast segmental motion and/or slow water exchange. In vivo studies were performed in nude mice grafted with human colorectal carcinoma LS 174T. For one group of animals, 24 h after injection of 0.001 mmol/kg of gadoliunium-labeled immunoconjugate, the tumor uptake in was 10−15% and a corresponding r_1 increase of 15−20% was noted. However, in another "MRI negative group" of mice, no difference was found between the control and injected mice.

Wu and co-workers have reported the preparation of metal-chelate-dendrimer-antibody constructs for use in imaging and radioimmunotherapy.[305] Dendrimers have the advantage of uniform surface chemistry and low polydispersity ratios, which in theory should make their conjugates more well-defined chemically than their polymeric counterparts. In this work, generation 2 polyamidoamine (PAMAM) dendrimers were modified by reaction with bifunctional DTPA or DOTA chelators followed by conjugation to monoclonal antibody. No significant effect on immunoreactivity was noted. While this work was primarily directed toward radioimmunotherapy, the approach was noted to be useful for gadolinium as well. Subsequently, Wiener reported the preparation of folate-conjugated MRI imaging agents using the dendrimer conjugation approach.[306] In this work, folic acid was attached to a generation four ammonia core dendrimer, which was then reacted with an isothiocyanate DTPA derivative to form the polymeric chelate f-PAMAM-TU-DTPA. Cells accumulated the folate-conjugated dendrimer in a receptor specific manner. When treated with 28 nM folate-conjugated PAMAM-TU-GdDTPA for 40 min, the longitudinal relaxation rate at 50 MHz increased by 109% as compared with ∼20% for the control. These data indicate that cellular relaxation rates can be modified by targeting receptors in vitro. However, as noted by the authors, layers of targeting and pharmacokinetic challenges remain before receptor-based MRI agents can be used in vivo.

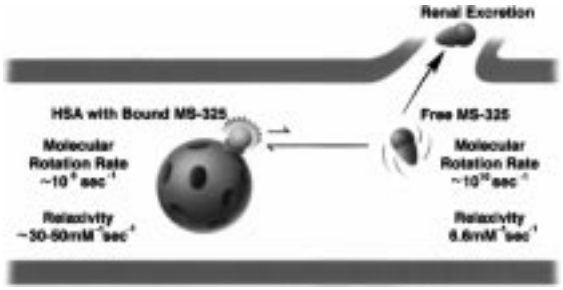

Figure 45. RIME mechanism of action for MS-325. The agent is shown schematically as consisting of two parts: a circular gadolinium chelate and a bullet-shaped protein-binding moiety. Within the bloodstream, MS-325 binds, on average, to one of many available sites on HSA. The bound form is in equilibrium with a small amount of the free form which is renally excreted steadily over time. The bound form of MS-325 has greatly enhanced relaxivity by virtue of its slower molecular tumbling rate.

VI. Relaxivity of Noncovalently Bound Adducts of Gadolinium(III) Complexes

Gadolinium(III) complexes that noncovalently bind to substrates have certain inherent advantages from a biophysical viewpoint over their bioconjugate cousins. This is the basis of the receptor induced magnetization enhancement (RIME) philosophy.[307] In this approach, a contrast agent is targeted to a particular protein or receptor molecule. The binding causes an increased concentration and retention of the Gd(III) complex in the area of the receptor molecule. Binding to a macromolecule also allows the Gd(III) complex to take on a rotational correlation time that is similar to that of the macromolecule. This increase in τ_R can cause a dramatic increase in relaxivity. Furthermore, the high relaxivity of the bound complex is much greater than that of the unbound, which leads to a high target-to-background ratio.

The RIME concept was articulated[307] in 1991 and is diagrammed schematically in Figure 45, using MS-325 (Chart 2) as an example. Relaxivity enhancement in the tissue of interest occurs not only by compartmentalization of the agent but also by improved relaxivity upon binding. This is a mechanism that is unique to MRI contrast agents and is unavailable to diagnostic nuclear medicine or ultrasound. Some of the early work in this area involved the binding of iron(III) complexes to HSA.[308]

MS-325 was the first complex to fully exploit the RIME concept. MS-325 was designed as a contrast agent for imaging the blood pool using serum albu-

min as the targeted binding molecule.[309,310] HSA is an attractive target for blood pool imaging. It constitutes about 4.5% of plasma (~ 0.67 mM) and is known to bind a variety of small molecules at multiple sites on the protein. In 4.5% HSA at 37 °C, MS-325 was highly bound at a contrast agent concentration of 0.1 mM. Under these conditions, the observed 20 MHz relaxivity was 42.0 mM^{-1} s^{-1}. The relaxivity of MS-325 in phosphate buffered saline (PBS) is only 6.6 mM^{-1} s^{-1}. This represents an almost 7-fold increase upon binding.

It was shown that MS-325 binds to more than one site on HSA and that the calculated bound relaxivity ($r_1^{bound} = \{r_1^{obs} - x^{free}r_1^{free}\}/x^{bound}$; x = mole fraction) is dependent on the binding binding site. As the MS-325 concentration increased, r_1^{bound} decreased from 45 to 30 mM^{-1} s^{-1}. These two points suggest that the use of the proton relaxation enhancement (PRE) method alone for determining binding constants is not a useful method for HSA ligand interactions.[311] With HSA there are often multiple nonidentical binding sites which can give rise to varying degrees of relaxation enhancement. Scatchard plots cannot be unambiguously fit, making the interpretation of data rather dubious.

It should also be noted at this point that defining relaxivity in terms of mM^{-1} s^{-1} in protein solutions can be misleading. Several reports use HSA concentrations greater than 3 mM; because of the high molecular weight of HSA, these solutions are more than 20% protein and hence less than 80% water. The molar concentration of 1 mmol of Gd(III) in a liter of 20% HSA is 1 mM, but the molal concentration would be 1.25 mmolal—the reported relaxivity is overestimated by 25%. A relaxivity enhancement has been reported for $[Gd(DOTA)(H_2O)]^-$ as a function of HSA concentration.[243] Although $[Gd(DOTA)(H_2O)]^-$ does not bind to HSA there is an apparent linear increase in r_1 with increasing HSA concentration which can be ascribed to the misleading definition of relaxivity.

MP-2269 (Chart 2) is another example of a blood pool agent which binds to HSA and exhibits enhanced relaxivity.[258] The relaxivity of MP-2269 was found to be about 3 times greater in the presence of 4% HSA versus its relaxivity in pure H_2O. Toth et al.[220] have studied MP-2269 in the presence and absence of 20% w/v bovine serum albumin (BSA) with NMRD and ^{17}O NMR. Their results suggest that the water exchange rate of MP-2269 does not change upon binding to BSA. They estimate the rotational correlation time of the bound complex to be about 1 ns which is about 7 times longer than the unbound complex. A 1 ns correlation time suggests that there is still some rotational flexibility within the bound complex.

Cavagna et al. have shown that increasing the number of benzyloxymethyl (BOM) groups on a DTPA or DOTA core (Charts 2 and 14) leads to increased relaxation enhancement in the presence of HSA. The multipurpose agent $[Gd(BOPTA)(H_2O)]^{2-}$ contains one BOM, group and B-21326/7 contains three BOM groups.[246] Both compounds showed enhanced relaxivity in plasma. B-21326/7 had a higher enhancement and appeared to be more rigidly bound

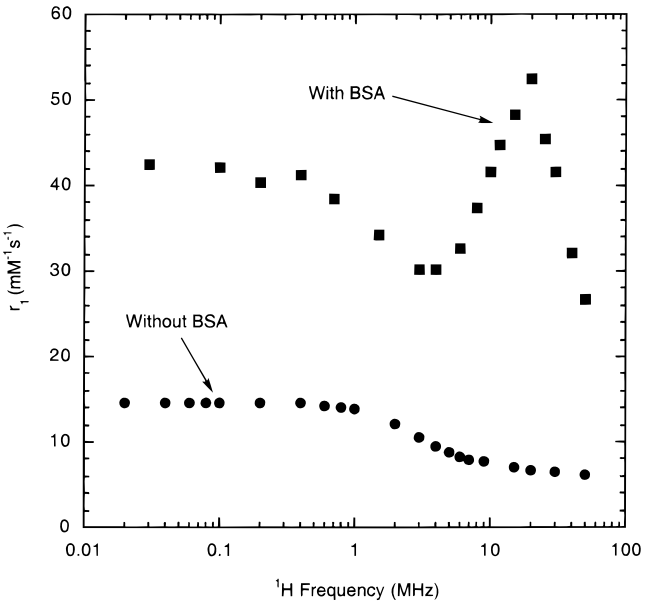

Figure 46. NMRD curves $[Gd\{(DOTA(BOM)_3\}(H_2O)]^-$ in the presence and absence of BSA. Note the large increase in relaxivity upon binding to the protein.

based on an NMRD profile. Aime et al. reported relaxation enhancements of $[Gd(DOTA\{BOM\}_n(H_2O)]^-$ complexes with HSA.[243] The relaxation enhancement increased with the number of BOM units added. Their data was fit to a two equal site binding model.

The NMRD curve of $[Gd(DOTA(BOM)_3)(H_2O)]^-$ is shown in Figure 46.[243] The calculated NMRD curve of $[Gd(DOTA(BOM)_3)(H_2O)]^-$ bound to BSA is also shown. The authors used the K_a from their PRE study to calculate how much complex was bound to BSA under these conditions. They then used these data to determine a bound relaxivity. The increase in r_1 upon binding is remarkable.

Anelli et al. have also reported a series of monoamide derivatives of DOTA in which the amide group is linked to an iodinated aryl ring.[263] They report six derivatives and use two aryl groups which find use in hepatobiliary X-ray contrast imaging, Chart 20. These compounds also bind to HSA. In a study at 20 MHz, the relaxivity of these compounds in saline and reconstituted human serum were compared. There is a 2- to 3-fold increase in r_1 and r_2 in serum compared to saline (Table 26).

The complex $[Gd(PCTP\text{-}[13])(H_2O)]^{3-}$ binds weakly to HSA with an association constant of 600 M^{-1} reported.[231] The authors claim a relaxivity of 45 mM^{-1} s^{-1} for the bound agent. They have also calculated a "bound" NMRD profile based on the association constant and used $[Gd(DOTP)]^{5-}$ as an outer-sphere model. The authors fit the NMRD curve to a rotational correlation time of 30 ns and a water residency time of 290 ns at 25 °C. On the basis of this analysis, the water exchange rate slows by about 2 orders of magnitude upon protein binding.

Aime and co-workers have also examined the q = 0 complex $[Gd(DOTPMBu)]^-$ (Chart 8) in the presence of HSA.[52] The butyl groups appear to enhance HSA binding (the ethyl analogue does not bind well), and they estimate a K_d of 1 mM. The relaxivity of $[Gd(DOTPMBu)]^-$ increases from 2.8 to 13.4 mM^{-1}

Chart 20

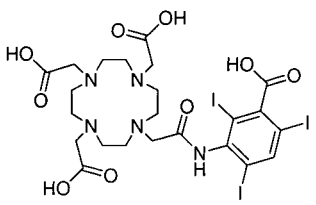
DO3A-L5

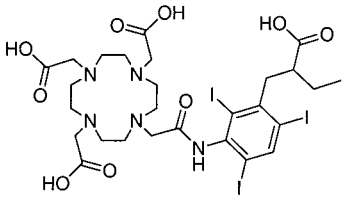
DO3A-L6

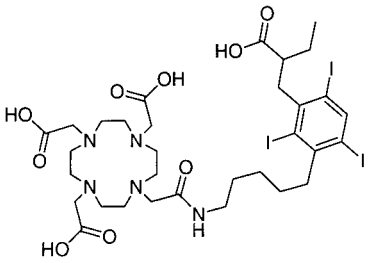
DO3A-L7

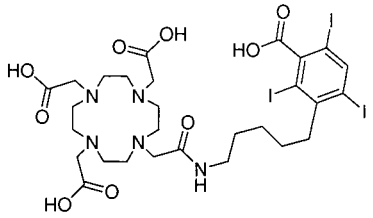
DO3A-L8

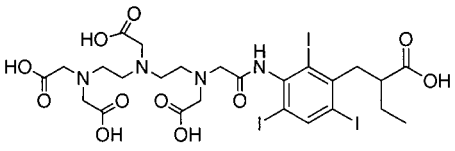
DTPA-L2

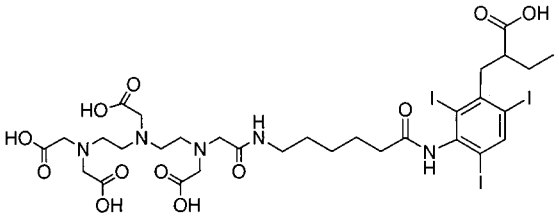
DTPA-L3

Table 26. Relaxivities (20 MHz, 39 °C) of Gd(III) Complexes Containing Iodinated Aryl Rings in Saline and in Seronorm (Reconstituted Human Plasma)[263]

ligand	r_1 (saline)	r_2 (saline)	r_1 (Seronorm)	r_2 (Seronorm)
DO3A-L5	5.01	7.01	10.57	12.08
DO3A-L6	5.59	7.33	14.23	16.57
DO3A-L7	5.07	6.60	18.19	21.50
DO3A-L8	4.80	6.25	10.51	12.51
DTPA-L2	5.91	7.96	12.92	14.46
DTPA-L3	5.48	6.17	18.39	21.12

s^{-1} on going from saline to 5% HSA solution. This is a very significant result to consider when trying to estimate the amount of inner-sphere relaxivity for a given compound. For systems with long τ_R, outer-sphere (second-sphere) relaxivity cannot be estimated from a small molecule such as $[Gd(TTHA)]^{3-}$.

Targeting of other macromolecules should increase relaxivity via the RIME mechanism. Two complexes which were designed with hepatobiliary contrast in mind are $[Gd(BOPTA)(H_2O)]^{2-}$ and $[Gd(EOB\text{-}DTPA)(H_2O)]^{2-}$. $[Gd(BOPTA)(H_2O)]^{2-}$ has a relaxivity of 4.4 $mM^{-1}\ s^{-1}$ in water, 6.9 $mM^{-1}\ s^{-1}$ in rat plasma, and $\sim$30 $mM^{-1}\ s^{-1}$ in rat hepatocytes.[312] $[Gd(EOB\text{-}DTPA)(H_2O)]^{2-}$ has a relaxivity (20 MHz, 37 °C) of 5.3 $mM^{-1}\ s^{-1}$ in water, 8.7 $mM^{-1}\ s^{-1}$ in rat plasma, and 16.9 $mM^{-1}\ s^{-1}$ in rat hepatocytes. [313]

Wiener and co-workers have prepared a folate conjugate of their PAMAM-tu-DTPA dendrimer (vide supra).[306] This compound was designed to target tumor cells which express the high-affinity folate receptor (hFR). They established that the complex binds to tumor cells with the hFR and that upon binding a 2-fold increase in relaxivity was observed.

Martin et al.[252] described the preparation of some DTPA-based dimers and tetramers (Chart 21). The authors also report relaxivities in water and in 4% BSA solution and observe an increase upon measuring r_1 in the protein solution (see Table 27).

Incorporation of a contrast agent into a liposome or membrane is another means of slowing tumbling times and increasing relaxivity.[314−319] The majority of studies have employed a DTPA-bisamide ligand where the amide group contains a long chain fatty acid such as a stearyl or myristyl derivative. This is largely a result of the synthetic ease of preparing symmetric bisamides from DTPA anhydride. Unfortunately, as outlined in sections IV and V, Gd(III) complexes of DTPA-bisamides have very slow water exchange rates and relaxivity can be limited by long τ_m values. Nevertheless, relaxivities in the teens to mid-twenties range have been reported for various liposome and membrane containing contrast agents. Liposomes have also been used to encapsulate contrast agents as a means of drug delivery;[320,321] encapsulated chelates do not show the same r_1 enhancement as those which form part of the liposome itself.

Aime and co-workers have reported several studies on the formation of ternary complexes between β-cyclodextrin and contrast agents. [35,95,228,253,256] Cyclodextrin binding serves to slow the molecular tumbling time and increase relaxivity. The relaxivity increases are modest compared to some of the systems mentioned above, but this is a much more well-defined system and more amenable to quantitative study.

Chart 21

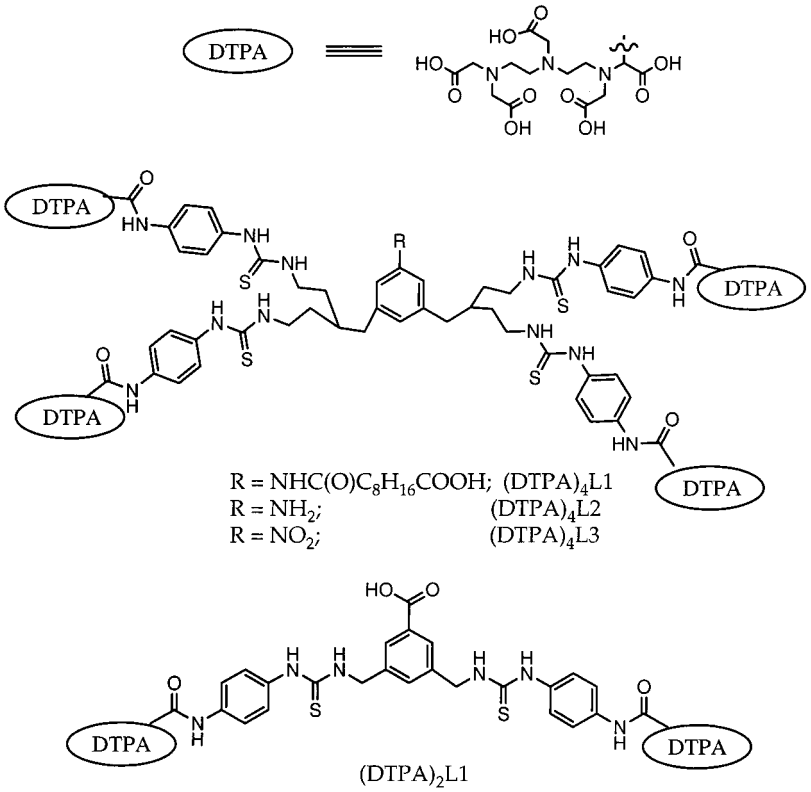

Table 27. Relaxivities (20 MHz) of DTPA Multimers in Water and in 4% Bovine Serum Albumin Solution[252]

ligand	r_1/Gd (H_2O)	r_1/mol (H_2O)	r_1/Gd (BSA)	r_1/mol (BSA)
DTPA-L1	3.7	3.7	12.6	12.6
$(DTPA)_2L1$	4.7	9.4	9.3	18.6
$(DTPA)_4L1$	10.4	41.6	24.6	98.4
$(DTPA)_4L2$	9.1	36.4	19.2	76.8
$(DTPA)_4L3$	13.3	53.2	20.4	81.6

The use of noncovalent binding to a macromolecular target is a field that shows a great deal of promise. Many impressive gains in relaxivity have already been reported. The quantitation of the parameters influencing relaxivity is even more difficult than in sections IV and V because a new variable—binding—is introduced. What is more difficult still is that proteins such as HSA do not have a single well-defined binding site. In many reports to date several assumptions have been made regarding binding. It is often assumed that multiple binding sites have the same binding constant and that the relaxivity at each site is the same, but this has never been proven. Intuitively one would expect contrast agents to bind to HSA with varying affinities to multiple sites on the protein since this is what happens with fatty acids and other small molecules.[322] Likewise, it is dangerous to assume that binding offers a uniform relaxivity. Because of these two discrepancies, proton relaxation enhancement curves cannot be uniquely fit to one model.[311] Until the speciation of the contrast agent−protein system is established by direct techniques, the interpretation of relaxation data is questionable.

VII. General Physicochemical Properties

Beyond the relatively esoteric functional attribute of relaxivity, MRI contrast agents exist and function in the body as drugs. As such, their in vivo properties, including biodistribution, pharmacokinetics, and safety, are dependent on the same combination of properties that determine drug behavior. These properties do not vary tremendously among the agents currently approved or in clinical trials. However, their cataloging does illuminate subtle differences, some of which have functional consequences. Table 28 shows the most frequently measured parameters for the relevant i.v. formulations.[323] Variations in hydrophobicity lead to the greatest differences in in vivo behavior, with potential to alter biodistribution, pharmacokinetics, and safety. Osmolality and viscosity are mainly discussed in reference to safety and ease of injection.

Hydrophobicity can be measured using traditional octanol/water or butanol/water partition experiments or HPLC.[324] Butanol/water coefficients are shown in Table 28 since they are more available in the literature and because very little of the more hydrophilic agents, such as $[Gd(DTPA)(H_2O)]^{2-}$, partition into octanol. The results show that MRI contrast agents are generally hydrophilic, a property that was well known to give rise to limited cell penetration and good tolerability. A more mundane advantage of hydrophilicity is good water solubility; this permits the substantial doses to be administered in small volumes.

The extracellular agents have log *P* values over a very limited range (−2 to −3.2). The lack of any substantial difference in in vivo properties among these agents seems to correlate with these measurements. The addition of aromatic or conjugated ring systems increases hydrophobicity and allows for varying degrees of targeting to proteins or cells (see

Table 28. Physicochemical Properties of MRI Contrast Agents[6,8,323,324]

chemical name	concn (M)	osmolality[a] (osmol kg^{-1})	viscosity (mP s)	log *P* ($BuOH/H_2O$)
$[Gd(DTPA)(H_2O)]^{2-}$	0.5	1.96	2.9	−3.16
$[Gd(DOTA)(H_2O)]^{-}$	0.5	1.35	2.0	
$[Gd(DTPA\text{-}BMA)(H_2O)]$	0.5	0.65	1.4	−2.13
$[Gd(HP\text{-}DO3A)(H_2O)]$	0.5	0.63	1.3	−1.98
$[Gd(DO3A\text{-}butrol)(H_2O)]$	0.5	0.57	1.43	−2
$[Gd(DO3A\text{-}butrol)(H_2O)]$	1.0	1.39	3.9	−2
$[Gd(DTPA\text{-}BMEA)(H_2O)]$	0.5			
$[Gd(BOPTA)(H_2O)]^{2-}$	0.5	1.97	5.3	−2.23
$[Gd(EOB\text{-}DTPA)(H_2O)]^{2-}$	0.25	0.89	1.22	−2.11
MS-325	0.25			−2.11

[a] Osmolality and viscosity measured at 37 °C.

section IX). Nonetheless, the agents remain very hydrophilic.

Osmolality is frequently measured for MRI contrast media more as a holdover from iodinated X-ray contrast agents than for any critical safety reason. Since very large doses of X-ray agents are used, some improvement in tolerability was obtained by switching from charged agents to neutral molecules which required no counterions and thus exhibited much lower osmolality. It was thought that the newer formulations were less irritating to the vascular system and kidneys since the solutions were much closer to the osmolality of serum. These notions guided commercial activities in MRI as well.[8]

Table 28 shows that similar reductions in osmolality have been achieved for the neutral extracellular MRI agents which require no positively charged counterions. While these neutral agents have been shown to have higher LD_{50}s in animals, the mechanisms responsible have not been elucidated. Moreover, some of the mild and reversible effects of ionic agents, such as vacuolization of the kidney tubular cells, were thought at one time to be osmotic in nature, but these effects were produced by the neutral agents as well.[325] Most importantly, clinical trials repeatedly showed no significant difference in adverse events between any of the extracellular agents.[326,327]

In addition to lower osmolality, the formulations of neutral agents also have lower viscosity. This could have some benefit in applications requiring rapid injection, although power injectors have largely replaced human hands for these applications. It was also thought that the injection of a less viscous solution would minimize sheer forces in the vein, but there is no evidence of any difference in vascular toxicity among the extracellular agents.

VIII. Safety

A. Low Molecular Weight Chelates

The extracellular class of MRI agents are widely known to be among the safest drugs ever introduced.[4,326−328] The reported adverse event rates range from 1 to 3%, including such mild effects as headache, nausea, and taste perversion (oddly, a "metallic" taste despite the fact that the chelates do not dissociate in vivo). As with any widely used drug, there are scattered reports of more serious reactions such as anaphylaxis, but the reported rates are extremely low (0.0003−0.01%). The hepatobiliary and blood pool chelates in development appear to have comparable safety.[329−334]

An important contributory factor to the safety of these agents is their efficient excretion from the body. This minimizes exposure to the drug and reduces the chance that slow uptake processes such as endocytosis might internalize the agents in cells. In addition, the agents are largely excreted unaltered by oxidation or conjugation.

There is no evidence that any of the clinical effects of gadolinium(III) chelates stem from free gadolinium(III). Most likely the effects are due to the intact, foreign molecule or the small amount of free ligand added in the formulation. As discussed earlier, both metal ions and ligands tend to be more toxic than their stable chelates. The lack of any metal-based toxicity in humans is consistent with biodistribution studies in animals showing no significant bone uptake of free gadolinium(III).[6,334]

Investigators have tried to use animal and in vitro studies to discriminate among the extracellular agents,[6,8,334] especially using LD_{50} values, zinc chelation results, or metal ion release data (vide supra, section II). As mentioned above, neutral chelates have higher LD_{50}s. Macrocyclic chelates, such as $[Gd(DOTA)(H_2O)]^{-}$ and $[Gd(HP\text{-}DO3A)(H_2O)]$, release somewhat less gadolinium(III) in vivo. However, none of these differences appear to be relevant clinically.

B. Macromolecular Agents

As opposed to the free excreted small molecules, macromolecular conjugates tend to have much longer dwell times in the body and less complete elimination. This increases the odds of cellular uptake and processing, leading potentially to the release of toxic byproducts including free gadolinium(III). Franano et al.[117] have shown that albumin-Gd-DTPA conjugates can be metabolized in vivo to form lysine-Gd-DTPA monomers. Since this is likely to occur in the low pH environment of a lysosome, it is not suprising that, depending on the strength of the chelate, a significant fraction of the chelates dissociated, and gadolinium was found in the bone.

Moreover, large multivalent molecules are more likely to be antigenic than small molecules, leading to drug-directed antibodies and potentially anaphy-

laxis. Probably as a result of these concerns, no macromolecular agents have progressed to human trials.

IX. Applications

Due to the appreciable concentrations of paramagnetic label required for MRI enhancement (10−100 μM), novel applications involving true "magic bullet" targeting to receptors have not emerged, at least clinically. As outlined 12 years ago,[1] the dominant classes of agents in use or in development stem from bulk biodistribution rather than any elegant uptake mechanism. Still, there are molecular features which are critical to their function and interesting to explore.

A. Extracellular Agents

This class of agents represents the dominant use of MRI contrast media in radiology. After injection, the agents distribute nonspecifically throughout the plasma and interstitial space of the body. The agents are excreted by the kidneys with an elimination half-life of 1.5 h. A typical use is the detection of tumors in the brain. New applications involve faster imaging during injection to obtain images of arteries or of blood flow to the heart.

B. Blood Pool Agents

After extracellular agents, the next largest class of applications may involve blood pool agents that enhance vascular structures for the entire period of the MRI exam. The clinical need for these types of agents stems largely from the desire for a noninvasive alternative to X-ray angiography, the standard, but potentially dangerous, procedure for obtaining high-resolution pictures of arterial blockages in the body. In X-ray angiography, an artery, such as the femoral artery in the groin, is punctured and a long cathether fed to the site of interest. Large volumes of iodinated X-ray contrast agent are rapidly injected to highlight arteries during X-ray exposure. In addition to high cost to the health care system, side effects include pain, damage to the puncture site, kidney damage, and occasionally limb loss or death.

MRI represents a more attractive procedure for patients and doctors. Images of enhanced vessels can be obtained easily using intravenous injections of contrast agents rather than arterial injections. In addition, gadolinium agents are used in lower doses than X-ray agents and do not cause kidney dysfunction.

MS-325 (AngioMARK) is the prototype MR angiographic agent.[310,333] In addition to high relaxivity, its strong binding to albumin in serum reduces the free concentration available for glomerular filtration in the kidneys, thus slowing the renal excretion rate and prolonging the blood half-life and imaging window. Animal (Figure 47) and human studies showed that vessels were strongly enhanced with MS-325 for over 1 h in comparison to the very short window available with extracellular agents (0.5−3 min). The added time available with MS-325 permits the use of very high-resolution MR pulse sequences, affording stunningly detailed images of the vascular system (Figure 48).

A critical element in the design of MS-325 was pharmacokinetic tuning. The same chemical features which give rise to albumin binding, hydrophobic groups, also lead to liver uptake which can decrease blood half-life. A structure−activity analysis afforded a general solution to this problem,[335] and the hydrophilic phosphodiester group in MS-325 is representative. Despite causing a decrease in the overall lipophilicity, this moiety, placed in a critical position between the hydrophobic diphenylcyclohexyl group and the chelate, allowed for high albumin binding affinity. Presumably, the critical positioning of this anionic group leads to electrostatic interactions with known cationic side chains in the albumin binding sites. At the same time, however, the decreased overall lipophilicity leads to decreased liver uptake and prolonged blood half-life.

The alternative approach to blood pool agents, using macromolecules with covalently attached chelates, has been plagued with manufacturing and safety concerns.[4] None of these agents has progressed to clinical trials to date.

C. Hepatobiliary Agents

The presence of hydrophobic groups on metal chelates can lead to hepatocellular uptake and excretion into the bile ducts, gall bladder, and intestines. This class of MRI agents has been actively investigated for years,[14] and the first gadolinium-based agent, $[Gd(BOPTA)(H_2O)]^{2-}$ (MultiHance), is approved in Europe.[329,330] Interestingly, the perceived clinical applications of this agent mirror the biochemical consequences of its chemical structure. The presence of an aromatic ring gives rise to both albumin binding in serum and liver uptake (with cytosolic binding inside hepatocytes), so the agent is being pursued as both a liver agent and a general agent with higher relaxivity due to albumin binding. Latter applications include the same uses as the extracellular agents, especially the temporary enhancement of vascular structures. Thus $[Gd(BOPTA)(H_2O)]^{2-}$ is the first RIME agent to be approved for human use.

A related chelate, $[Gd(EOB\text{-}DTPA)(H_2O)]^{2-}$ (Eovist), is currently in phase III clinical trials.[331,332] This agent is excreted to a greater extent via the liver (roughly 50% for $[Gd(EOB\text{-}DTPA)(H_2O)]^{2-}$ vs 2−4% for $[Gd(BOPTA)(H_2O)]^{2-}$), resulting in stronger liver enhancement.

The mechanism for chelate uptake by the liver has not been clarified. Presumably it occurs from passive dissolution in the hepatocyte membrane or via discrete receptors. However, studies with MRI agents have confirmed that the transport from the hepatocyte into bile occurs via a specific organic anion transporter critical in the excretion of bilirubin, the toxic heme breakdown product. In the case of $[Gd(EOB\text{-}DTPA)(H_2O)]^{2-}$, prolonged trapping in the liver

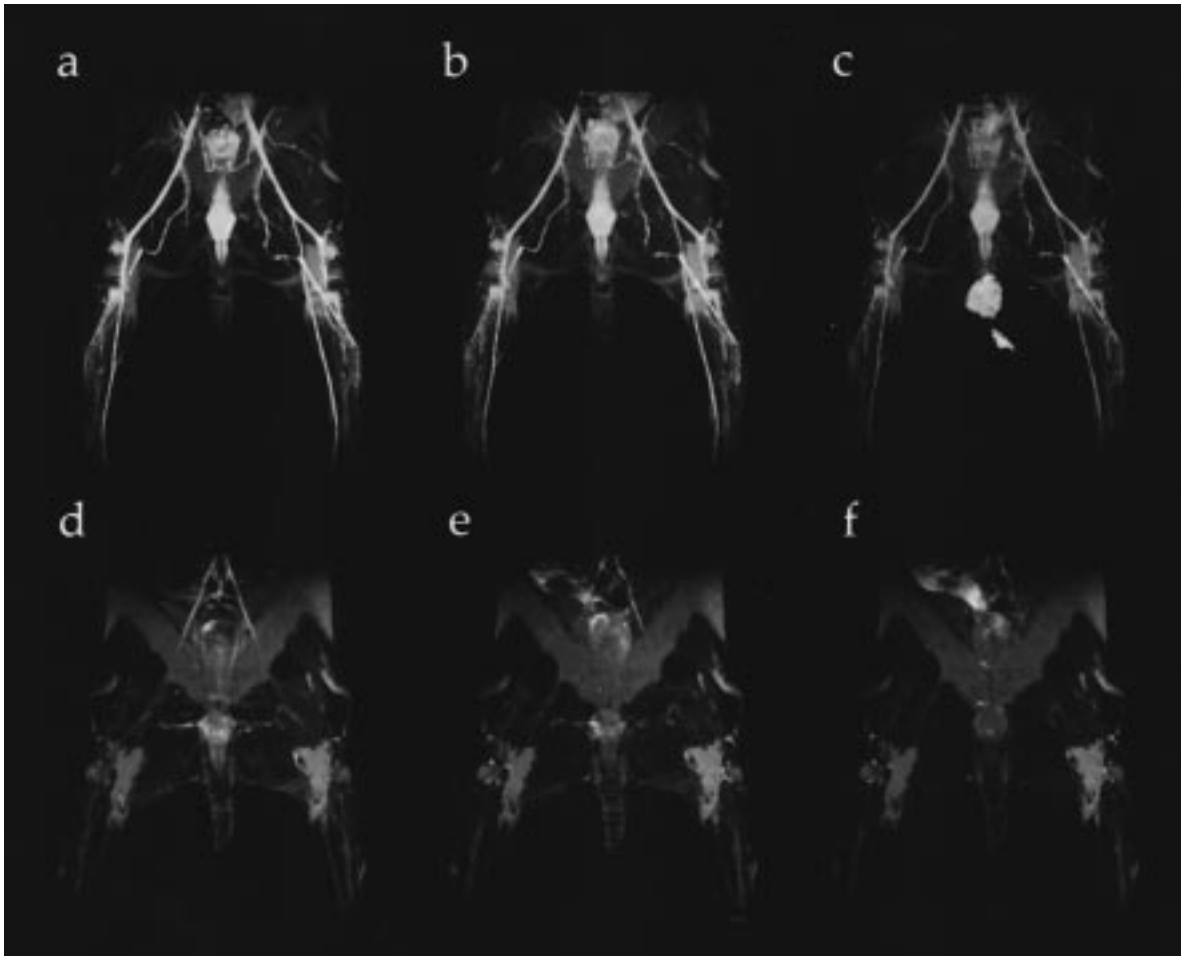

Figure 47. MR images (FISP 40/10/60 deg) of rabbit hindquarters after injection of either MS-325 (0.025 mmol/kg; a−c) or Gd-DTPA (0.1 mmol/kg; d−f). Images shown are 5 (a, d), 30 (b, e), and 60 min postinjection (c, f). Strong, persistent vascular enhancement is evident for MS-325 compared to transient enhancement available with Gd-DTPA.

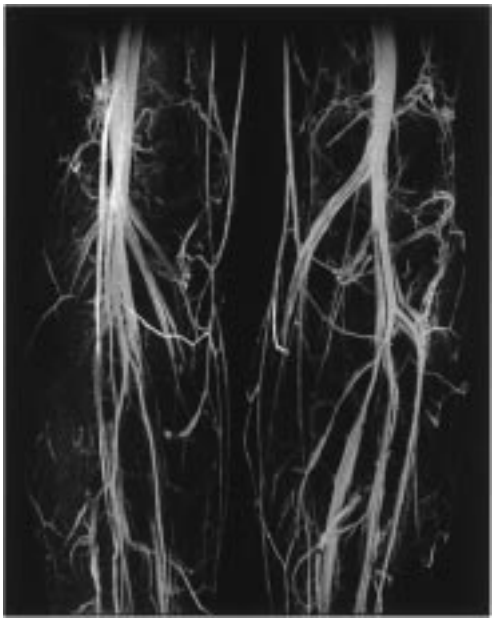

Figure 48. MRI image of the legs in a volunteer after injection of AngioMARK (MS-325). The prolonged increase in blood $1/T_1$ and signal enables noninvasive, high-resolution imaging of the vascular system, including detailed depictions of artery/vein pairs.

and strongly reduced biliary excretion were observed in mutant rats lacking this transporter.[336]

D. Other Agents

Many targeted contrast agents for MRI have been proposed and studied in vitro and in animals. Most of these have not progressed to advanced development or clinical trials due to metal chelate instability, insufficient targeting, high cost, toxicity, or small perceived market. An interesting discussion by Nunn et al. analyzes the reasons in more detail.[271] The following discussion summarizes a few notable areas that have attracted the most attention.

Metalloporphyrins have been evaluated as MRI agents for many years. The nonspecific binding of porphyrins to the interstitial space in tumors, known for over 50 years, attracted early interest in tumor imaging. One expanded porphyrin, PCI-120 ([Gd-(Tx)]$^{2+}$), is currently in clinical trials as a radiation sensitizer for brain cancer,[337] properties that stem from the unique delocalized ring structure, not the metal ion (see Scheme 1 for ligand structure). As a side benefit, the presence of a gadolinium(III) ion in the agent also creates prolonged enhancement of the tumors on MRI images. There are no reports that the agent has any advantages over extracellular agents for tumor detection, however.

One application for porphyrins that may have more promise is the prolonged enhancement of necrotic tissue, especially of myocardial infarcts. Schering AG has developed gadophrin-2, a Gd-DTPA chelate teth-

Scheme 2

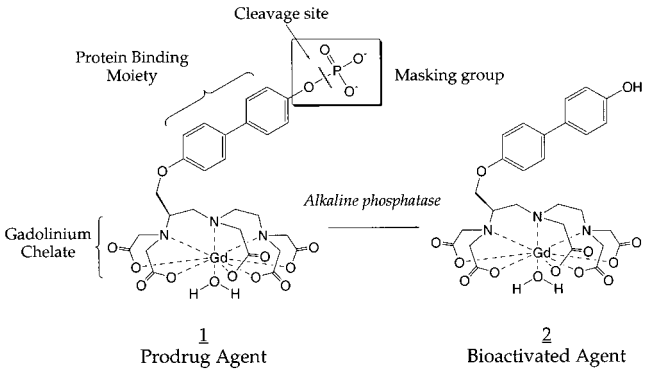

ered to a mesoporphrin (see Chart 16).[338,339] The mechanism for the avidity to necrosis is unknown, but may involve binding to cellular proteins released upon cell death or even to albumin which fills the necrotic area.

E. Bioactivated Agents

Recent reports show the potential of MRI agents which sense their biochemical environment, either through enzyme-induced relaxivity changes or changes due to the concentration of a particular substance. Once these strategies are made practical by proper choices of chelates, biochemical targets, and clinical indications, this approach may permit the detailed images of biological function.

Two recent reports show the potential to MRI agents which sense the presence of particular enzymes via enzyme-induced relaxivity changes. Meade and co-workers[340] synthesized (4,7,10-tri(acetic acid)-1-(2-β-galactopyranosylethoxy)-1,4,7,10-tetraazacyclododecane)gadolinium(III), a substrate for β-galactosidase. The galactose group coordinates to the Gd(III), lowering the relaxivity. The enzyme cleaves the galactopyranose group, increasing q from 0.7 to 1.2 and increasing the relaxivity by 20%.

McMurry and co-workers[341] used protein binding changes to increase relaxivity. This is shown schematically in Scheme 2. A substrate for alkaline phosphatase, prodrug **1**, was selected for its low binding affinity for HSA. Reaction with the enzyme yielded a 70% increase in $1/T_1$ in 4.5% HSA. Hydrolysis of the phosphate moiety increases the hydrophobicity of the aryl group, permitting stronger HSA binding affinity. Higher binding of **2**, the bioactivated agent, increases relaxivity.

Finally, Li et al.[342] sythesized a calcium-responsive agent, DOPTA-Gd, based on well-known calcium-chelating EGTA fluorophores. In the presence of low concentrations of calcium, the aromatic iminoacetate groups may coordinate in some fashion to the gadolinium ions, maintaining low (outer sphere?) relaxivity. As the concentration of calcium approaches micromolar, the EGTA chelate binds calcium, possibly releasing the Gd(III) coordinated iminoacetates, and increases relaxivity from 3.26 to 5.76 mM^{-1} s^{-1}. This interesting compound certainly merits more attention. The mechanism of relaxivity increase is speculative, and a detailed study of hydration is warranted.

X. Conclusion

MRI contrast media represent a complex field of technical endeavor. Much like other multidisciplinary areas such as high-temperature superconductors, the progress is at once encouraging but frustratingly slow.

We have seen great progress in understanding why different complexes have different relaxivities, yet we have been unable to drastically increase the values to enable targeting low-concentration receptors. The structure−activity relationships seen with water exchange behavior are most notable, but this is just a tuning fork, not the ultimate answer. In addition, the structure of the transition states and, thus, the real reasons why each complex has a different τ_m are unknown.

Most frustrating has been the lack of hard data and new theories regarding electron spin relaxation and its field dependent effects on relaxivity. Why are there countless dissertations on the electronic properties of obscure metalloenzymes and essentially none on gadolinium?

The ultimate beneficiaries of this hard work are, of course, patients. MRI, with the help of contrast agents, can eliminate painful, invasive procedures and provide diagnostic information earlier in the clinical workup. The authors have heard countless stories of clinical trial patients comparing a torturous X-ray angiography procedure to a safe, painless AngioMARK MRI. The efforts of chemists, along with their colleagues in other disciplines, have a lot to do with this progress.

It will be interesting to see how much more we can say in another decade.

XI. Acknowledgments.

The authors acknowledge Prof. André Merbach and Dr. Éva Tóth for providing data and a preprint of ref 281. Professor Silvio Aime is thanked for providing the NMRD data in Figures 39 and 46. Professor Bill Armstrong is kindly acknowledged for the use of his software and facilities in preparing the ORTEP drawings used throughout.

XII. References

(1) Lauffer, R. B. *Chem. Rev.* **1987**, *87*, 901−927.
(2) Banci, L.; Bertini, I.; Luchinat, C. *Nuclear and Electron Relaxation*; VCH: Weinheim, 1991.
(3) Aime, S.; Botta, M.; Fasano, M.; Terreno, E. *Chem. Soc. Rev.* **1998**, *27*, 19−29.
(4) Brasch, R. C. *Radiology* **1992**, *183*, 1−11.
(5) Tweedle, M. F. *J. Alloys Compd.* **1992**, *180*, 317−23.
(6) Tweedle, M. F. *Invest. Radiol.* **1992**, *27*, 2−6.
(7) Lauffer, R. B. *Magn. Reson. Quart.* **1990**, *6*, 65−84.
(8) Rocklage, S. M.; Watson, A. D.; Carvlin, M. J. In *Magnetic Resonance Imaging*; Stark, D. D., Bradley, W. G., Eds.; Mosby: St. Louis, 1992; Vol. 1.
(9) Øksendal, A. N.; Hals, P.-A. *Magn. Reson. Imaging* **1993**, *3*, 157−165.
(10) Mathur-De Vré, R.; Lemort, M. *Brit. J. Radiol.* **1995**, *68*, 225−247.
(11) Mitchell, D. G. *J. Magn. Reson. Imaging* **1997**, *7*, 1−4.
(12) Low, R. N. *J. Magn. Reson. Imag.* **1997**, *7*, 56−67.
(13) Mahfouz, A.-E.; Hamm, B.; Taupitz, M. *Eur. Radiol.* **1997**, *7*, 507−513.
(14) Schuhmann-Giampieri, G. *Invest. Radiol.* **1993**, *8*, 753−761.
(15) Peters, J. A.; Huskens, J.; Raber, D. J. *Prog. Nucl. Magn. Reson. Spectrosc.* **1996**, *28*, 283−350.

(16) Weissleder, R.; Papisov, M. *Rev. Magn. Reson. Med.* **1992**, *4*, 1−20.
(17) Gupta, H.; Weissleder, R. *MRI Clinics of North America* **1996**, *4*, 171.
(18) Albert, M. S.; Cates, G. D.; Driehuys, B.; Happer, W.; Saam, B.; Springer, C. S., Jr.; Wishnia, A. *Nature* **1994**, *370*, 199.
(19) Guggenberger, L. J.; Muetterties, E. L. *J. Am. Chem. Soc.* **1976**, *98*, 7221−5.
(20) Gries, H.; Miklautz, H. *Physiol. Chem. Phys. Med. NMR* **1984**, *16*, 105−12.
(21) Stezowski, J. J.; Hoard, J. L. *Isr. J. Chem.* **1984**, *24*, 323−34.
(22) Jin, T.; Zhao, S.; Xu, G.; Han, Y.; Shi, N.; Ma, Z. *Huaxue Xuebao* **1991**, *49*, 569−75.
(23) Inoue, M. B.; Inoue, M.; Fernando, Q. *Inorg. Chim. Acta* **1995**, *232*, 203−6.
(24) Sakagami, N.; Homma, J.-i.; Konno, T.; Okamoto, K.-i. *Acta Crystallogr., Sect. C: Cryst. Struct. Commun.* **1997**, *C53*, 1378−1381.
(25) Ruloff, R.; Gelbrich, T.; Hoyer, E.; Sieler, J.; Beyer, L. *Z. Naturforsch., B: Chem. Sci.* **1998**, *53*, 955−959.
(26) Caulfield, T. J.; Guo, P.; Illig, C. R.; Kellar, K. E.; Liversidge, E.; Shen, J.; Wellons, J.; Ladd, D.; Peltier, N.; Toner, J. L. *Bioorg. Med. Chem. Lett.* **1995**, *5*, 1657−62.
(27) Tyeklar, Z.; Midelfort, K.; Dunham, S.; Lauffer, R.; McMurry, T.; Hollander, F. Unpublished results.
(28) Uggeri, F.; Aime, S.; Anelli, P. L.; Botta, M.; Brocchetta, M.; de Haën, C.; Ermondi, G.; Grandi, M.; Paoli, P. *Inorg. Chem.* **1995**, *34*, 633−42.
(29) Dapporto, P.; Fedelli, F.; Paoli, P.; Uggeri, F. *Acta Crystallogr., Sect. C: Cryst. Struct. Commun.* **1996**, *C52*, 1438−1441.
(30) Selvin, P. R.; Jancarik, J.; Li, M.; Hung, L.-W. *Inorg. Chem.* **1996**, *35*, 700−5.
(31) Ehnebom, L.; Fjaertoft Pedersen, B. *Acta Chem. Scand.* **1992**, *46*, 126−30.
(32) Konings, M. S.; Dow, W. C.; Love, D. B.; Raymond, K. N.; Quay, S. C.; Rocklage, S. M. *Inorg. Chem.* **1990**, *29*, 1488−91.
(33) Bligh, S. W. A.; Chowdhury, A. H. M. S.; McPartlin, M.; Scowen, I. J.; Bulman, R. A. *Polyhedron* **1995**, *14*, 567−9.
(34) Wang, Y.-M.; Cheng, T.-H.; Sheu, R.-S.; Chen, I.-T.; Chiang, M. Y. *J. Chin. Chem. Soc. (Taipei)* **1997**, *44*, 123−128.
(35) Aime, S.; Benetollo, F.; Bombieri, G.; Colla, S.; Fasano, M.; Paoletti, S. *Inorg. Chim. Acta* **1997**, *254*, 63−70.
(36) Parker, D.; Pulukkody, K.; Smith, F. C.; Batsanov, A.; Howard, J. A. K. *J. Chem. Soc., Dalton Trans.* **1994**, 689−93.
(37) Inoue, M. B.; Inoue, M.; Fernando, Q. *Acta Crystallogr., Sect. C: Cryst. Struct. Commun.* **1994**, *C50*, 1037−40.
(38) Inoue, M. B.; Inoue, M.; Munoz, I. C.; Bruck, M. A.; Fernando, Q. *Inorg. Chim. Acta* **1993**, *209*, 29−34.
(39) Inoue, M. B.; Navarro, R. E.; Inoue, M.; Fernando, Q. *Inorg. Chem.* **1995**, *34*, 6074−9.
(40) Inoue, M. B.; Oram, P.; Inoue, M.; Fernando, Q.; Alexander, A. L.; Unger, E. C. *Magn. Reson. Imaging* **1994**, *12*, 429−32.
(41) Franklin, S. J.; Raymond, K. N. *Inorg. Chem.* **1994**, *33*, 5794−804.
(42) Spirlet, M. R.; Rebizant, J.; Desreux, J. F.; Loncin, M. F. *Inorg. Chem.* **1984**, *23*, 359−63.
(43) Dubost, J. P.; Leger, J. M.; Langlois, M. H.; Meyer, D.; Schaefer, M. *C. R. l'Academie Sci., Ser. II Univers* **1991**, *312*, 349−54.
(44) Chang, C. A.; Francesconi, L. C.; Malley, M. F.; Kumar, K.; Gougoutas, J. Z.; Tweedle, M. F.; Lee, D. W.; Wilson, L. J. *Inorg. Chem.* **1993**, *32*, 3501−8.
(45) Aime, S.; Barge, A.; Botta, M.; Fasano, M.; Ayala, J. D.; Bombieri, G. *Inorg. Chim. Acta* **1996**, *246*, 423−429.
(46) Aime, S.; Barge, A.; Benetollo, F.; Bombieri, G.; Botta, M.; Uggeri, F. *Inorg. Chem.* **1997**, *36*, 4287−4289.
(47) Kumar, K.; Chang, C. A.; Francesconi, L. C.; Dischino, D. D.; Malley, M. F.; Gougoutas, J. Z.; Tweedle, M. F. *Inorg. Chem.* **1994**, *33*, 3567−75.
(48) Platzek, J.; Blaszkiewicz, P.; Gries, H.; Luger, P.; Michl, G.; Mueller-Fahrnow, A.; Raduechel, B.; Suelzle, D. *Inorg. Chem.* **1997**, *36*, 6086−6093.
(49) Aime, S.; Anelli, P. L.; Botta, M.; Fedeli, F.; Grandi, M.; Paoli, P.; Uggeri, F. *Inorg. Chem.* **1992**, *31*, 2422−8.
(50) Howard, J. A. K.; Kenwright, A. M.; Moloney, J. M.; Parker, D.; Woods, M.; Port, M.; Navet, M.; Rousseau, O. *Chem. Commun.* **1998**, 1381−1382.
(51) Kang, S. I.; Ranganathan, R. S.; Emswiler, J. E.; Kumar, K.; Gougoutas, J. Z.; Malley, M. F.; Tweedle, M. F. *Inorg. Chem.* **1993**, *32*, 2912−18.
(52) Aime, S.; Batsanov, A. S.; Botta, M.; Howard, J. A. K.; Parker, D.; Senanayake, K.; Williams, G. *Inorg. Chem.* **1994**, *33*, 4696−706.
(53) Aime, S.; Batsanov, A. S.; Botta, M.; Dickins, R. S.; Faulkner, S.; Foster, C. E.; Harrison, A.; Howard, J. A. K.; Moloney, J. M.; Norman, T. J.; Parker, D.; Royle, L.; Williams, J. A. G. *J. Chem. Soc., Dalton Trans.* **1997**, 3623−3636.
(54) Dale, J. *Isr. J. Chem.* **1980**, *20*, 3−11.
(55) Spirlet, M.-R.; Rebizant, J.; Wang, X.; Jin, T.; Gilsoul, D.; Comblin, V.; Maton, F.; Muller, R. N.; Desreux, J. F. *J. Chem. Soc., Dalton Trans.* **1997**, 497−500.
(56) Spirlet, M. R.; Rebizant, J.; Loncin, M. F.; Desreux, J. F. *Inorg. Chem.* **1984**, *23*, 4278−83.
(57) Ruloff, R.; Prokop, P.; Sieler, J.; Hoyer, E.; Beyer, L. *Z. Naturforsch., B: Chem. Sci.* **1996**, *51*, 963−968.
(58) Wang, R.-Y.; Li, J.-R.; Jin, T.-Z.; Xu, G.-X.; Zhou, Z.-Y.; Zhou, X.-G. *Polyhedron* **1997**, *16*, 1361−1364.
(59) Ruloff, R.; Gelbrich, T.; Sieler, J.; Hoyer, E.; Beyer, L. *Z. Naturforsch., B: Chem. Sci.* **1997**, *52*, 805−809.
(60) Mondry, A.; Starynowicz, P. *Inorg. Chem.* **1997**, *36*, 1176−1180.
(61) Wang, R.-Y.; Li, J.-R.; Jin, T.-Z.; Xu, G.-X.; Zhou, Z.-Y.; Zhou, X.-G. *Polyhedron* **1997**, *16*, 2037−2040.
(62) Mondry, A.; Starynowicz, P. *J. Chem. Soc., Dalton Trans.* **1998**, 859−863.
(63) Chen, D.-F.; Yang, W.-C.; Wang, R.-Y.; Jin, T.-Z. *Huaxue Xuebao* **1997**, *55*, 672−677.
(64) Xu, J.; Franklin, S. J.; Whisenhunt, D. W., Jr.; Raymond, K. N. *J. Am. Chem. Soc.* **1995**, *117*, 7245−6.
(65) Sessler, J. L.; Mody, T. D.; Hemmi, G. W.; Lynch, V. *Inorg. Chem.* **1993**, *32*, 3175−87.
(66) Lisowski, J.; Sessler, J. L.; Lynch, V.; Mody, T. D. *J. Am. Chem. Soc.* **1995**, *117*, 2273−85.
(67) Alexander, V. *Chem. Rev.* **1995**, *95*, 273−342.
(68) Schauer, C. K.; Anderson, O. P. *J. Chem. Soc., Dalton Trans.* **1989**, 185−91.
(69) Morita, K.; Yukawa, Y.; Inomata, Y.; Howell, F. S.; Takeuchi, T. *Kidorui* **1996**, *28*, 218−219.
(70) Okamura, D.; Inomata, Y.; Howell, F. S. *Kidorui* **1997**, *30*, 324−325.
(71) Amin, S.; Voss, D. A., Jr.; Horrocks, W. D.; Lake, C. H.; Churchill, M. R.; Morrow, J. R. *Inorg. Chem.* **1995**, *34*, 3294−300.
(72) Dickins, R. S.; Howard, J. A. K.; Lehmann, C. W.; Moloney, J.; Parker, D.; Peacock, R. D. *Angew. Chem., Int. Ed. Engl.* **1997**, *36*, 521−523.
(73) Alderighi, L.; Bianchi, A.; Calabi, L.; Dapporto, P.; Giorgi, C.; Losi, P.; Paleari, L.; Paoli, P.; Rossi, P.; Valtancoli, B.; Virtuani, M. *Eur. J. Inorg. Chem.* **1998**, 1581−1584.
(74) Horrocks, W. D., Jr.; Sudnick, D. R. *J. Am. Chem. Soc.* **1979**, *101*, 334−40.
(75) Bryden, C. C.; Reilley, C. N. *Anal. Chem.* **1982**, *54*, 610−15.
(76) Alpoim, M. C.; Urbano, A. M.; Geraldes, C. F. G. C.; Peters, J. A. *J. Chem. Soc., Dalton Trans.* **1992**, 463−7.
(77) Geraldes, C. F. G. C.; Sherry, A. D.; Cacheris, W. P.; Kuan, K. T.; Brown, R. D., III.; Koenig, S. H.; Spiller, M. *Magn. Reson. Med.* **1988**, *8*, 191−9.
(78) Chang, C. A.; Brittain, H. G.; Telser, J.; Tweedle, M. F. *Inorg. Chem.* **1990**, *29*, 4468−73.
(79) Anelli, P. L.; Balzani, V.; Prodi, L.; Uggeri, F. *Gazz. Chim. Ital.* **1991**, *121*, 359−64.
(80) Geraldes, C. F. G. C.; Urbano, A. M.; Hoefnagel, M. A.; Peters, J. A. *Inorg. Chem.* **1993**, *32*, 2426−32.
(81) Bovens, E.; Hoefnagel, M. A.; Boers, E.; Lammers, H.; van Bekkum, H.; Peters, J. A. *Inorg. Chem.* **1996**, *35*, 7679−7683.
(82) Frey, S. T.; Chang, C. A.; Carvalho, J. F.; Varadarajan, A.; Schultze, L. M.; Pounds, K. L.; Horrocks, W. D., Jr. *Inorg. Chem.* **1994**, *33*, 2882−9.
(83) Bryden, C. C.; Reilley, C. N.; Desreux, J. F. *Anal. Chem.* **1981**, *53*, 1418−25.
(84) Albin, M.; Horrocks, W. D., Jr.; Liotta, F. J. *Chem. Phys. Lett.* **1982**, *85*, 61−4.
(85) Zhang, X.; Chang, C. A.; Brittain, H. G.; Garrison, J. M.; Telser, J.; Tweedle, M. F. *Inorg. Chem.* **1992**, *31*, 5597−600.
(86) Murru, M.; Parker, D.; Williams, G.; Beeby, A. *J. Chem. Soc., Chem. Commun.* **1993**, 1116−18.
(87) Kim, W. D.; Kiefer, G. E.; Huskens, J.; Sherry, A. D. *Inorg. Chem.* **1997**, *36*, 4128−4134.
(88) Shannon, R. D. *Acta Crystallogr., Sect. A* **1976**, *A32*, 751−67.
(89) Peters, J. A. *J. Magn. Reson.* **1986**, *68*, 240−51.
(90) Geraldes, C. F. G. C.; Urbano, A. M.; Alpoim, M. C.; Hoefnagel, M. A.; Peters, J. A. *J. Chem. Soc., Chem. Commun.* **1991**, 656−8.
(91) Peters, J. A. *Inorg. Chem.* **1988**, *27*, 4686−91.
(92) Jenkins, B. G.; Lauffer, R. B. *Inorg. Chem.* **1988**, *27*, 4730−8.
(93) Jacques, V.; Desreux, J. F. *Inorg. Chem.* **1994**, *33*, 4048−53.
(94) Hoeft, S.; Roth, K. *Chem. Ber.* **1993**, *126*, 869−73.
(95) Aime, S.; Botta, M.; Ermondi, G.; Terreno, E.; Anelli, P. L.; Fedeli, F.; Uggeri, F. *Inorg. Chem.* **1996**, *35*, 2726−36.
(96) Aime, S.; Botta, M.; Ermondi, G. *Inorg. Chem.* **1992**, *31*, 4291−9.
(97) Shukla, R. B. *J. Magn. Reson., Ser. A* **1995**, *113*, 196−204.
(98) Schmitt−Willich, H.; Brehm, M.; Ewers, Ch. L. J.; Michl, G.; Müller−Fahrnow, A.; Petrov, O.; Platzek, J.; Radüchel, B.; Sülzle, D. *Inorg. Chem.* **1999**, *38*, 1134−1144.
(99) Cummins, C. H.; Rutter, E. W., Jr.; Fordyce, W. A. *Bioconjugate Chem.* **1991**, *2*, 180−186.

(100) Lammers, H.; Maton, F.; Pubanz, D.; Van Laren, M. W.; Van Bekkum, H.; Merbach, A. E.; Muller, R. N.; Peters, J. A. *Inorg. Chem.* **1997**, *36*, 2527−2538.
(101) White, D. H.; DeLearie, L. A.; Dunn, T. J.; Rizkalla, E. N.; Imura, H.; Choppin, G. R. *Invest. Radiol.* **1991**, *28*, S229−S231.
(102) Aime, S.; Botta, M.; Fasano, M.; Marques, M. P. M.; Geraldes, C. F. G. C.; Pubanz, D.; Merbach, A. E. *Inorg. Chem.* **1997**, *36*, 2059−2068.
(103) Desreux, J. F. *Inorg. Chem.* **1980**, *19*, 1319−24.
(104) Brittain, H. G.; Desreux, J. F. *Inorg. Chem.* **1984**, *23*, 4459−66.
(105) Geraldes, C. F. G. C.; Sherry, A. D.; Kiefer, G. E. *J. Magn. Reson.* **1992**, *97*, 290−304.
(106) Ren, J.; Sherry, A. D. *J. Magn. Reson., Ser. B* **1996**, *111*, 178−182.
(107) Sherry, A. D.; Ren, J.; Huskens, J.; Bruecher, E.; Toth, E.; Geraldes, C. F. C. G.; Castro, M. M. C. A.; Cacheris, W. P. *Inorg. Chem.* **1996**, *35*, 4604−4612.
(108) Sherry, A. D.; Malloy, C. R.; Jeffrey, M. H.; Cacheris, W. P.; Geraldes, C. F. G. C. *J. Magn. Reson.* **1988**, *76*, 528−533.
(109) Buster, D. C.; Castro, M. M. C. A.; Geraldes, C. F. G. C.; Malloy, C. R.; Sherry, A. D.; Siemers, T. C. *Magn. Reson. Med.* **1990**, *15*, 25−32.
(110) Bansal, N.; Germann, M. J.; Seshan, V.; Shires, G. T., III.; Malloy, C. R.; Sherry, A. D. *Biochemistry* **1993**, *32*, 5638−43.
(111) Seshan, V.; Germann, M. J.; Preisig, P.; Malloy, C. R.; Sherry, A. D.; Bansal, N. *Magn. Reson. Med.* **1995**, *34*, 25−31.
(112) Sherry, A. D. *J. Alloys Compd.* **1997**, *249*, 153−157.
(113) Pulukkody, K. P.; Norman, T. J.; Parker, D.; Royle, L.; Broan, C. J. *J. Chem. Soc., Perkin Trans. 2* **1993**, 605−20.
(114) Loncin, M. F.; Desreux, J. F.; Merciny, E. *Inorg. Chem.* **1986**, *25*, 5, 2646−8.
(115) Holz, R. C.; Horrocks, W. D., Jr. *Inorg. Chim. Acta* **1990**, *171*, 193−8.
(116) Mondry, A.; Riehl, J. P. *Acta Phys. Pol., A* **1993**, *84*, 969−74.
(117) Franano, F. N.; Edwards, W. B.; Welch, M. J.; Brechbiel, M. W.; Gansow, O. A.; Duncan, J. R. *Magn. Reson. Imaging* **1995**, *13*, 201−14.
(118) Wedeking, P.; Tweedle, M. *Nucl. Med. Biol.* **1988**, *15*, 395−402.
(119) Wedeking, P.; Kumar, K.; Tweedle, M. F. *Nucl. Med. Biol.* **1993**, *20*, 679−91.
(120) Smith, R. M.; Martell, A. E. *Critical Stability Constants*; Plenum: New York, 1974.
(121) Wedeking, P.; Kumar, K.; Tweedle, M. F. *Magn. Reson. Imaging* **1992**, *10*, 641−8.
(122) Cacheris, W. P.; Quay, S. C.; Rocklage, S. M. *Magn. Reson. Imaging* **1990**, *8*, 467−81.
(123) Kumar, K.; Tweedle, M. F.; Malley, M. F.; Gougoutas, J. Z. *Inorg. Chem.* **1995**, *34*, 6472−80.
(124) Meyer, D.; Schaefer, M.; Doucet, D. *Invest. Radiol.* **1990**, *25*, S53−S55.
(125) Runge, V. M.; Gelblum, D. Y.; Jacobson, S. *Magn. Reson. Imaging* **1991**, *9*, 79−87.
(126) White, D. H.; DeLearie, L. A.; Moore, D. A.; Wallace, R. A.; Dunn, T. J.; Cacheris, W. P.; Imura, H.; Choppin, G. R. *Invest. Radiol.* **1991**, *26*, S226−S228.
(127) Cacheris, W. P.; Nickle, S. K.; Sherry, A. D. *Inorg. Chem.* **1987**, *26*, 958−60.
(128) Clarke, E. T.; Martell, A. E. *Inorg. Chim. Acta* **1991**, *190*, 37−46.
(129) Smith, R. M.; Motekaitis, R. J.; Martell, A. E. *NIST Standard Reference Database #46*, 3.0 ed.; National Institute of Standards and Technology: Washington, DC, 1997.
(130) Wang, X.; Jin, T.; Comblin, V.; Lopez-Mut, A.; Merciny, E.; Desreux, J. F. *Inorg. Chem.* **1992**, *31*, 1095−9.
(131) Puttagunta, N. R.; Gibby, W. A.; Smith, G. T. *Invest. Radiol.* **1996**, *31*, 739−742.
(132) Puttagunta, N. R.; Gibby, W. A.; Puttagunta, V. L. *Invest. Radiol.* **1996**, *31*, 619−624.
(133) Tweedle, M. F.; Hagan, J. J.; Kumar, K.; Mantha, S.; Chang, C. A. *Magn. Reson. Imaging* **1991**, *9*, 409−15.
(134) Kumar, K.; Tweedle, M. F. *Inorg. Chem.* **1993**, *32*, 4193−9.
(135) Brucher, E.; Sherry, A. D. *Inorg. Chem.* **1990**, *29*, 1555−9.
(136) Choi, K.-Y.; Kim, K. A.; Kim, J. C. *Polyhedron* **1994**, *13*, 567−571.
(137) Kumar, K.; Chang, C. A.; Tweedle, M. F. *Inorg. Chem.* **1993**, *32*, 587−93.
(138) Kumar, K.; Jin, T.; Wang, X.; Desreux, J. F.; Tweedle, M. F. *Inorg. Chem.* **1994**, *33*, 3823−9.
(139) Harrison, A.; Walker, C. A.; Pereira, K. A.; Parker, D.; Royle, L.; Pulukkody, K.; Norman, T. J. *Magn. Reson. Imaging* **1993**, *11*, 761−70.
(140) Rizkalla, E.; Choppin, G.; Cacheris, W. *Inorg. Chem.* **1993**, *32*, 582−586.
(141) Wang, Y.-M.; Cheng, T.-H.; Liu, G.-C.; Sheu, R.-S. *J. Chem. Soc., Dalton Trans.* **1997**, 833−837.
(142) Wang, Y.-M.; Lin, S.-T.; Wang, Y.-J.; Sheu, R.-S. *Polyhedron* **1998**, *17*, 2021−2028.
(143) Wang, Y.-M.; Lee, C.-H.; Liu, G.-C.; Sheu, R.-S. *J. Chem. Soc., Dalton Trans.* **1998**, 4113−4118.
(144) Varadarajan, J. A.; Crofts, S. P.; Carvalho, J. F.; Fellmann, J. D.; Kim, S.-H.; Chang, C. A.; Watson, A. D. *Invest. Radiol.* **1994**, *29*, S18−S20.
(145) Paul-Roth, C.; Raymond, K. N. *Inorg. Chem.* **1995**, *34*, 1408−12.
(146) Harris, W. R.; Raymond, K. N.; Weitl, F. L. *J. Am. Chem. Soc.* **1981**, *103*, 2667−75.
(147) Caravan, P.; Mehrkhodavandi, P.; Orvig, C. *Inorg. Chem.* **1997**, 13166-1321.
(148) Thompson, L.; Shafer, B.; Edgar, J.; Mannila, K. *Adv. Chem. Ser.* **1967**, *71*, 169−179.
(149) Wiegers, C. B.; Welch, M. J.; Sharp, T. L.; Brown, J. J.; Perman, W. H.; Sun, Y.; Motekaitis, R. J.; Martell, A. E. *Magn. Reson. Imaging* **1992**, *10*, 903−11.
(150) Wagner, M.; Ruloff, R.; Hoyer, E.; Grunder, W. *Z. Naturforsch., C: Biosci.* **1997**, *52*, 508−515.
(151) Sherry, A. D. *J. Less-Common Met.* **1989**, *149*, 133−41.
(152) Kim, W. D.; Hrncir, D. C.; Kiefer, G. E.; Sherry, A. D. *Inorg. Chem.* **1995**, *34*, 2225−32.
(153) Hong, C.; Kim, D. W.; Choi, K.-Y. *Bull. Korean Chem. Soc.* **1997**, *18*, 1158−1161.
(154) Delgado, R.; Sun, Y.; Motekaitis, R. J.; Martell, A. E. *Inorg. Chem.* **1993**, *32*, 3320−6.
(155) Brucher, E.; Cortes, S.; Chavez, F.; Sherry, A. D. *Inorg. Chem.* **1991**, *30*, 2092−7.
(156) Wu, S. L.; Horrocks, W. D., Jr. *J. Chem. Soc., Dalton Trans.* **1997**, 1497−1502.
(157) Wu, S. L.; Horrocks, W. D., Jr. *Anal. Chem.* **1996**, *68*, 394−401.
(158) Sherry, A. D.; Brown, R. D., III; Geraldes, C. F. G. C.; Koenig, S. H.; Kuan, K. T.; Spiller, M. *Inorg. Chem.* **1989**, *28*, 620−2.
(159) Lazar, I.; Sherry, A. D.; Ramasamy, R.; Brucher, E.; Kiraly, R. *Inorg. Chem.* **1991**, *30*, 5016−19.
(160) Geraldes, C. F. G. C.; Sherry, A. D.; Lázár, I.; Miseta, A.; Bogner, P.; Berenyi, E.; Sumegi, B.; Kiefer, G. E.; McMillan, K.; Maton, F.; Muller, R. N. *Magn. Reson. Med.* **1993**, *30*, 696−703.
(161) Geraldes, C. F. G. C.; Brown, R. D., III; Cacheris, W. P.; Koenig, S. H.; Sherry, A. D.; Spiller, M. *Magn. Reson. Med.* **1989**, *9*, 94−104.
(162) Parker, D.; Pulukkody, K.; Norman, T. J.; Harrison, A.; Royle, L.; Walker, C. *J. Chem. Soc., Chem. Commun.* **1992**, 1441−3.
(163) Broan, C. J.; Cole, E.; Jankowski, K. J.; Parker, D.; Pulukkody, K.; Boyce, B. A.; Beeley, N. R. A.; Millar, K.; Millican, A. T. *Synthesis* **1992**, 63−8.
(164) Aime, S.; Botta, M.; Parker, D.; Williams, J. A. G. *J. Chem. Soc., Dalton Trans.* **1996**, 17−23.
(165) Choppin, G. R. *J. Alloys Compd.* **1995**, *225*, 242−245.
(166) McMurry, T. J.; Pippin, C. G.; Wu, C.; Deal, K. A.; Brechbiel, M. W.; Mirzadeh, S.; Gansow, O. A. *J. Med. Chem.* **1998**, *41*, 3546−3549.
(167) Luz, Z.; Meiboom, S. *J. Chem. Phys.* **1964**, *40*, 2686.
(168) Swift, T. J.; Connick, R. E. *J. Chem. Phys.* **1962**, *37*, 307.
(169) Kowalewski, J.; Nordenskioeld, L.; Benetis, N.; Westlund, P. O. *Prog. Nucl. Magn. Reson. Spectrosc.* **1985**, *17*, 141−85.
(170) Bertini, I.; Luchinat, C. *Coord. Chem. Rev.* **1996**, *150*, 1−295.
(171) Cossy, C.; Helm, L.; Powell, D. H.; Merbach, A. E. *New J. Chem.* **1995**, *19*, 27−35.
(172) Helm, L.; Merbach, A. E. *Eur. J. Solid State Inorg. Chem.* **1991**, *28*, 245−50.
(173) Benazeth, S.; Purans, J.; Chalbot, M.-C.; Nguyen-van-Duong, M. K.; Nicolas, L.; Keller, F.; Gaudemer, A. *Inorg. Chem.* **1998**, *37*, 3667−3674.
(174) Yamaguchi, T.; Nomura, M.; Wakita, H.; Otaki, H. *J. Chem. Phys.* **1988**, *89*, 5153−9.
(175) Steele, M. L.; Wertz, D. L. *J. Am. Chem. Soc.* **1976**, *98*, 4424−8.
(176) Clarkson, R. B.; Hwang, J. H.; Belford, R. L. *Magn. Reson. Med.* **1993**, *29*, 521−7.
(177) Powell, D. H.; Ni Dhubhghaill, O. M.; Pubanz, D.; Helm, L.; Lebedev, Y. S.; Schlaepfer, W.; Merbach, A. E. *J. Am. Chem. Soc.* **1996**, *118*, 9333−9346.
(178) Chen, J. W.; Auteri, F. P.; Budil, D. E.; Belford, R. L.; Clarkson, R. B. *J. Phys. Chem.* **1994**, *98*, 13452−9.
(179) Chen, J. W.; Belford, R. L.; Clarkson, R. B. *J. Phys. Chem. A* **1998**, *102*, 2117−2130.
(180) Halle, B.; Wennerström *J. Magn. Reson.* **1981**, *44*, 89.
(181) Aime, S.; Nano, R. *Invest. Radiol.* **1988**, *23*, S264−S266.
(182) Vander Elst, L.; Laurent, S.; Muller, R. N. *Invest. Radiol.* **1998**, *33*, 828−834.
(183) Lakowicz, J. R. *Principles of Fluorescence Spectroscopy*; Plenum: New York, 1983.
(184) Micskei, K.; Helm, L.; Brucher, E.; Merbach, A. E. *Inorg. Chem.* **1993**, *32*, 3844−50.
(185) Aime, S.; Barge, A.; Botta, M.; Parker, D.; De Sousa, A. S. *J. Am. Chem. Soc.* **1997**, *119*, 4767−4768.
(186) Strandberg, E.; Westlund, P.-O. *J. Magn. Reson., Ser. A* **1996**, *122*, 179−191.
(187) Abernathy, S. M.; Miller, J. C.; Lohr, L. L.; Sharp, R. R. *J. Chem. Phys.* **1998**, *109*, 4035−4046.
(188) Abernathy, S. M.; Sharp, R. R. *J. Chem. Phys.* **1997**, *106*, 9032−9043.

(189) Abernathy, S. M.; Sharp, R. R. *J. Phys. Chem. A* **1997**, *101*, 3692−3698.
(190) Sharp, R.; Abernathy, S. M.; Lohr, L. L. *J. Chem. Phys.* **1997**, *107*, 7620−7629.
(191) Sharp, R. R. *J. Chem. Phys.* **1993**, *98*, 912−21.
(192) Sharp, R. R. *J. Chem. Phys.* **1993**, *98*, 2507−15.
(193) Sharp, R. R. *J. Chem. Phys.* **1993**, *98*, 6092−101.
(194) Sharp, R. R. *J. Magn. Reson.* **1992**, *100*, 491−516.
(195) Bovet, J. M.; Sharp, R. R. *J. Chem. Phys.* **1993**, *99*, 18−26.
(196) Westlund, P.-O. *J. Chem. Phys.* **1998**, *108*, 4945−4953.
(197) Westlund, P. O.; Larsson, T. P.; Teleman, O. *Mol. Phys.* **1993**, *78*, 1365−84.
(198) Banci, L.; Bertini, I.; Briganti, F.; Luchinat, C. *J. Magn. Reson.* **1986**, *66*, 58−65.
(199) Benetis, N.; Kowalewski, J.; Nordenskioeld, L.; Wennerstroem, H.; Westlund, P. O. *Mol. Phys.* **1983**, *48*, 329−46.
(200) Larsson, T.; Westlund, P.-O.; Kowalewski, J.; Koenig, S. H. *J. Chem. Phys.* **1994**, *101*, 1116−28.
(201) Lipari, G.; Szabo, A. *J. Am. Chem. Soc.* **1982**, *104*, 4546−4559.
(202) Freed, J. *J. Chem. Phys.* **1978**, *68*, 4034.
(203) Pfeifer, H. *Ann. Phys. (Leipzig)* **1961**, *8*, 1.
(204) Geraldes, C. F. G. C.; Urbano, A. M.; Alpoim, M. C.; Sherry, A. D.; Kuan, K.-T.; Rajagopalan, R.; Maton, F.; Muller, R. N. *Magn. Reson. Imaging* **1995**, *13*, 401−20.
(205) Koenig, S. H. *Invest. Radiol.* **1994**, *29*, S127−S130.
(206) Southwood-Jones, R. V.; Earl, W. L.; Newman, K. E.; Merbach, A. E. *J. Chem. Phys.* **1980**, *73*, 5909−18.
(207) Micskei, K.; Powell, D. H.; Helm, L.; Brucher, E.; Merbach, A. E. *Magn. Reson. Chem.* **1993**, *31*, 1011−20.
(208) Gonzalez, G.; Powell, D. H.; Tissieres, V.; Merbach, A. E. *J. Phys. Chem.* **1994**, *98*, 53−9.
(209) Powell, D. H.; Gonzalez, G.; Tissieres, V.; Micskei, K.; Bruecher, E.; Helm, L.; Merbach, A. E. *J. Alloys Compd.* **1994**, *207−208*, 20−4.
(210) Helm, L.; Powell, D. H.; Merbach, A. E. *High-Pressure Research* **1994**, *13*, 109−113.
(211) Powell, D. H.; Favre, M.; Graeppi, N.; Dhubhghaill, O. M. N.; Pubanz, D.; Merbach, A. *J. Alloys Compd.* **1995**, *225*, 246−252.
(212) Toth, E.; Pubanz, D.; Vauthey, S.; Helm, L.; Merbach, A. E. *Chem. Eur. J.* **1996**, *2*, 1607−1615.
(213) Toth, E.; Vauthey, S.; Pubanz, D.; Merbach, A. E. *Inorg. Chem.* **1996**, *35*, 3375−9.
(214) Aime, S.; Barge, A.; Borel, A.; Botta, M.; Chemerisov, S.; Merbach, A. E.; Mueller, U.; Pubanz, D. *Inorg. Chem.* **1997**, *36*, 5104−5112.
(215) Toth, E.; Burai, L.; Brucher, E.; Merbach, A. E. *J. Chem. Soc., Dalton Trans.* **1997**, 1587−1594.
(216) Toth, E.; Connac, F.; Helm, L.; Adzamli, K.; Merbach, A. E. *Eur. J. Inorg. Chem.* **1998**, 2017−2021.
(217) Toth, E.; Helm, L.; Merbach, A. E.; Hedinger, R.; Hegetschweiler, K.; Janossy, A. *Inorg. Chem.* **1998**, *37*, 4104−4113.
(218) Ruloff, R.; Muller, R. N.; Pubanz, D.; Merbach, A. E. *Inorg. Chim. Acta* **1998**, *275−276*, 15−23.
(219) Toth, E.; Van Uffelen, I.; Helm, L.; Merbach, A. E.; Ladd, D.; Briley-Saebo, K.; Kellar, K. E. *Magn. Reson. Chem.* **1998**, *36*, S125−S134.
(220) Toth, E.; Connac, F.; Helm, L.; Adzamli, K.; Merbach, A. E. *J. Biol. Inorg. Chem.* **1998**, *3*, 606−613.
(221) Aime, S.; Barge, A.; Botta, M.; De Sousa, A. S.; Parker, D. *Angew. Chem., Int. Ed. Engl.* **1998**, *37*, 2673−2675.
(222) Pubanz, D.; Gonzalez, G.; Powell, D. H.; Merbach, A. E. *Inorg. Chem.* **1995**, *34*, 4447−53.
(223) Graeppi, N.; Powell, D. H.; Laurenczy, G.; Zekany, L.; Merbach, A. E. *Inorg. Chim. Acta* **1995**, *235*, 311−26.
(224) Toth, E.; Burai, L.; Brucher, E.; Merbach, A. *J. Chem Soc. Dalton Trans.* **1997**, 1587−1594.
(225) Aime, S.; Botta, M.; Crich, S. G.; Giovenzana, G.; Pagliarin, R.; Sisti, M.; Terreno, E. *Magn. Reson. Chem.* **1998**, *36*, S200−S208.
(226) Aime, S.; Botta, M.; Crich, S. G.; Giovenzana, G. B.; Jommi, G.; Pagliarin, R.; Sisti, M. *Inorg. Chem.* **1997**, *36*, 2992−3000.
(227) Aime, S.; Botta, M.; Fasano, M.; Paoletti, S.; Terreno, E. *Chem. Eur. J.* **1997**, *3*, 1499−1504.
(228) Aime, S.; Crich, S. G.; Gianolio, E.; Terreno, E.; Beltrami, A.; Uggeri, F. *Eur. J. Inorg. Chem.* **1998**, 1283−1289.
(229) Kim, W. D.; Kiefer, G. E.; Maton, F.; McMillan, K.; Muller, R. N.; Sherry, A. D. *Inorg. Chem.* **1995**, *34*, 2233−43.
(230) Aime, S.; Botta, M.; Dickins, R. S.; Maupin, C. L.; Parker, D.; Riehl, J. P.; Williams, J. A. G. *J. Chem. Soc., Dalton Trans.* **1998**, 881−892.
(231) Aime, S.; Botta, M.; Crich, S. G.; Giovenzana, G. B.; Pagliarin, R.; Piccinini, M.; Sisti, M.; Terreno, E. *J. Biol. Inorg. Chem.* **1997**, *2*, 470−479.
(232) Aime, S.; Fasano, M.; Paoletti, S.; Terreno, E. *Gazz. Chim. Ital.* **1995**, *125*, 125−31.
(233) Aime, S.; Botta, M.; Nonnato, A.; Terreno, E.; Anelli, P. L.; Uggeri, F. *J. Alloys Compd.* **1995**, *225*, 274−8.
(234) Aime, S.; Botta, M.; Fasano, M.; Paoletti, S.; Anelli, P. L.; Uggeri, F.; Virtuani, M. *Inorg. Chem.* **1994**, *33*, 4707−11.
(235) Aime, S.; Botta, M.; Terreno, E.; Anelli, P. L.; Uggeri, F. *Magn. Reson. Med.* **1993**, *30*, 583−91.
(236) Geraldes, C. F. G. C.; Sherry, A. D.; Vallet, P.; Maton, F.; Muller, R. N.; Mody, T. D.; Hemmi, G.; Sessler, J. L. *Magn. Reson. Imaging* **1995**, *5*, 725−729.
(237) Geraldes, C. F. G. C.; Brown, R. D., III; Brucher, E.; Koenig, S. H.; Sherry, A. D.; Spiller, M. *Magn. Reson. Med.* **1992**, *27*, 284−95.
(238) Aime, S.; Botta, M.; Dastru, W.; Fasano, M.; Panero, M.; Arnelli, A. *Inorg. Chem.* **1993**, *32*, 2068−71.
(239) Hall, J.; Haner, R.; Aime, S.; Botta, M.; Faulkner, S.; Parker, D.; de Sousa, A. S. *New J. Chem.* **1998**, *22*, 627−631.
(240) Sur, S. K.; Bryant, R. G. *J. Magn. Reson.* **1996**, *B 111*, 105−108.
(241) Shukla, R. B.; Kumar, K.; Weber, R.; Zhang, X.; Tweedle, M. *Acta Radiologica* **1997**, *38*, 121−123.
(242) Powell, D. H.; Merbach, A. E.; Gonzalez, G.; Bruecher, E.; Micskei, K.; Ottaviani, M. F.; Koehler, K.; von Zelewsky, A.; Grinberg, O. Y.; Lebedev, Y. S. *Helv. Chim. Acta* **1993**, *76*, 2129−46.
(243) Aime, S.; Botta, M.; Fasano, M.; Crich, S. G.; Terreno, E. *J. Biol. Inorg. Chem.* **1996**, *1*, 312−319.
(244) Sessler, J. L.; Mody, T. D.; Hemmi, G. W.; Lynch, V.; Young, S. W.; Miller, R. A. *J. Am. Chem. Soc.* **1993**, *115*, 10368−9.
(245) Smith, P. H.; Reyes, Z. E.; Lee, C. W.; Raymond, K. N. *Inorg. Chem.* **1988**, *27*, 4154−65.
(246) Cavagna, F. M.; Maggioni, F.; Castelli, P. M.; Dapra, M.; Imperatori, L. G.; Lorusso, V.; Jenkins, B. G. *Invest. Radiol.* **1997**, *32*, 780−796.
(247) Zhang, X.; Pillai, R.; Shukla, R.; Ranganathan, R. S.; Tweedle, M. *Invest. Radiol.* **1994**, *29*, S69−S70.
(248) Bligh, S. W. A.; Choi, N.; Evagorou, E. G.; McPartlin, M.; Cummins, W. J.; Kelly, J. D. *Polyhedron* **1992**, *11*, 2571−3.
(249) Bligh, S. W. A.; Harding, C. T.; McEwen, A. B.; Sadler, P. J.; Kelly, J. D.; Marriott, J. A. *Polyhedron* **1994**, *13*, 1937−43.
(250) Bligh, S. W. A.; Choi, N.; Geraldes, C. F. G. C.; Knoke, S.; McPartlin, M.; Sanganee, M. J.; Woodroffe, T. M. *J. Chem. Soc., Dalton Trans.* **1997**, 4119−4126.
(251) Bligh, S. W. A.; Drew, M. G. B.; Martin, N.; Maubert, B.; Nelson, J. *J. Chem. Soc., Dalton Trans.* **1998**, 3711−3714.
(252) Martin, V. V.; Ralston, W. H.; Hynes, M. R.; Keana, J. F. W. *Bioconjugate Chem.* **1995**, *6*, 616−23.
(253) Aime, S.; Botta, M.; Panero, M.; Grandi, M.; Uggeri, F. *Magn. Reson. Chem.* **1991**, *29*, 923−7.
(254) Aime, S.; Botta, M.; Ermondi, G. *J. Magn. Reson.* **1991**, *92*, 572−80.
(255) Aime, S.; Botta, M.; Crich, S. G.; Giovenzana, G. B.; Jommi, G.; Pagliarin, R.; Sisti, M. *J. Chem. Soc., Chem. Commun.* **1995**, 1885−6.
(256) Aime, S.; Botta, M.; Parker, D.; Williams, J. A. G. *J. Chem. Soc., Dalton Trans.* **1995**, 2259−66.
(257) Shukla, R.; Fernandez, M.; Pillai, R. K.; Ranganathan, R.; Ratsep, P. C.; Zhang, X.; Tweedle, M. F. *Magn. Reson. Med.* **1996**, *35*, 928−931.
(258) Wallace, R. A.; Haar, J. P., Jr.; Miller, D. B.; Woulfe, S. R.; Polta, J. A.; Galen, K. P.; Hynes, M. R.; Adzamli, K. *Magn. Reson. Med.* **1998**, *40*, 733−739.
(259) Periasamy, M.; White, D.; DeLearie, L.; Moore, D.; Wallace, R.; Lin, W.; Dunn, J.; Hirth, W.; Cacheris, W. *Invest. Radiol.* **1991**, *26*, S217−S220.
(260) Weinmann, H. J.; Schuhmann-Giampieri, G.; Schmitt-Willich, H.; Vogler, H.; Frenzel, T.; Gries, H. *Magn. Reson. Med.* **1991**, *22*, 233−7.
(261) Geze, C.; Mouro, C.; Hindre, F.; Le Plouzennec, M.; Moinet, C.; Rolland, R.; Alderighi, L.; Vacca, A.; Simonneaux, G. *Bull. Soc. Chim. Fr.* **1996**, *133*, 267−272.
(262) Claire, P. P. K.; Jones, C. J.; Chiu, K. W.; Thornback, J. R.; McPartlin, M. *Polyhedron* **1992**, *11*, 499−500.
(263) Anelli, P. L.; Calabi, L.; de Haen, C.; Fedeli, F.; Losi, P.; Murru, M.; Uggeri, F. *Gazz. Chim. Ital.* **1996**, *126*, 89−97.
(264) Adzamli, I. K.; Blau, M. *Magn. Reson. Med.* **1991**, *17*, 141−8.
(265) Ranganathan, R. S.; Fernandez, M. E.; Kang, S. I.; Nunn, A. D.; Ratsep, P. C.; Pillai, K. M. R.; Zhang, X.; Tweedle, M. F. *Invest. Radiol.* **1998**, *33*, 779−797.
(266) Smith, P. H.; Brainard, J. R.; Morris, D. E.; Jarvinen, G. D.; Ryan, R. R. *J. Am. Chem. Soc.* **1989**, *111*, 7437−43.
(267) Burai, L.; Hietapelto, V.; Kiraly, R.; Toth, E.; Brucher, E. *Magn. Reson. Med.* **1997**, *38*, 146−150.
(268) Lindqvist-Reis, P.; Muñoz-Páez, A.; Díaz-Moreno, S.; Pattanaik, S.; Persson, I.; Sandström, M. *Inorg. Chem.* **1998**, *37*, 6675−6683.
(269) Bleuzen, A.; Foglia, F.; Furet, E.; Helm, L.; Merbach, A.; Weber, J. *J. Am. Chem. Soc.* **1996**, *118*, 12777.
(270) Brasch, R. C. *Magn. Reson. Med.* **1991**, *22*, 282−7.
(271) Nunn, A. D.; Linder, K.; Tweedle, M. *Quart. J. Nuc. Med.* **1997**, *41*, 155−62.
(272) Brinkley, M. *Bioconjugate Chem.* **1992**, *3*, 2−13.

(273) Schuhmann-Giampieri, G.; Schmitt-Willich, H.; Frenzel, T.; Press: W. R.; Weinmann, H. J. *Invest. Radiol.* **1991**, *26*, 969−74.
(274) Sieving, P. F.; Watson, A. D.; Rocklage, S. M. *Bioconjugate Chem.* **1990**, *1*, 65−71.
(275) Spanoghe, M.; Lanens, D.; Dommisse, R.; Van der Linden, A.; Alder Weireldt, F. *Magn. Reson. Imaging* **1992**, *10*, 913−17.
(276) Desser, T.; Rubin, D.; Muller, H.; Qing, F.; Khodor, S.; Zanazzi; Young, S.; Ladd, D.; Wellons, J.; Kellar, K.; Toner, J.; Snow, R. *J. Magn. Reson. Imaging* **1994**, *4*, 467−472.
(277) Frank, H.; Weissleder, R.; Bogdanov, A.; Brady, T. *Am. J. Radiol.* **1994**, 1041−1046.
(278) Bogdanov, A. A.; Weissleder, R.; Frank, H. W.; Bogdanova, A. V.; Nossif, N.; Schaffer, B. K.; Tsai, E.; Papisov, M. I.; Brady, T. J. *Radiology* **1993**, *187*, 701−6.
(279) Bogdanov, A. A. J.; Weissleder, R.; Brady, T. J. *Adv. Drug Delivery Rev.* **1995**, *16*, 335−48.
(280) Kellar, K. E.; Henrichs, P. M.; Hollister, R.; Koenig, S. H.; Eck, J.; Wei, D. *Magn. Reson. Med.* **1997**, *38*, 712−716.
(281) Toth, E.; Helm, L.; Kellar, K. E.; Merbach, A. E. *Chem. Eur. J.* **1999**, *5*, 1202−1211.
(282) Tomalia, D.; Naylor, A.; Goddard, W., III. *Angew. Chem., Int. Ed. Engl.* **1990**, *29*, 138−175.
(283) Tomalia, D. A.; Durst, H. D. *Top. Curr. Chem.* **1993**, *165*, 193−313.
(284) Wiener, E. C.; Auteri, F. P.; Chen, J. W.; Brechbiel, M. W.; Gansow, O. A.; Schneider, D. S.; Belford, R. L.; Clarkson, R. B.; Lauterbur, P. C. *J. Am. Chem. Soc.* **1996**, *118*, 7774−7782.
(285) Bryant, L. H., Jr.; Brechbiel, M. W.; Wu, C.; Bulte, J. W. M.; Herynek, V.; Frank, J. A. Proceedings of the 6th International Society of Magnetic Resonance in Medicine Conference, Sydney, Australia, 1998.
(286) Margerum, L. D.; Campion, B. K.; Koo, M.; Shargill, N.; Lai, J.-J.; Marumoto, A.; Sontum, P. C. *J. Alloys Compd.* **1997**, *249*, 185−190.
(287) Tacke, J.; Adam, G.; Claben, H.; Muhler, A.; Prescher, A.; Gunther, R. W. *Magn. Reson. Imaging* **1997**, *7*, 678−682.
(288) Roberts, H. C.; Saeed, M.; Roberts, T. P. L.; Muhler, A.; Shames, D. M.; Mann, J. S.; Stiskal, M.; Demsar, F.; Brasch, R. C. *Magn. Reson. Imaging* **1997**, *7*, 331−338.
(289) Roberts, H. C.; Saeed, M.; Roberts, T. P. L.; Brasch, R. C. *Acad. Radiol.* **1998**, *5*, S31−S33.
(290) Raduechel, B.; Schmitt-Willich, H.; Platzek, J.; Ebert, W.; Frenzel, T.; Misselwitz, B.; Weinmann, H.-J. *Book of Abstracts*; 216th ACS National Meeting, Boston, August 23−27, 1998; p PMSE−278.
(291) Dong, Q.; Hurst, D. R.; Weinmann, H. J.; Chenevert, T. L.; Londy, F. J.; Prince, M. R. *Invest. Radiol.* **1998**, *33*, 699−708.
(292) Adam, G.; Neuerburg, J.; Spuntrup, E.; Muhler, A.; Scherer, K.; Gunther, R. W. *Magn. Reson. Imaging* **1994**, *4*, 462−466.
(293) Wiener, E. C.; Brechbiel, M. W.; Brothers, H.; Magin, R. L.; Gansow, O. A.; Tomalia, D. A.; Lauterbur, P. C. *Magn. Reson. Med.* **1994**, *31*, 1−8.
(294) Lauffer, R. B.; Brady, T. J. *Magn. Reson. Imaging* **1985**, *3*, 11−16.
(295) Schmiedl, U.; Ogan, M.; Paajanen, H.; Marotti, M.; Crooks, L. E.; Brito, A. C.; Brasch, R. C. *Radiology* **1987**, *162*, 205−10.
(296) Casali, C.; Janier, M.; Canet, E.; Obadia, J. F.; Benderbous, S.; Carot, C.; Revel, D. *Acad Radiol* **1998**, *5*, S214−S218.
(297) Meyer, D.; Schaeffer, M.; Bouillot, A.; Beaute, S.; Chambon, C. *Invest. Radiol.* **1991**, *26*, S50−S52.
(298) Armitage, F. E.; Richardson, D. E.; Li, K. C. P. *Bioconjugate Chem.* **1990**, *1*, 365−74.
(299) Rebizak, R.; Schaefer, M.; Dellacherie, E. *Bioconjugate Chem.* **1997**, *8*, 605−610.
(300) Corot, C.; Schaefer, M.; Beaute, S.; Bourrinet, P.; Zehaf, S.; Benize, V.; Sabatou, M.; Meyer, D. *Acta Radiologica* **1997**, *38*, 91−99.
(301) Siauve, N.; Clement, O.; Cuenod, C.-A.; Benderbous, S.; Frija, G. *Magn. Reson. Imaging* **1996**, *14*, 381−390.
(302) Rebizak, R.; Schaefer, M.; Dellacherie, E. *Bioconjugate Chem.* **1998**, *9*, 94−99.
(303) Dellacherie, É. In *Polysaccharides in Medicinal Applications*; Dumitriu, S., Ed.; Marcel Dekker: New York, 1996.
(304) Curtet, C.; Maton, F.; Havet, T.; Slinkin, M.; Mishra, A.; Chatal, J.-F.; Muller, R. N. *Invest. Radiol.* **1998**, *33*, 752−761.
(305) Wu, C.; Brechbiel, M. W.; Kozak, R. W.; Gansow, O. A. *Bioorg. Med. Chem. Lett.* **1994**, *4*, 449−54.
(306) Wiener, E. C.; Konda, S.; Shadron, A.; Brechbiel, M.; Gansow, O. *Invest. Radiol.* **1997**, *32*, 748−754.
(307) Lauffer, R. B. *Magn. Reson. Med.* **1991**, *22*, 339.
(308) Jenkins, B. G.; Armstrong, E.; Lauffer, R. B. *Magn. Reson. Med.* **1991**, *17*, 164−178.
(309) Parmelee, D. J.; Walovitch, R. C.; Ouellet, H. S.; Lauffer, R. B. *Invest. Radiol.* **1997**, *32*, 741−747.
(310) Lauffer, R. B.; Parmelee, D. J.; Dunham, S. U.; Ouellet, H. S.; Dolan, R. P.; Witte, S.; McMurry, T. J.; Walovitch, R. C. *Radiology* **1998**, *207*, 529−538.
(311) Dwek, R. A. *Nuclear Magnetic Resonance (N.M.R.) in Biochemistry*; Oxford University Press: Oxford, 1973.
(312) Cavagna, F.; Tirone, P.; Felder, E.; De Haen, C. In *Liver Imaging: Current Trends and New Techniques*; Ferrucci, J. T., Stark, D. D., Eds.; Andover Medical Publishers: Boston, 1990.
(313) Schuhmann-Giampieri, G.; Schmitt-Willich, H.; Press: W.-R.; Negishi, C.; Weinmann, H. J.; Speck, U. *Radiology* **1992**, *183*, 59−64.
(314) Kim, S. K.; Pohost, G. M.; Elgavish, G. A. *Magn. Reson. Med.* **1991**, *22*, 57−67.
(315) Tilcock, C.; Ahkong, Q. F.; Koenig, S. H.; Brown, R. D., III.; Davis, M.; Kabalka, G. *Magn. Reson. Med.* **1992**, *27*, 44−51.
(316) Kabalka, G. W.; Davis, M. A.; Moss, T. H.; Buonocore, E.; Hubner, K.; Holmberg, E.; Maruyama, K.; Huang, L. *Magn. Reson. Med.* **1991**, *19*, 406−15.
(317) Kim, S. K.; Pohost, G. M.; Elgavish, G. A. *Bioconjugate Chem.* **1992**, *3*, 20−6.
(318) Kabalka, G. W.; Davis, M. A.; Holmberg, E.; Maruyama, K.; Huang, L. *Magn. Reson. Imaging* **1991**, *9*, 373−7.
(319) Zhao, X.; Zhuo, R.; Lu, Z.; Liu, W. *Polyhedron* **1997**, *16*, 2755−2759.
(320) Fossheim, S. L.; Colet, J.-M.; Mansson, S.; Fahlvik, A. K.; Muller, R. N.; Klaveness, J. *Invest. Radiol.* **1998**, *33*, 810−821.
(321) Unger, E.; Fritz, T.; Wu, G.; Shen, D.; Kulik, B.; New, T.; Crowell, M.; Wilke, N. *J. Liposome Res.* **1994**, *4*, 811−34.
(322) Peters, T. J. *All About Albumin: Biochemistry, Genetics, and Medical Applications*; Academic Press: San Diego, 1996.
(323) Vogler, H.; Platzek, J.; Schuhmann-Giampieri, G.; Frenzel, T.; Weinmann, H.-J.; Radüchel, B.; Press: W.-R. *Eur. J. Radiol.* **1995**, *21*, 1−10.
(324) Kumar, K.; Sukumaran, K.; Taylor, S.; Chang, C. A.; Nunn, A. D.; Tweedle, M. F. *J. Liq. Chromatogr.* **1994**, *17*, 3735−46.
(325) Harpur, E. S.; Worah, D.; Hals, P.-A.; Holtz, E.; Furuhama, K.; Nomura, H. *Invest. Radiol.* **1993**, *28*, S28−S-43.
(326) Hieronim, D. E.; Kanal, E.; Swanson, D. P. *Am. J. Health-Syst. Pharm.* **1995**, *52*, 2556.
(327) Murphy, K. J.; A., B. J.; Cohan, R. H. *Am. J. Radiol.* **1996**, *167*, 847.
(328) Nelson, K. L.; Gifford, L. M.; Lauber-Huber, C.; Gross, C. A.; Lasser, T. A. *Radiology* **1995**, *196*, 439−443.
(329) Vogl, T. J.; Pegios, W.; McMahon, C. *AJR* **1992**, *158*, 887−892.
(330) Rosati, G.; Pirovano, G.; Spinazzi, A. *Invest. Radiol.* **1994**, *29*, S183.
(331) Hamm, B.; Staks, T.; Muhler, A.; Bollow, M.; Taupitz, M.; Frenzel, T.; Wolf, K.-J.; Weinmann, H.-J.; Lange, L. *Radiology* **1995**, *195*, 785−792.
(332) Reimer, P.; Rummeny, E. J.; Shamsi, K.; Balzer, T.; Daldrup, H. E.; Peters, P. E. *Radiology* **1996**, *199*, 177−183.
(333) Grist, T. M.; Korosec, F. R.; Peters, D. C.; Witte, S.; Walovitch, R. C.; Dolan, R. P.; Bridson, W. E.; Yucel, E. K.; Mistretta, C. A. *Radiology* **1998**, *207*, 539−544.
(334) Tweedle, M. F.; Wedeking, P.; Kumar, K. *Invest. Radiol.* **1995**, *30*, 372−80.
(335) McMurry, T. J.; Sajiki, H.; Scott, D. M.; Lauffer, R. B. PCT Int. Appl. WO9623526 1996; *Chem. Abstr.* **1996**, *125*, 230822.
(336) Mühler, A.; Oulde Elferink, R. P. J.; Weinmann, H.-J. *MAGMA* **1993**, *1*, 134−139.
(337) Young, S. W.; Qing, F.; Harriman, A.; Sessler, J. L.; Dow, W. C.; Mody, T. D.; Hemmi, G. W.; Hao, Y.; Miller, R. A. *Proc. Natl. Acad. Sci.* **1996**, *93*, 6610−6615.
(338) Ni, Y.; Pislaru, C.; Bosmans, H.; Pislaru, S.; Miao, Y.; Dymarkowski, S.; Bogaert, J.; Van de Werf, F.; Semmler, W.; Marchal, G. Proceedings of the 6th International Society of Magnetic Resonanace in Medicine Conference, Sydney, Australia, 1998; p 551.
(339) Kraitchman, D. L.; Oznur, I.; Faranesh, A. Z.; McVeigh, E. R.; Weinmann, H.-J. Proceedings of the 6th International Society of Magnetic Resonanace in Medicine Conference, Sydney, Australia, 1998; p 552.
(340) Moats, R. A.; Fraser, S. E.; Meade, T. J. *Angew. Chem., Int. Ed. Engl.* **1997**, *36*, 726−728.
(341) Lauffer, R. B.; McMurry, T. J.; Dunham, S. O.; Scott, D. M.; Parmelee, D. J.; Dumas, S. PCT Int. Appl. WO9736619, 1997; *Chem. Abstr.* **1997**, *127*, 316334.
(342) Li, W.-h.; Fraser, S. E.; Meade, T. J. *J. Am. Chem. Soc.* **1999**, *121*, 1413−1414.
(343) Beeby, A.; Clarkson, I. M.; Dickins, R. S.; Faulkner, S.; Parker, D.; Royle, L.; de Sousa, A. S.; Williams, J. A. G.; Woods, M. *J. Chem. Soc., Perkin Trans. 2* **1999**, 493−504.

CR980440X